Model Calculations of the Atmospheric Effects of Supersonic Aviation Which Were Used in the IPCC Special Report on Aviation and the Global Atmosphere

Lead Author:
Debra Weisenstein, AER, Inc., U.S.A.

Technical Support:
Karen Sage, NASA Langley Research Center, U.S.A.
Donald Brown, NASA Langley Research Center, U.S.A.

Co-Authors:
Richard S. Eckman, NASA Langley Research Center, U.S.A.
Malcolm K.W. Ko, AER, Inc., U.S.A.

Contributors:
Steven L. Baughcum, Boeing Company, U.S.A.
Martyn Chipperfield, University of Cambridge, U.K.
Michael Gauss, University of Oslo, Norway
William L. Grose, NASA Langley Research Center, U.S.A.
Robert S. Harwood, University of Edinburgh, U.K.
Ivar Isaksen, University of Oslo, Norway
Charles H. Jackman, NASA Goddard Space Flight Center, U.S.A.
Douglas E. Kinnison, Lawrence Livermore National Laboratory, U.S.A.
Giovanni Pitari, University L'Aquila, Italy
Helen Rogers, University of Cambridge, U.K.
Courtney J. Scott, AER, Inc., U.S.A.
Peter F. Vohralik, CSIRO, Australia
Vicky West, University of Edinburgh, U.K.

May 1999

Rationale

This report is intended to expand upon the IPCC Special Report on Aviation and the Global Atmosphere. It provides additional detail regarding the supersonic emission scenario calculations presented in Chapter 4—Modeling the Future Atmosphere. Due to the space limitations in that document, detailed plots and discussion for a majority of the model calculations were omitted. This document is intended to fill that gap and has been compiled for two reasons: (1) to aid those called upon to review the IPCC Special Report, and (2) to archive and document the calculations performed by nine modeling groups for up to 50 scenarios each. This document does not attempt to provide a synthesis of the modeling results or draw conclusions regarding the impact of aircraft on the atmosphere. That function is provided by the IPCC report.

The model descriptions and model results presented in this document represent the state of those models in 1997 when the calculations were performed. Because models are continually evolving and undergoing further development, these results should be considered as a historical snapshot. Please do not cite results presented herein without first obtaining permission from the group which performed the calculations.

Contents

Chapter 3

Background Atmospheres

Atmospheric perturbations due to emissions by supersonic aircraft are computed relative to the 2015 and 2050 atmospheres. Modeling of both future years is important because the concentrations of atmospheric chlorine and other trace gases are changing with time. HSCT perturbations are believed to be sensitive to concentrations of these background gases. Boundary conditions for 1992, 2015 and 2050 were specified for the modelers and are listed in Table 3.1. The future atmosphere boundary conditions were based on the IPCC IS92a scenario from past IPCC reports (1992, 1995). The halocarbon boundary conditions correspond to 3.7, 3.0, and 2.0 ppbv of Cl_y in the upper stratosphere in 1992, 2015, and 2050, respectively. Concentrations of Br_y in the upper stratosphere are 15, 12.5, and 11.1 pptv for the same years.

The sulfate surface area density (SAD) for the background atmosphere (designated SA0) was that given in Table 8-8 of *WMO* (1992) and is displayed in Figure 3.1. Maximum sulfate surface area density occurs in the lower stratosphere at middle to high latitudes in both hemispheres and decreases with height, with zero surface area density above 32 km. The profile is specified at two times during the year (April and October) and modelers were instructed to use the April profile for the first half of the year and the October profile for the second half. SA0 represents an atmosphere with minimal volcanic influence. To approximate the effects of an active period of volcanic eruptions (e.g., the last two decades), some scenarios employed an SAD enhanced by a factor of 4 relative to the nonvolcanic case (designated 4xSA0). The surface area of polar stratospheric clouds (PSCs) was not specified. Those models with the capability to calculate PSC surface area (AER, GSFC, UNIVAQ, SCTM1, SLIMCAT, and LARC) followed their standard treatment, while LLNL and THINAIR used an approach based on current climatology.

There were a total of seven baseline scenarios for the year 2015 and three baseline scenarios for the year 2050. These are listed, along with their scenario designations, in Table 3.2. Each includes a subsonic aircraft fleet, which was reduced in the HSCT scenarios to account for displacement of the subsonic fleet by the supersonic fleet. Scenario D is the standard 2015 baseline scenario. Scenario D3 includes a volcanically perturbed sulfate surface area density at 4xSA0. Scenario D4 has the PSC parameterizations removed. Scenarios D5 and D6 use different Cl_y amounts, 1.0 and 4.0 ppbv, respectively. Scenarios D7 and D8 include interactive sulfate aerosol microphysics. Scenario D9 uses the 2050 boundary conditions, resulting in 2.0 ppbv of Cl_y, though the subsonic aircraft fleet is the same as that used for the 2015 scenarios. Scenarios F and G also represent 2050 and employ projected subsonic fleets appropriate to 2050.

3.1 Scenario D Results

Nine models submitted results for Scenario D which employs boundary conditions appropriate to 2015, background aerosol surface area SA0, and a subsonic aircraft fleet. Figure 3.2 shows the integrated ozone column as a function of time of year and latitude expressed in Dobson Units (DU) for Scenario D. All nine models calculate the seasonal behavior of ozone in a manner consistent with observations, such as those from the TOMS instrument for 1990, shown in Figure 3.3. Features of note include the tropical minimum, reproduced in all models at approximately 260-280 DU, except in the SLIMCAT-3D model where the tropical minimum is slightly higher at 300 DU. The northern hemisphere high latitude winter/spring maximum is seen in all models, but with widely varying maximum levels, ranging from 420 DU in the CSIRO and

Table 3.1: Recommendations for Species Concentrations in 1992, 2015, and 2050

Species	1992 (3.6 ppbv Cl_y)	2015 (3 ppbv Cl_y)	2050 (2 ppbv Cl_y)
CFC-11	268 pptv	220 pptv	120 pptv
CFC-12	503 pptv	470 pptv	350 pptv
CFC-113	82 pptv	80 pptv	60 pptv
CCl_4	132 pptv	70 pptv	35 pptv
HCFC-22	100 pptv	250 pptv	15 pptv
CH_3CCl_3	135 pptv	3 pptv	0 pptv
HCFC-141b†	2 pptv	12 pptv	0 pptv
Halon-1301	3 pptv	1.4 pptv	0.9 pptv
Halon-1211	2 pptv	1.1 pptv	0.2 pptv
CH_3Cl	600 pptv	600 pptv	600 pptv
CH_3Br	10 pptv	10 pptv	10 pptv
CH_4	1714 ppbv	2052 ppbv	2793 ppbv
N_2O	311 ppbv	333 ppbv	371 ppbv
CO_2	356 ppmv	405 ppmv	509 ppmv

†For those models that cannot handle HCFC-141b, the recommendation is to put it in as CH_3CCl_3 after adjusting for the number of chlorine atoms per molecule, i.e., multiply the HCFC-141b mixing ratio by 2/3 and add to CH_3CCl_3. The stratospheric lifetimes for CH_3CCl_3 and HCFC-141b are 50 years and 75 years, respectively. These lifetimes are sufficiently close that supplementing CH_3CCl_3 with HCFC-141b should be a reasonable approximation.

Table 3.2: Specifications for Baseline Scenarios which Include a Subsonic Aircraft Fleet

Scenario	Year	Cl_y (ppbv)	Subsonic Fleet Projection	PSC Representation	SAD Representation
D	2015	3.0	2015	Included	SA0
D3	2015	3.0	2015	Included	4xSA0
D4	2015	3.0	2015	Removed	SA0
D5	2015	1.0	2015	Included	SA0
D6	2015	4.0	2015	Included	SA0
D7	2015	3.0	2015	Included	Sulfate microphysics with SO_2 gas to particle conversion of 50%
D8	2015	3.0	2015	Included	Sulfate microphysics with SO_2 gas to particle conversion of 100%
D9	2050	2.0	2015	Included	SA0
F	2050	2.0	2050 IS92a	Included	SA0
G	2050	2.0	2050 High Demand	Included	SA0

SLIMCAT-3D models to 500 DU in the AER, LLNL, UNIVAQ, and SCTM1 models. The high latitude summer decrease is seen in all models, but with widely varying rates of decrease, and minimum values from 320 to 380 DU. In the southern hemisphere, the winter/spring midlatitude maximum is simulated by all models with levels ranging from 360 DU to 500 DU. The models that include polar stratospheric chemistry (all but CSIRO) calculate a springtime minimum in southern polar ozone ranging from 240 DU to 320 DU, somewhat higher than typical present day levels.

In the zonal mean, the model O_3 fields also compare well with available observations as evidenced in Figure 3.4, showing zonal mean O_3 versus height in June. Peak ozone mixing ratios occur in the tropics near 30 km with levels of 8 to 11 ppmv. The vertical decrease through the upper stratosphere and mesosphere is similar in all models, with levels of 2 ppmv reached at 50 km in the tropics for most models, though the SLIMCAT-3D and THINAIR-2D models calculate slightly higher mesospheric ozone and the SCTM-3D model slightly lower. The SLIMCAT-3D and THINAIR-2D models both use θ as the vertical coordinate, and conversion onto the common UADP grid in log-pressure coordinates is only approximate. In addition, the SLIMCAT-3D and SCTM1-3D models have coarse vertical resolution in the upper stratosphere and mesosphere. Therefore these three models (SLIMCAT, SCTM1, and THINAIR) are expected to differ from the others in the upper stratosphere/mesosphere.

Figures 3.5, 3.6, and 3.7 shows the ozone number density profile at 45^{o}N, the equator, and 45^{o}S during June as a function of altitude. Most of the models show similar ozone maxima at approximately 25 km in midlatitudes with levels of 4-5x10^{12} molecules/cm^3. AER and LLNL, while similar to other models at 25 km, have higher concentrations (up to 5-6x10^{12} molecules/cm^3) between 15 and 25 km at 45^{o}N. Among other models, there is a moderate spread in calculated O_3 in the lower stratosphere. Above 28 km, all models yield similar ozone profiles, except that UNIVAQ is a bit higher. Model differences in background ozone, particularly in the lower stratosphere, are likely to yield differences in the response to HSCT emissions, particularly as HSCT emissions peak at northern midlatitudes, coincident with projected flight corridors.

The partitioning within the odd oxygen family is further illustrated in Figures 3.8 and 3.9. In Figure 3.8, zonal mean atomic oxygen mixing ratios are plotted as a function of latitude and height for June. The 2-D models reported daytime average values of atomic oxygen, while the 3-D models reported 24-hour averages. Model behavior is broadly similar in all cases. The O/O_3 ratio (Figure 3.9) shows odd oxygen partitioning in the upper stratosphere and lower mesosphere. This ratio is largely controlled by the photolysis of ozone, which is not expected to differ significantly between models because the models' photodissociation schemes have been previously benchmarked. Some differences may be due to the averaging interval used for atomic oxygen. Also, the temperature in this region (and the corresponding neutral density) may be a factor in this difference. As the mesospheric contribution to the ozone column is minimal, these differences would not be expected to have a substantial impact on stratospheric ozone levels (as evidenced in Figure 3.4).

N_2O, a longer-lived constituent, is shown in Figure 3.10. Differences are apparent between the models, which implies differences in transport. The CSIRO, GSFC and LARC models have more latitudinal variation in the upper stratosphere while the LARC and SLIMCAT N_2O fields are flatter in the lower stratosphere than others. This points to significant differences in mixing rates and transport time scales between different regions of the atmosphere. These differences in transport characteristics will impact the calculated HSCT effluent accumulation and distribution among, and thus the ozone impact.

Model water vapor fields are shown in Figure 3.11. H_2O is the principal source of atmospheric odd hydrogen which dominates ozone loss processes in the lower stratosphere and troposphere, as well as in the upper stratosphere and mesosphere. The models show similar H_2O distributions with stratospheric maxima of approximately 6 ppmv, though the THINAIR-2D model calculates a lower stratospheric maximum of only 5 ppmv. Differences are apparent in the tropical lower and middle stratosphere, with many models showing distinct local minima and others with less apparent local minima (e.g., CSIRO, SLIMCAT-3D, and THINAIR). The LARC H_2O distribution is specified from a 2D model distribution derived from an older version of the NOCAR model, rather than calculated self- consistently.

Zonal mean hydoxyl radical mixing ratio is plotted in Figure 3.12. The 3-D models reported 24-hour average values of radical species (ie. zonal means of the 3-D results), whereas the 2-D models reported daytime average values, so the OH fields in the 3-D models differ from the 2-D models by a factor of 2, roughly. Concentrations are generally similar in all models, if adjusted for averaging period. This general consistency, particularly in the lower stratosphere suggests that ozone loss rates due to odd hydrogen chemistry should be reasonably consistent among the models.

Figure 3.13 shows the model NO_y fields. Substantial differences are evident between the models. Maximum NO_y concentrations occur between 35 and 40 km with mixing ratios of between 18 and 26 ppbv. Figures 3.14, 3.15, and 3.16 show profiles of NO_y mixing ratio at 45^{o}N, the equator, and 45^{o}S in June. The large spread of model results is evident above 35 km in the tropics and at all stratospheric altitudes at midlatitudes. In the lower stratosphere, the AER, GSFC, LLNL, and THINAIR models have greater NO_y. In the upper stratosphere, the CSIRO, GSFC, LLNL, and THINAIR models have greater NO_y. As NO_y is a principal emission product of an HSCT fleet, differences in background lower stratospheric levels would have an impact on any calculated perturbations. The NO_x (or NO+NO_2) to NO_y ratio is shown in Figure 3.17. Despite the differences in total NO_y, these values are broadly similar among the models suggesting that the partitioning is similar in all cases. Large differences in NO_x/NO_y in the tropical upper troposphere likely reflect different treatments of the NO_x lightning source.

As expected by the differing peak NO_y values, the sum of NO and NO_2 (Figure 3.18) reveals differences in the maximum values, with mixing ratios from approximately 15 ppbv in the LARC model to 24 ppbv in the CSIRO, GSFC, and LLNL models. NO_2 fields are shown in Figure 3.19, with maxima from 6 to 10 ppbv at 35 km. Lower stratospheric differences are also apparent. Differences in the calculated NO_y (and NO_x) fields could have several sources: the photolysis of NO (which impacts atomic N that participates in the destruction of NO_y); the N_2O distribution (which is the principal source of NO_y); O_3 and O(1D), the latter reacting with N_2O to produce NO_y, and atmospheric transport. Such intercomparisons are beyond the scope of this document, but a more detailed study of these NO_y differences is warranted.

The odd chlorine family is examined in the next group of figures. Zonal mean Cl_y is shown in Figure 3.20 for the six models reporting this quantity. Results are similar and appropriate to the boundary conditions (~3.0 ppbv), except for the THINAIR result, which shows only 2.0 ppbv in the upper stratosphere. Figures 3.21, 3.22, and 3.23 show vertical profiles of Cl_y mixing ratio at 45^{o}N, the equator, and 45^{o}S in June. Most models yield very similar Cl_y concentrations at 60 km, exceptions being the THINAIR model which is quite low compared to the other models and the LARC and SCTM1 models which are a bit higher. Modest variation in Cl_y concentration among the models is found in the lower stratosphere.

ClO mixing ratios reveal distinct differences (Figure 3.24). Stratospheric maxima vary from levels of 0.5 ppbv (CSIRO and UNIVAQ) to 1.0 ppbv (AER and SCTM1-3D at about 40 km in the northern hemisphere. The THINAIR model shows much smaller maximum concentrations (only 0.1 ppbv) related to the smaller Cl_y concentrations in this model. Equator to pole gradients in the middle stratosphere vary from strong (AER, LLNL, SCTM1) to weak (CSIRO, UNIVAQ, SLIMCAT). Some of these differences are related to the way the models treat the reaction between OH and ClO. JPL 1997 makes no recommendation of product yields. The CSIRO, SLIMCAT, and LARC models include non-zero yields for the minor channel $ClO+OH \rightarrow HCl+O_2$. The inclusion of this channel would tend to lower the level of ClO at the peak. In the lower stratosphere, calculated mixing ratios are in better agreement, though ozone loss due to odd chlorine is a minor component in this region outside the poles. The ratio of ClO to Cl_y (Figure 3.25) also shows differences, with higher values of this ratio in the AER and SCTM1-3D models, and smaller values in the LARC and THINAIR models.

Total odd bromine (Br_y) is shown in Figure 3.26 as a function of latitude and altitude and in Figures 3.27, 3.28, and 3.29 as a function of latitude only at 45^{o}N, the equator, and 45^{o}S. Based on tropospheric boundary conditions of the organic halogens, Br_y levels in the upper stratosphere are expected to be 12.5 pptv. The AER, CSIRO, GSFC, and SCTM1 models show about 12 pptv of Br_y in the upper stratosphere, while the LARC model shows 14 pptv, the THINAIR model 20 pptv, and the SLIMCAT model 8 pptv. BrO concentrations, shown in Figure 3.30 for all nine models, have maxima near 40 km. Maximum concentrations range from 6 to 10 pptv, except for the THINAIR model which shows a maximum of 14 pptv. Lower stratospheric concentrations of BrO are in fair agreement. The ratio of BrO to Br_y is shown in Figure 3.31. Some difference in the partitioning are evident, with AER, CSIRO, and THINAIR calculating a partitioning of 70% active bromine near 40 km, GSFC and LARC calculating 60% active bromine, and SCTM1 calculating only 30-40%.

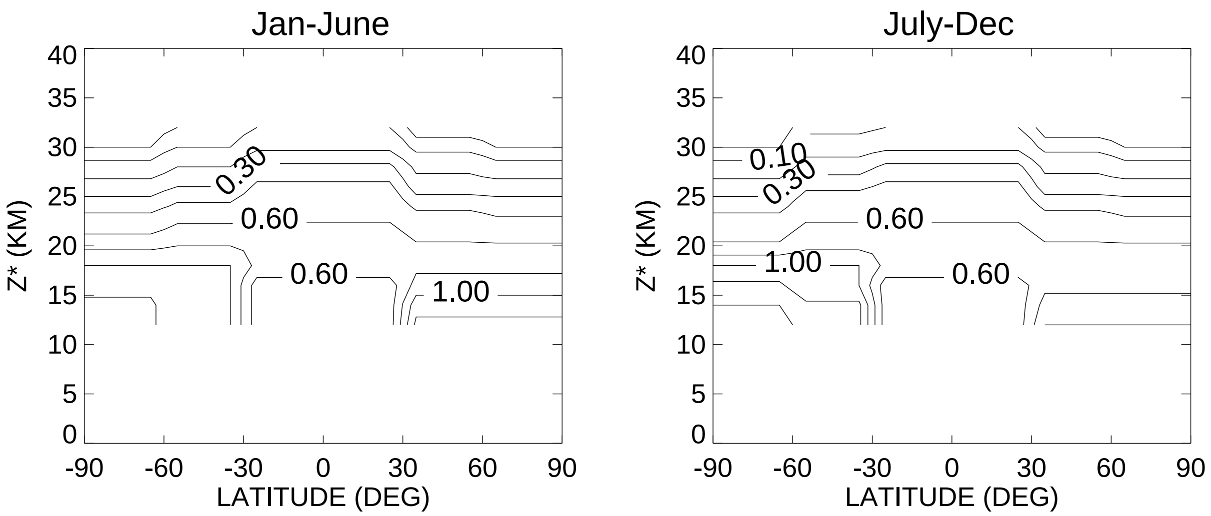

Figure 3.1: Surface area density ($\mu m^2/cm^3$) used for background atmospheres in 2015 and 2050 under volcanically clean conditions. This surface area density is designated SA0 and comes from *WMO* (1992). Contours are 0, 0.1, 0.2, 0.3, 0.4, 0.6, 0.8, 1.0, 1.2, 1.5.

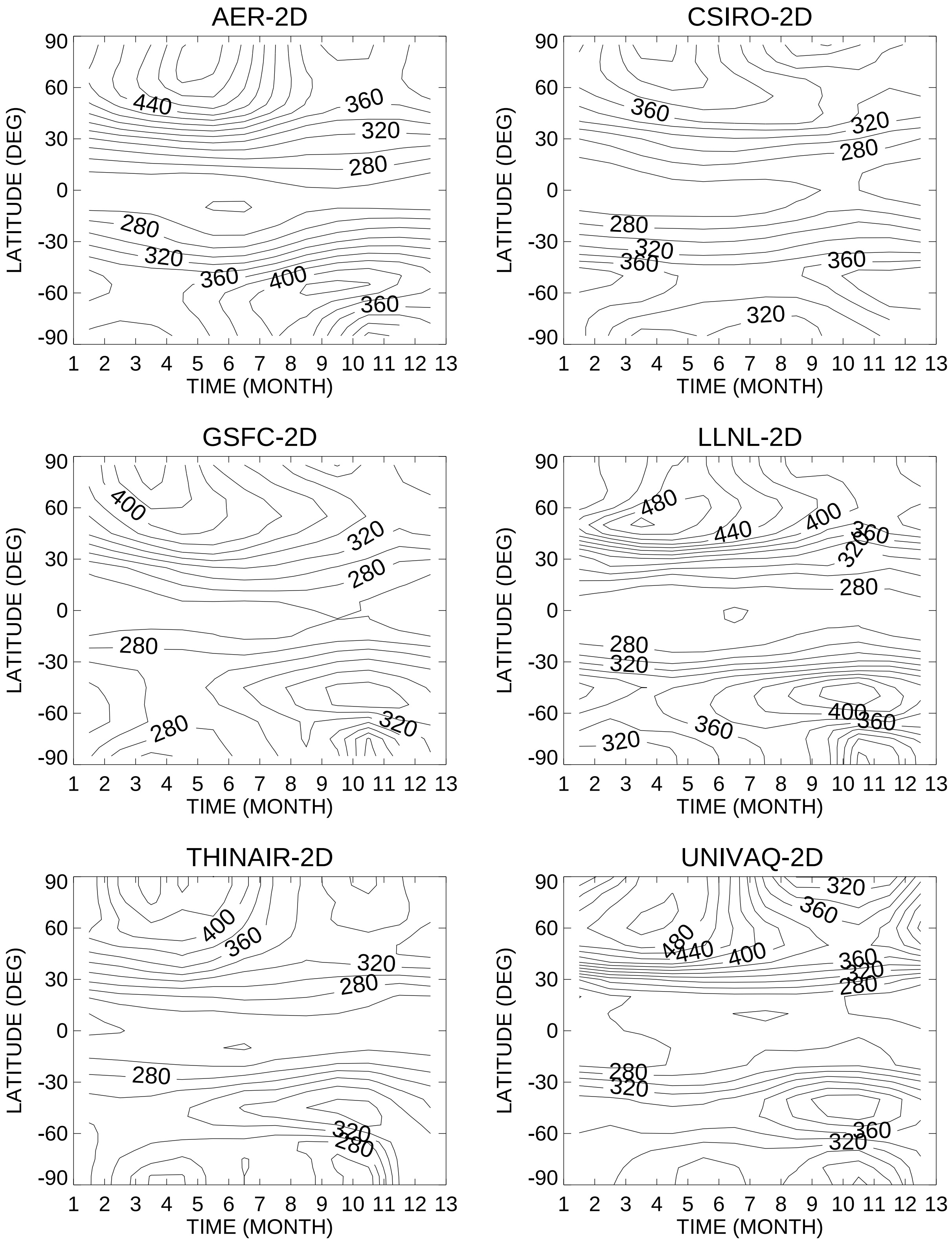

Figure 3.2: Total column ozone (Dobson Units) as a function of latitude and season calculated by the models for Scenario D, the 2015 background atmosphere with subsonic aircraft. The contour interval is 20 DU.

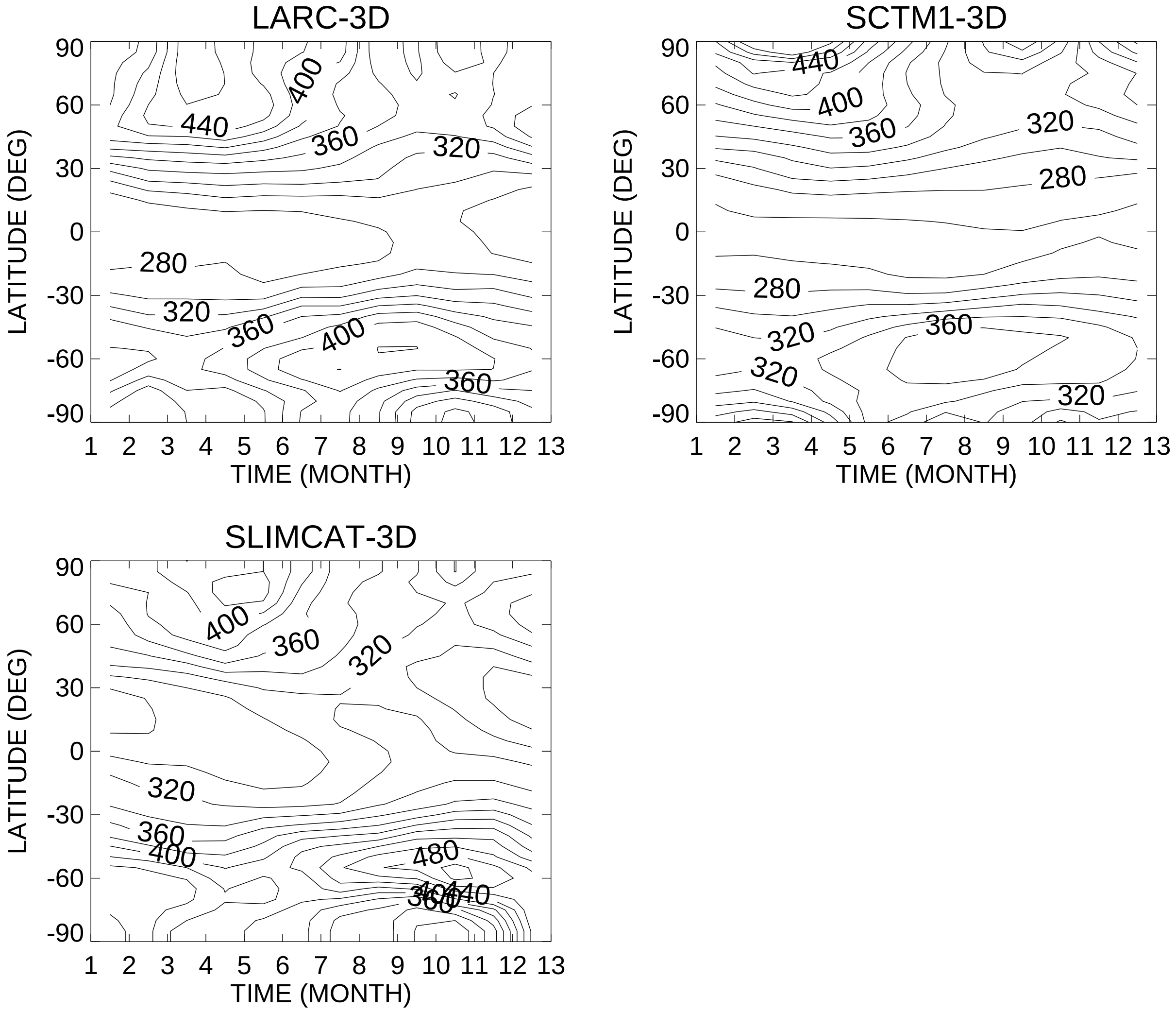

Figure 3.2: continued

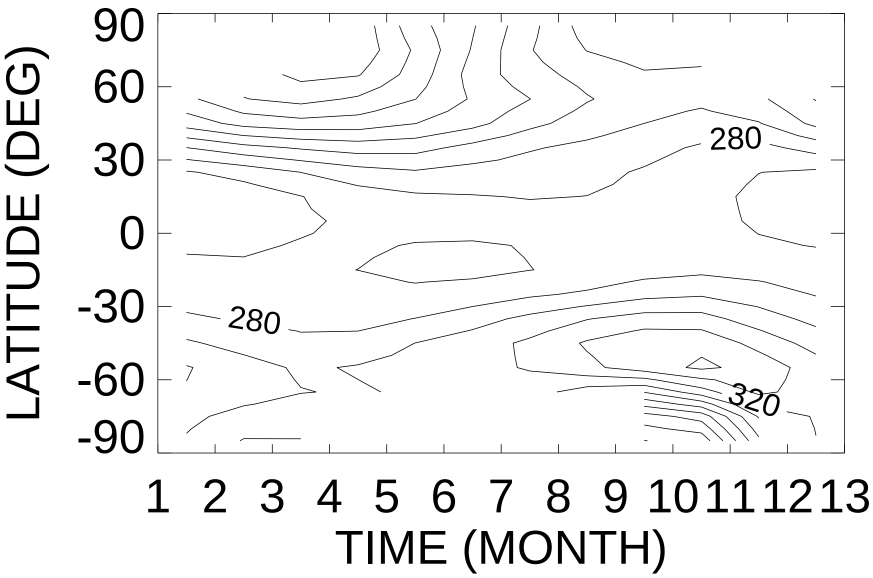

Figure 3.3: Total column ozone (Dobson Units) as a function of latitude and season for 1990 as observed by the TOMS instrument. The contour interval is 20 DU.

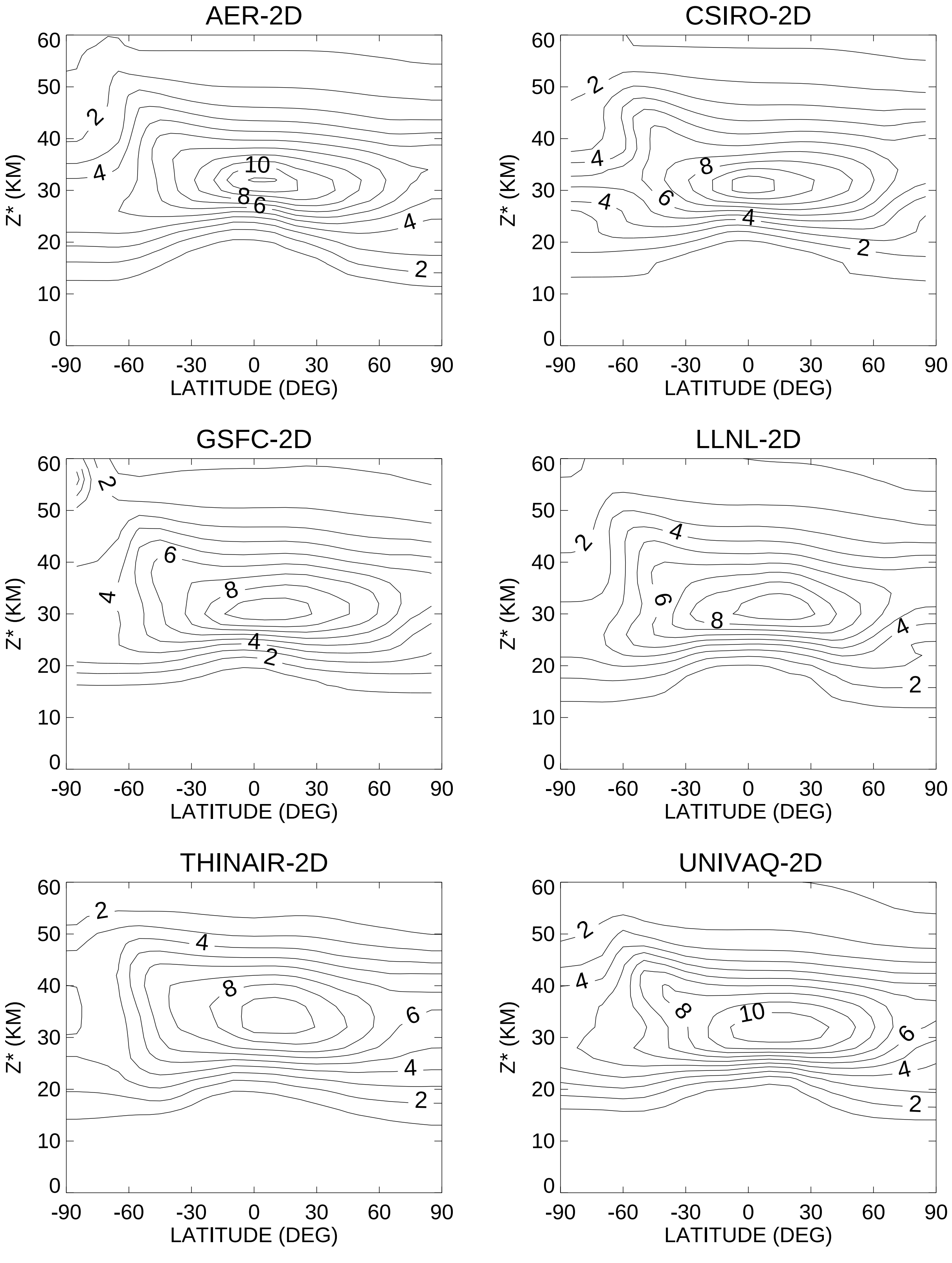

Figure 3.4: Calculated ozone mixing ratios (ppmv) as a function of latitude and altitude for Scenario D in June of 2015. The contour interval is 1 ppmv.

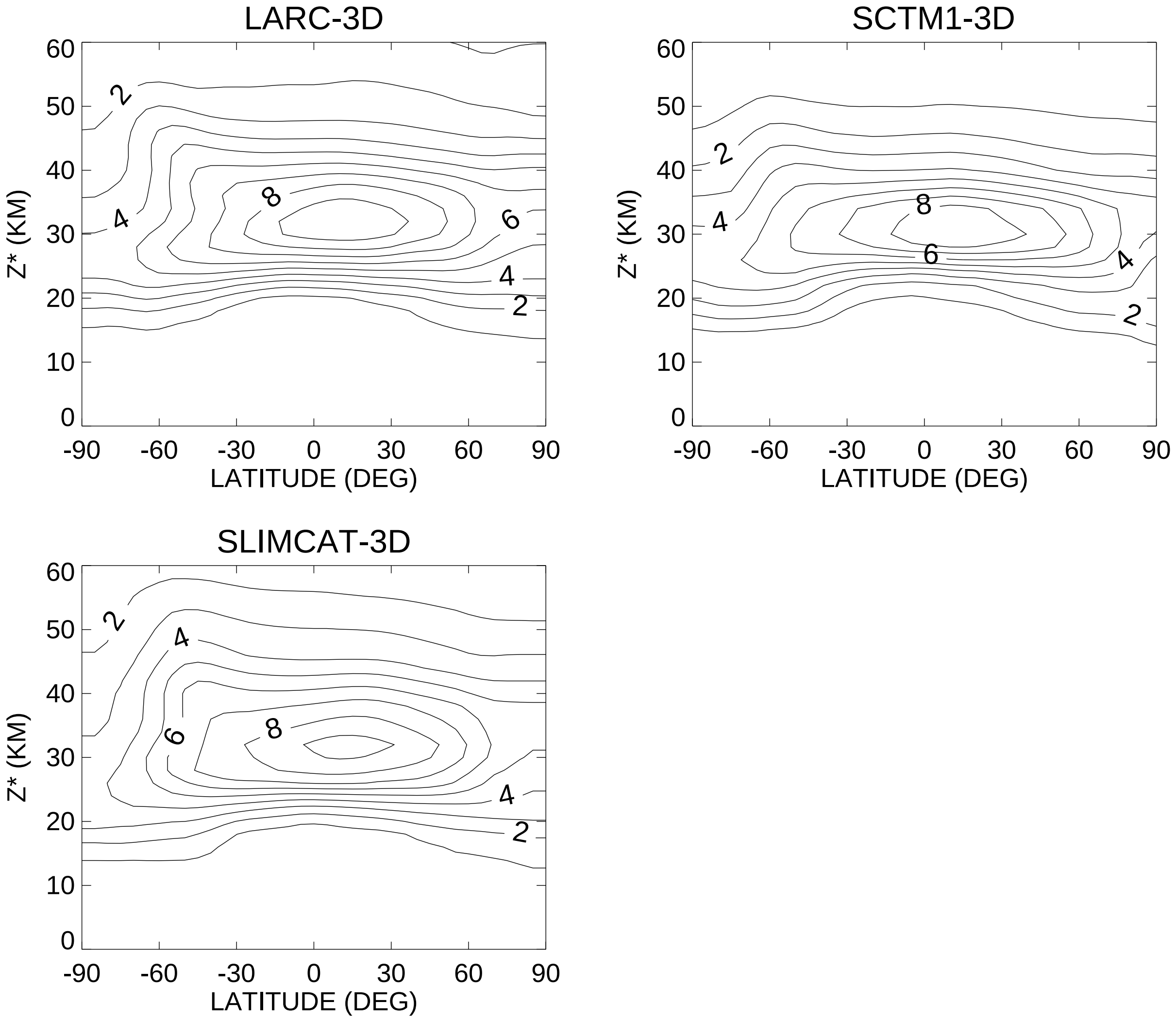

Figure 3.4: continued

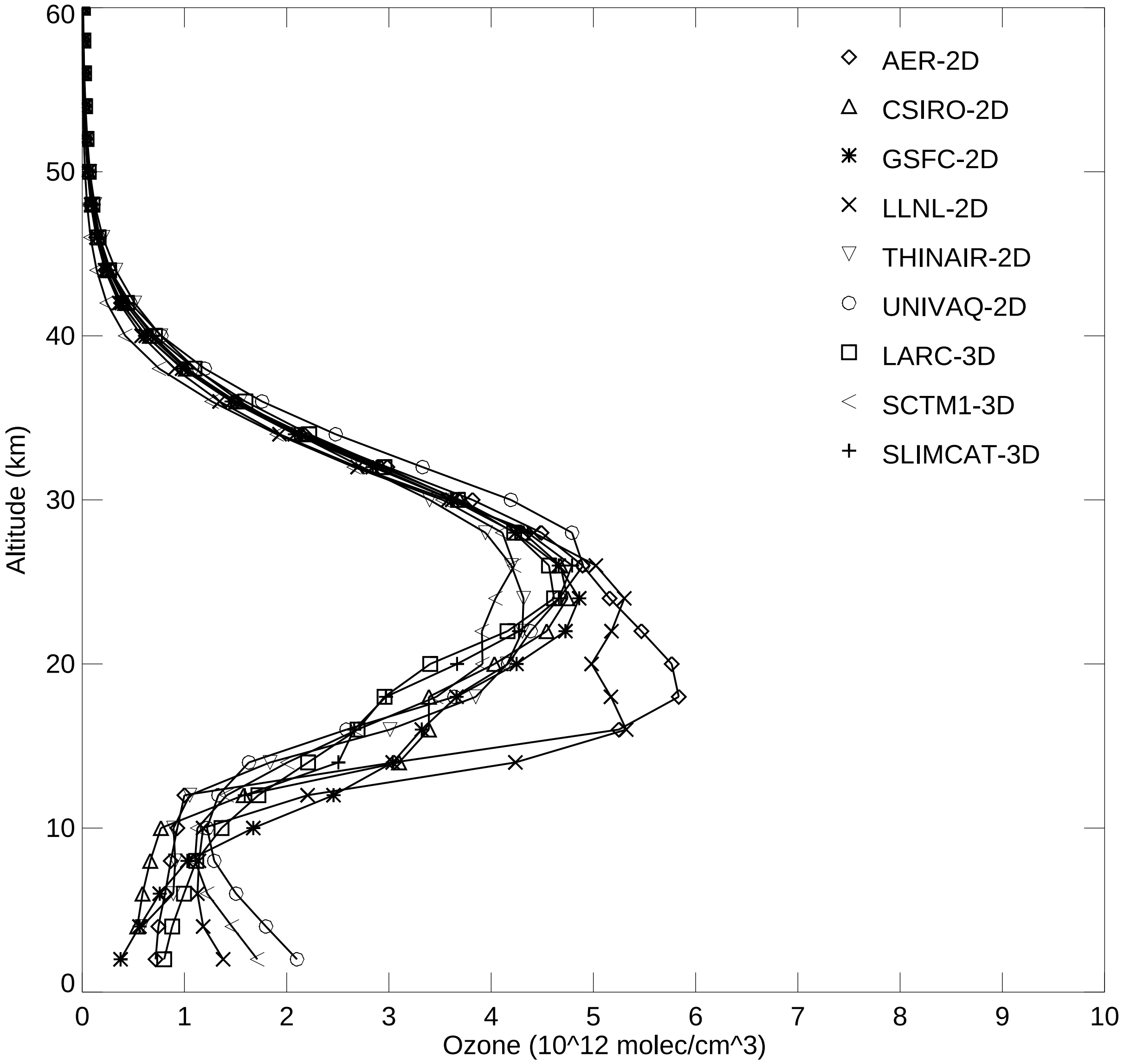

Figure 3.5: Calculated ozone concentration (molecules/cm^3) as a function of altitude for Scenario D at 45^{o}N in June.

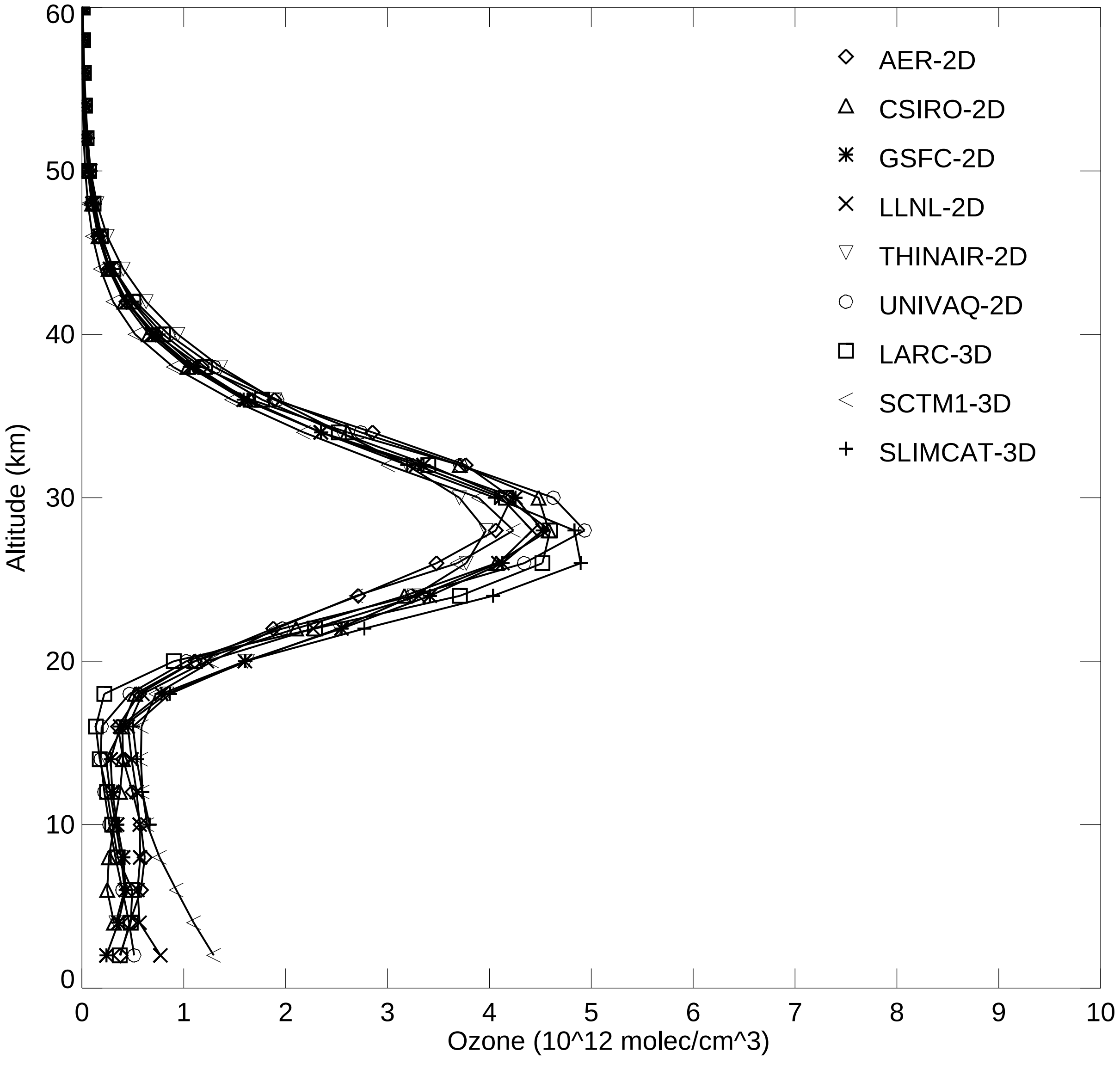

Figure 3.6: Calculated ozone concentration (molecules/cm^3) as a function of altitude for Scenario D at the equator in June.

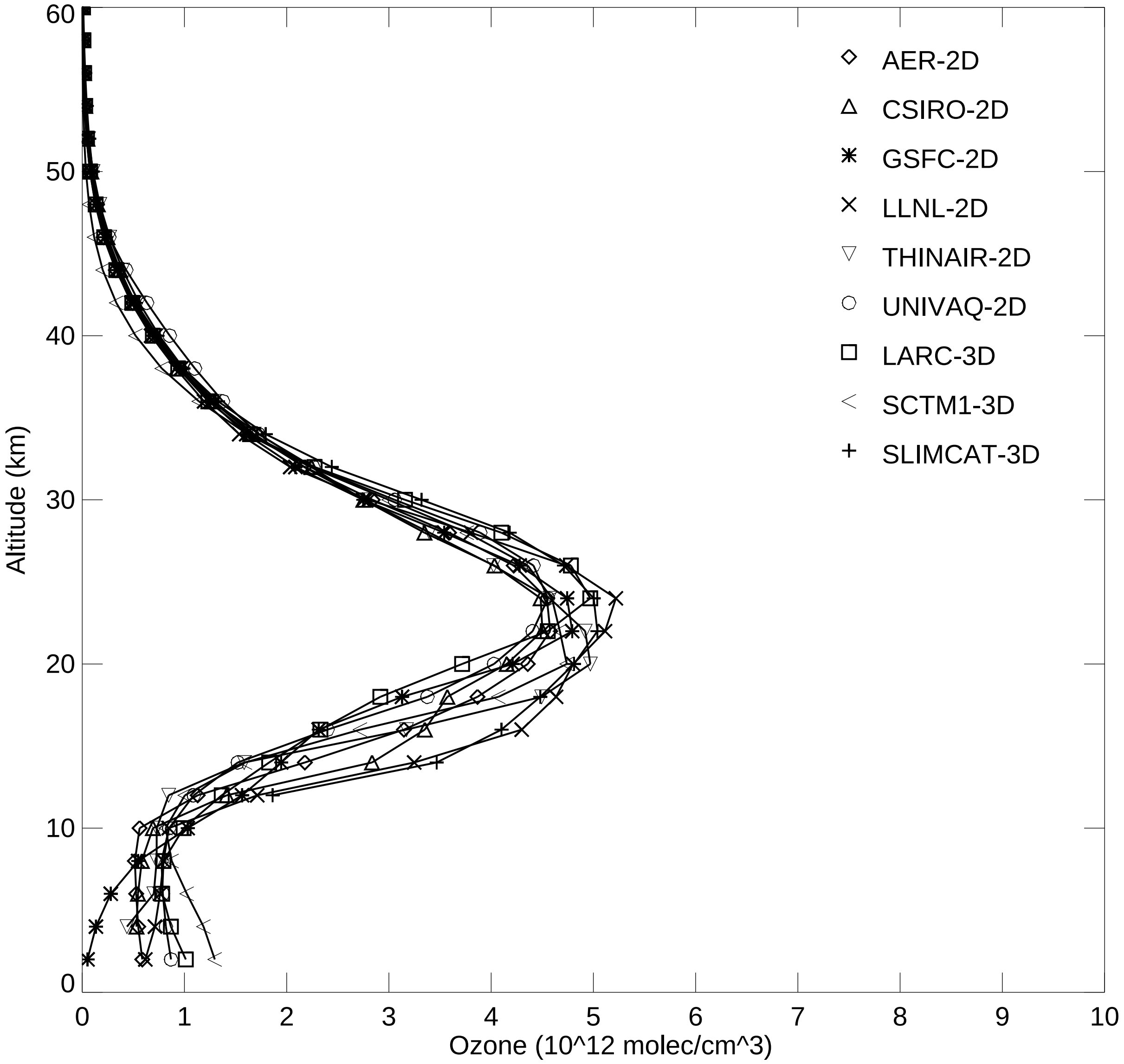

Figure 3.7: Calculated ozone concentration (molecules/cm^3) as a function of altitude for Scenario D at 45^oS in June.

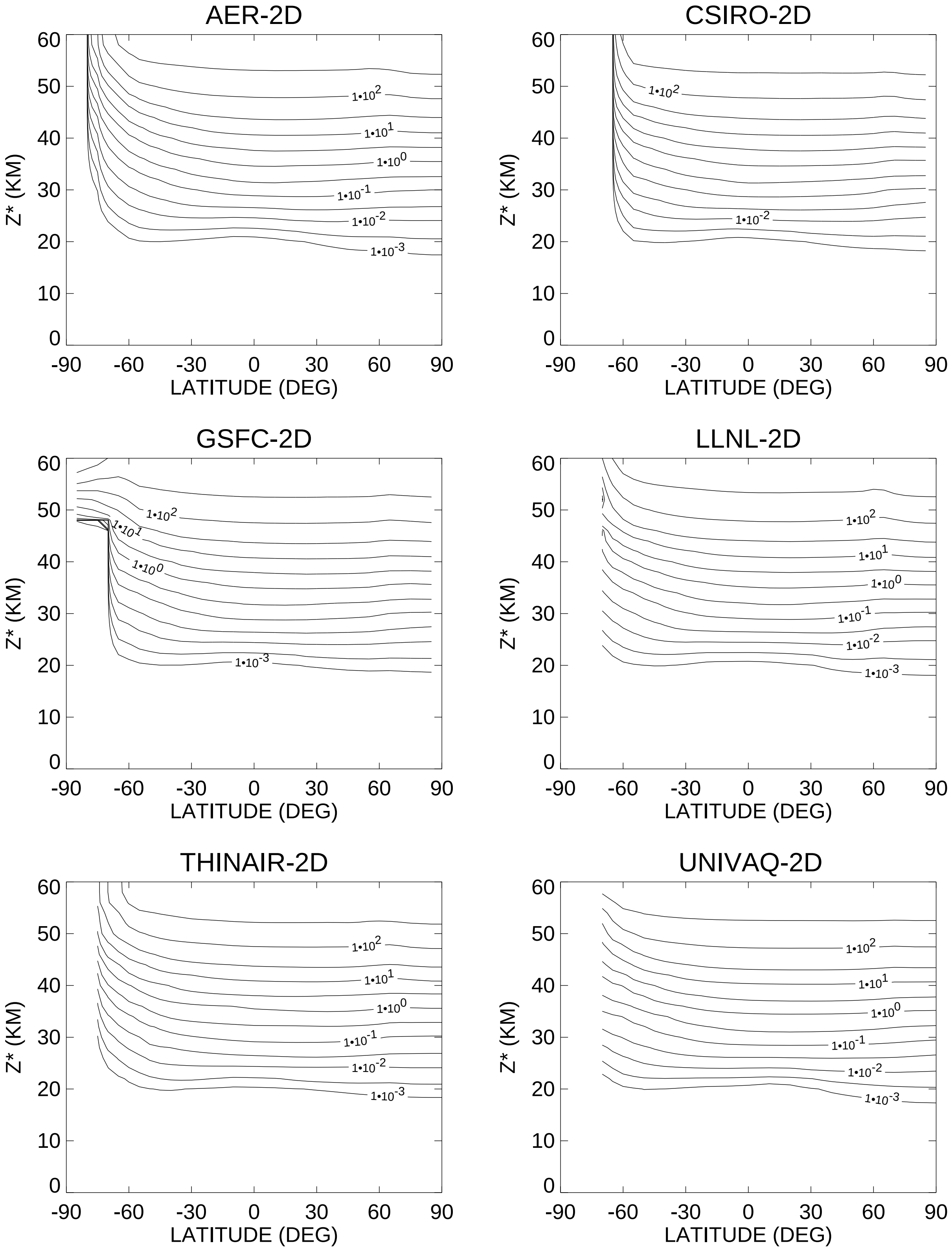

Figure 3.8: Calculated atomic oxygen mixing ratios (pptv) as a function of latitude and altitude for Scenario D in June of 2015. Daytime averages are shown for 2-D models, 24-hour averages for 3-D models. Contours are .001, .003, .01, .03, .1, .3, 1, 3, 10, 30, 100, 300, 1000 ppbv.

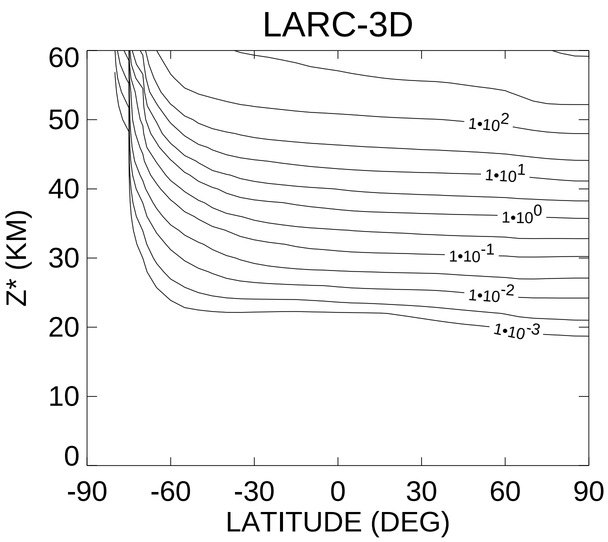

Figure 3.8: continued

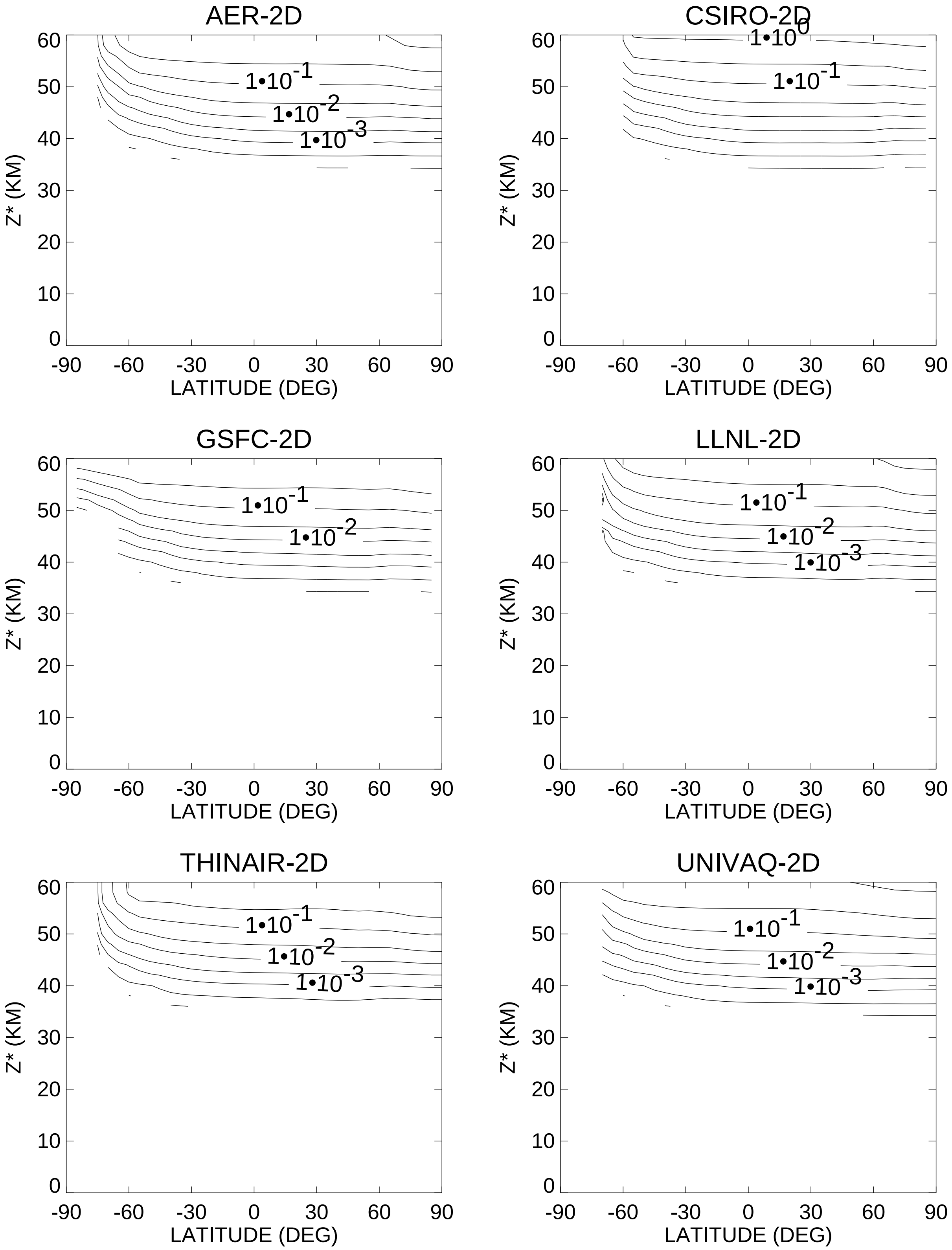

Figure 3.9: Calculated O/O_3 ratio as a function of latitude and altitude for Scenario D in June of 2015. Contours are .0001, .0003, .001, .003, .01, .03, .1, .3, 1.0.

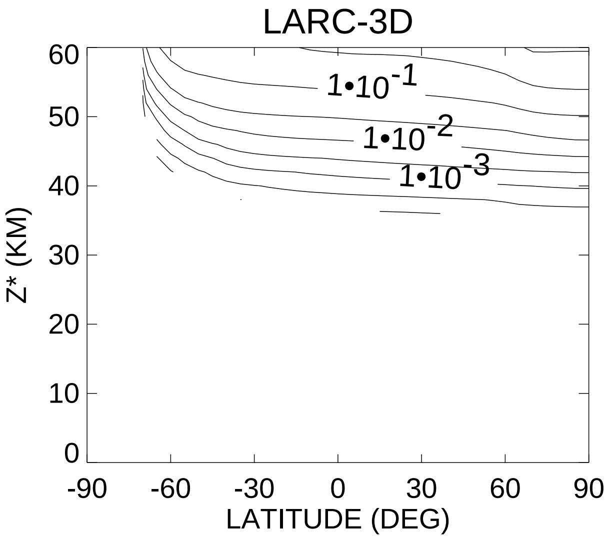

Figure 3.9: continued

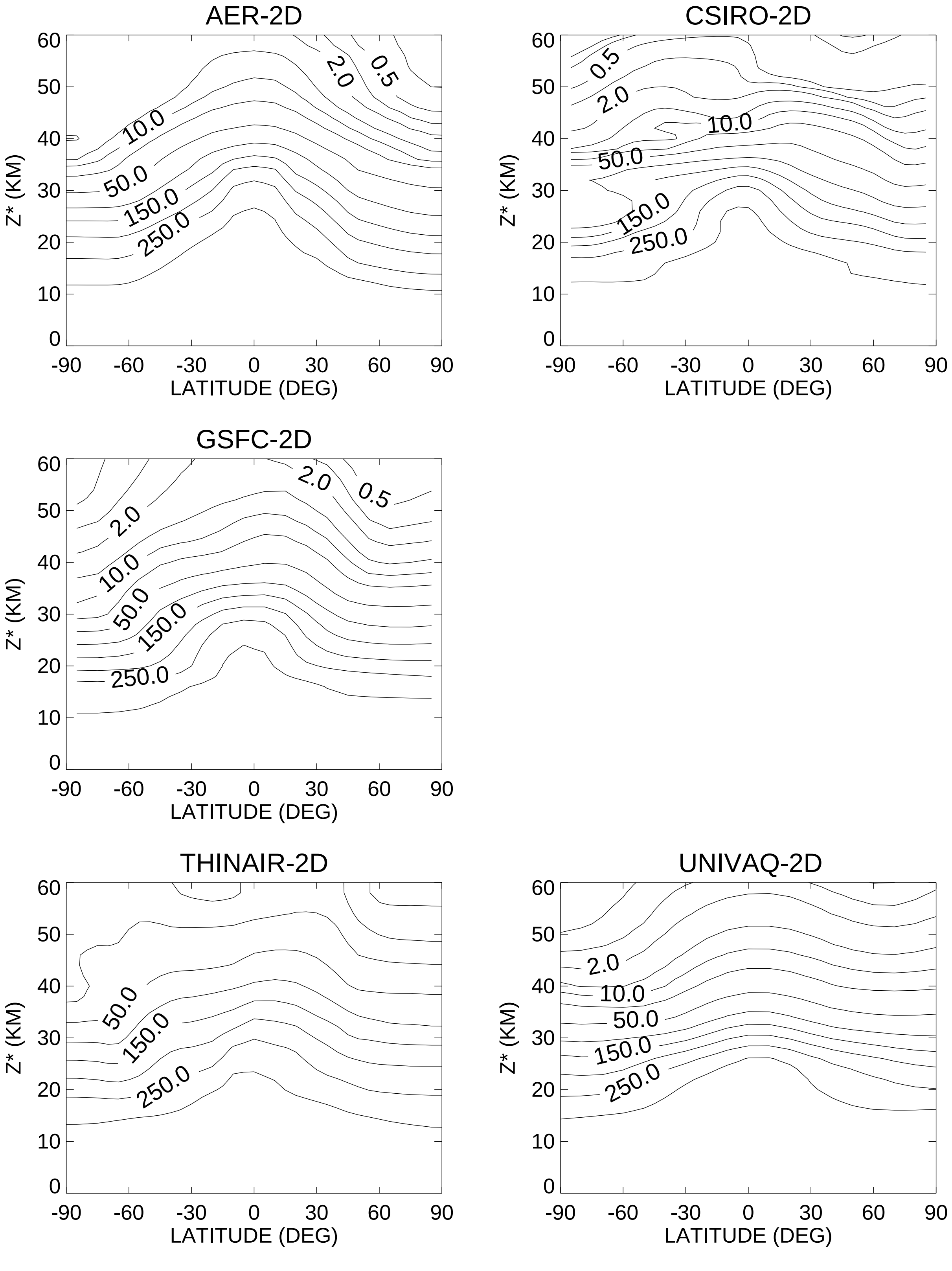

Figure 3.10: Calculated N_2O mixing ratios (ppbv) as a function of latitude and altitude for Scenario D in June of 2015. Contours are 0.1, 0.2, 0.5, 1, 2, 5, 10, 20, 50, 100, 150, 200, 250, 300 ppbv.

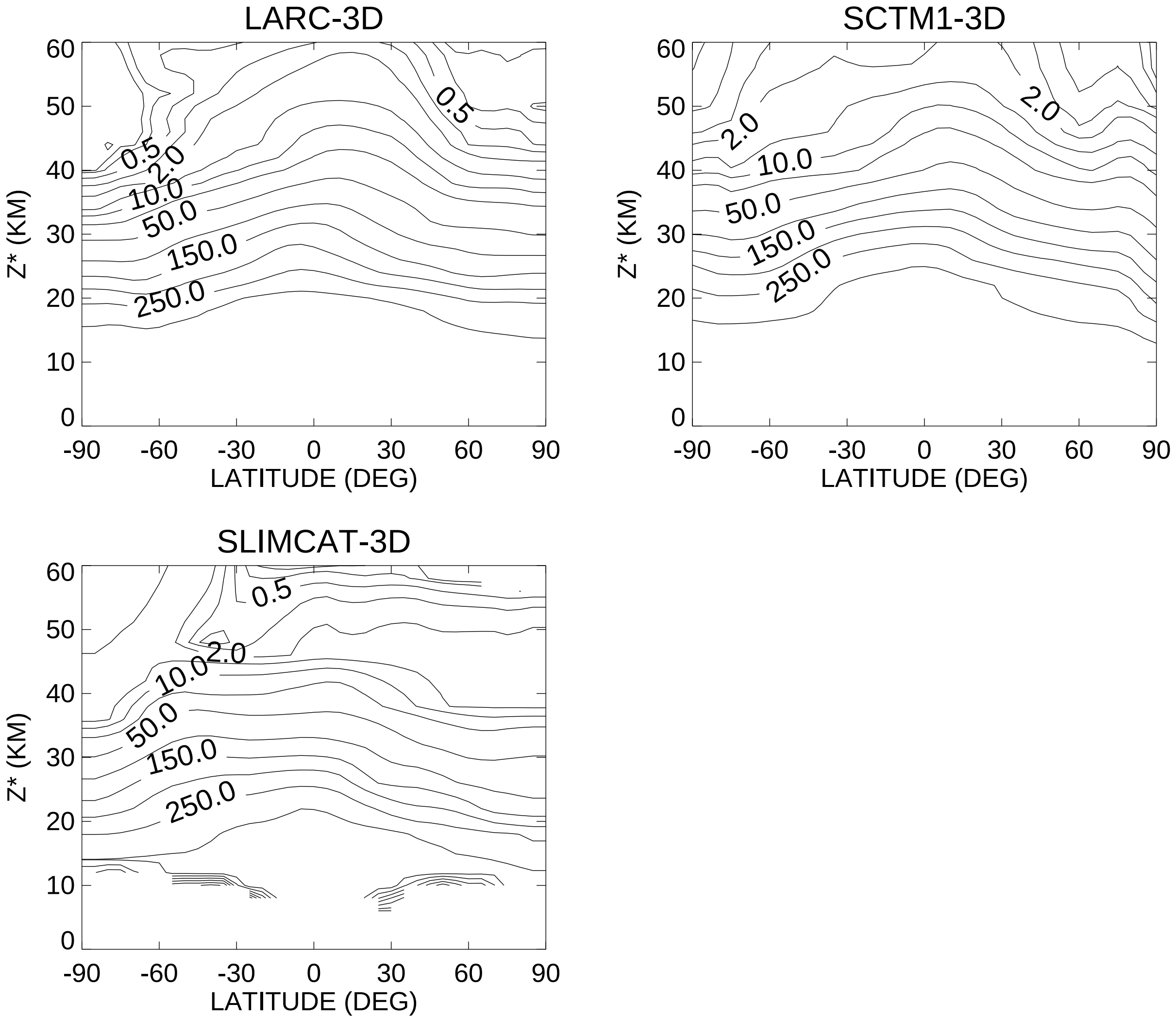

Figure 3.10: continued

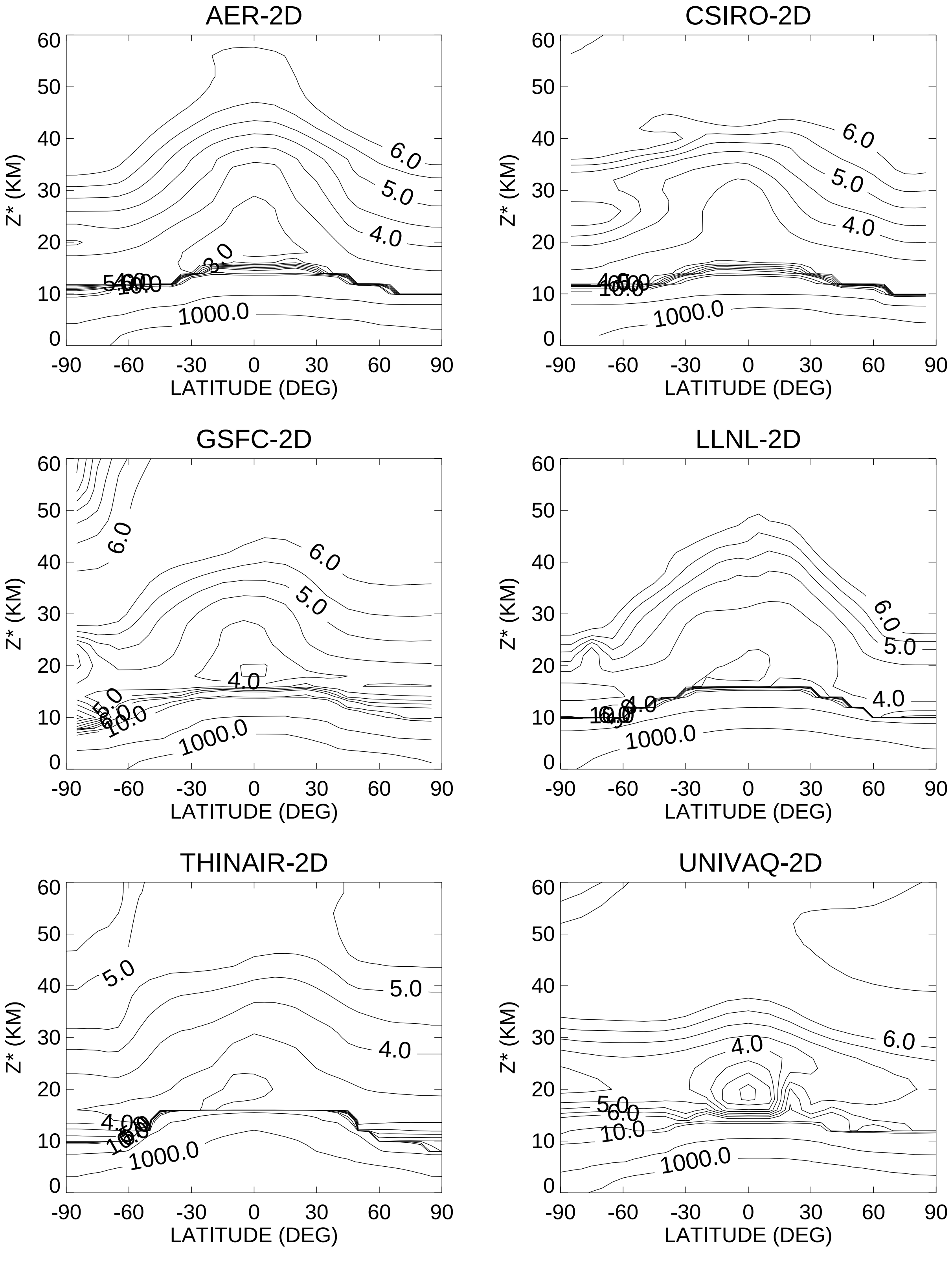

Figure 3.11: Calculated H_2O mixing ratios (ppmv) as a function of latitude and altitude for Scenario D in June of 2015. Contours are 2.5 to 6.5 by 0.5 ppmv and 10, 100, 1000 ppmv.

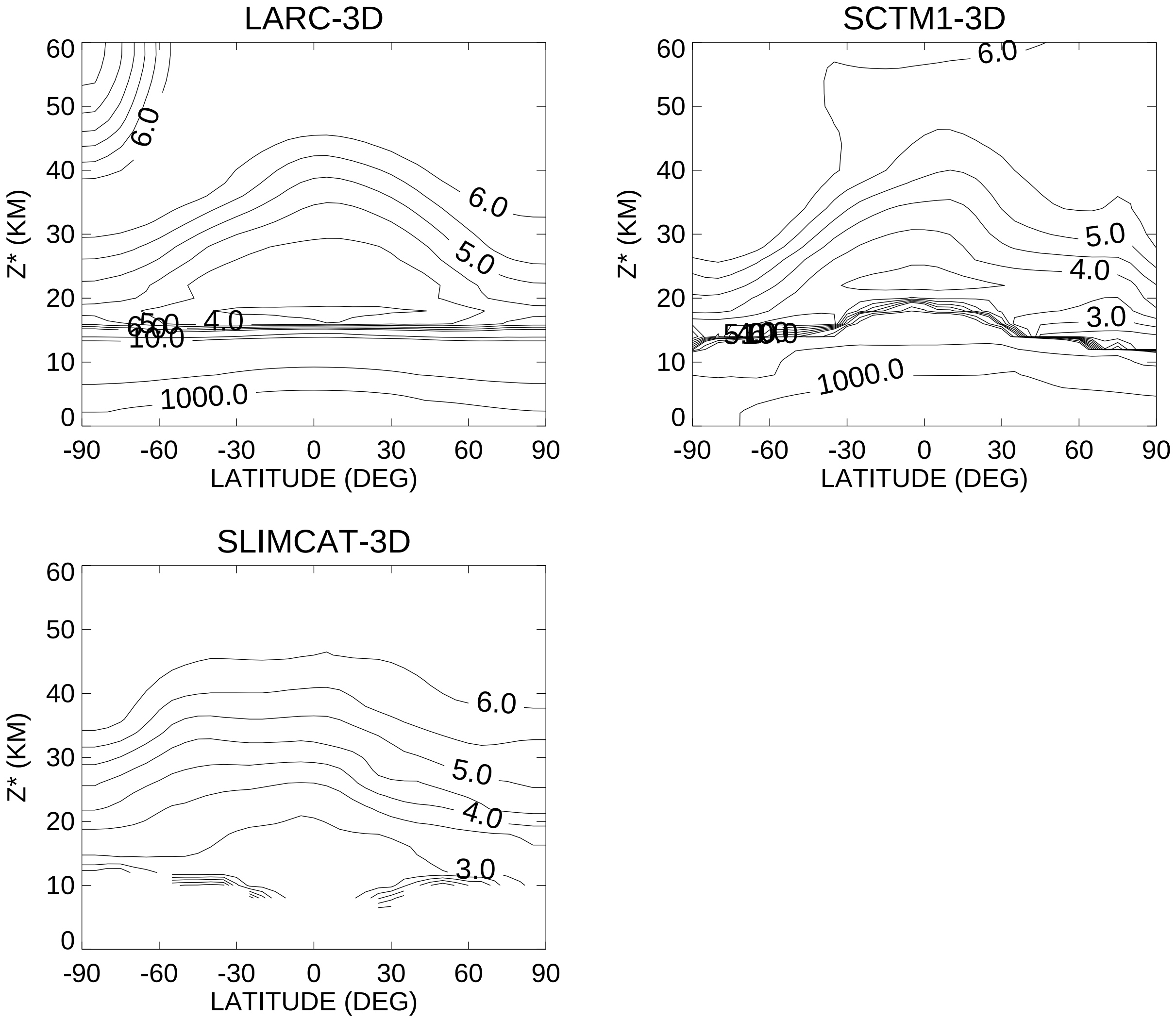

Figure 3.11: continued

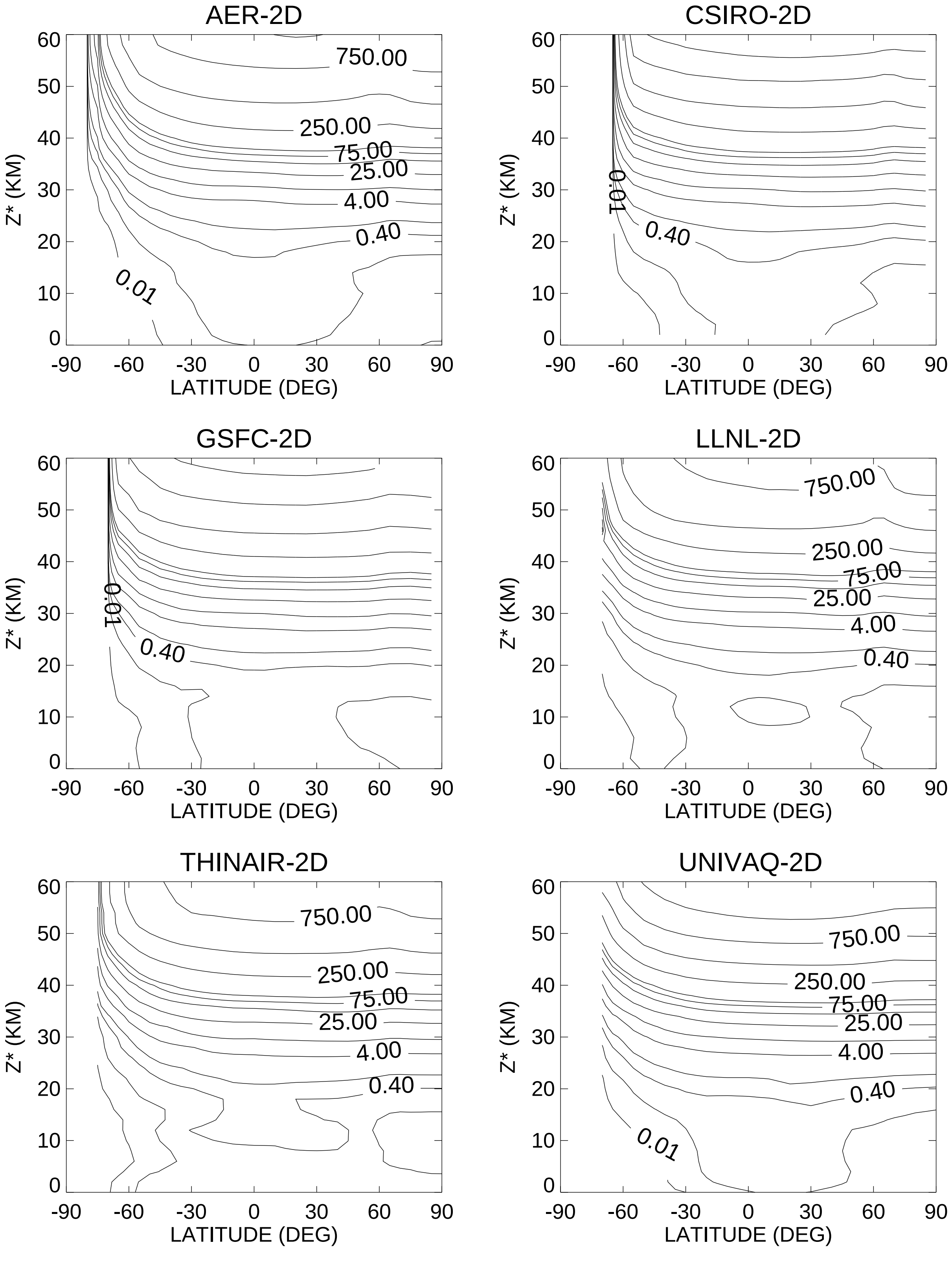

Figure 3.12: Calculated OH mixing ratios (pptv) as a function of latitude and altitude for Scenario D in June of 2015. Daytime averages are shown for 2-D models, 24-hour averages for 3-D models. Contours are .01, .1, .4, 1, 4, 10, 25, 50, 75, 100, 250, 500, 750 pptv.

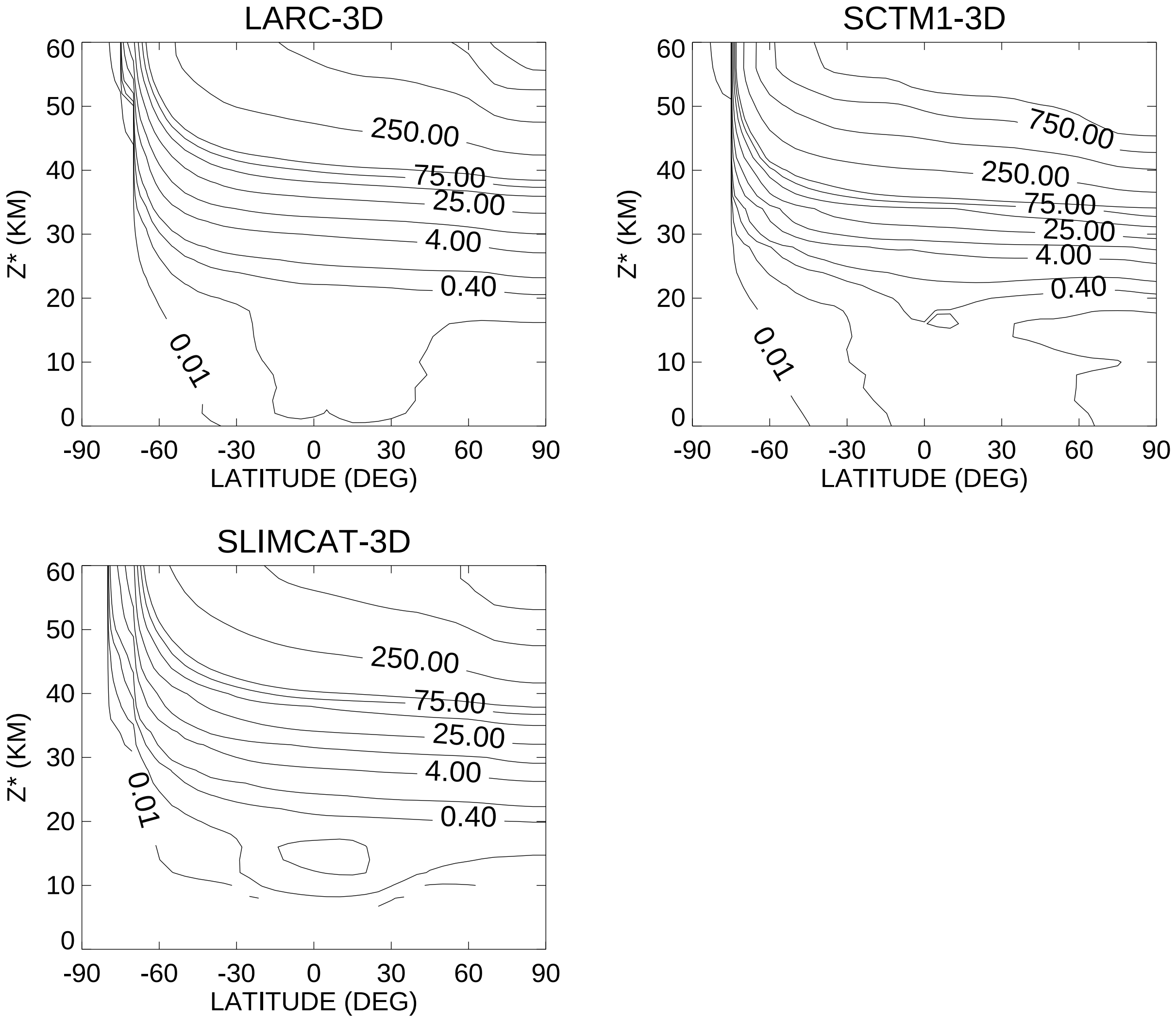

Figure 3.12: continued

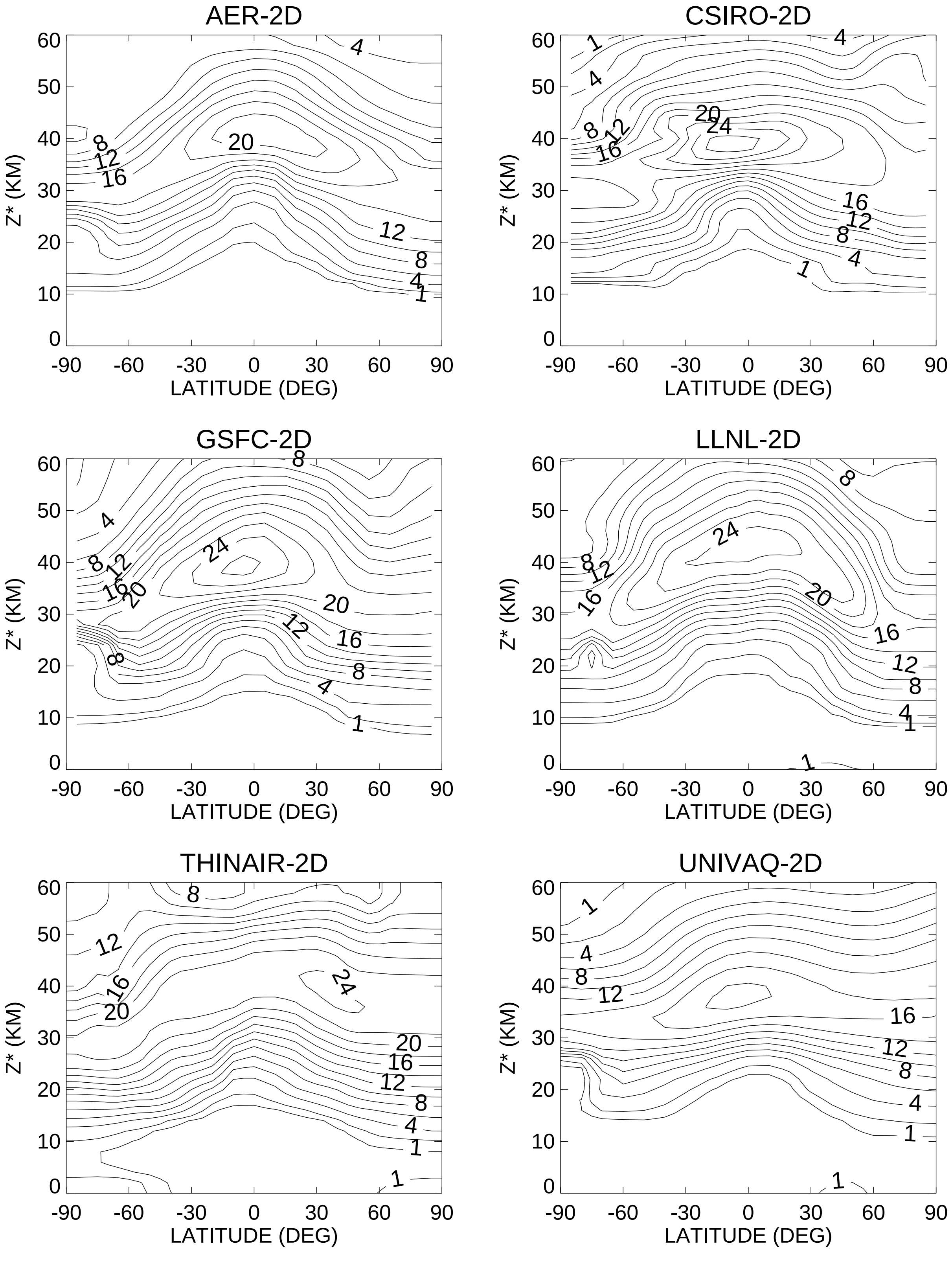

Figure 3.13: Calculated NO_y mixing ratios (ppbv) as a function of latitude and altitude for Scenario D in June of 2015. Contours are 1 ppbv and from 2 to 26 ppbv by 2 ppbv.

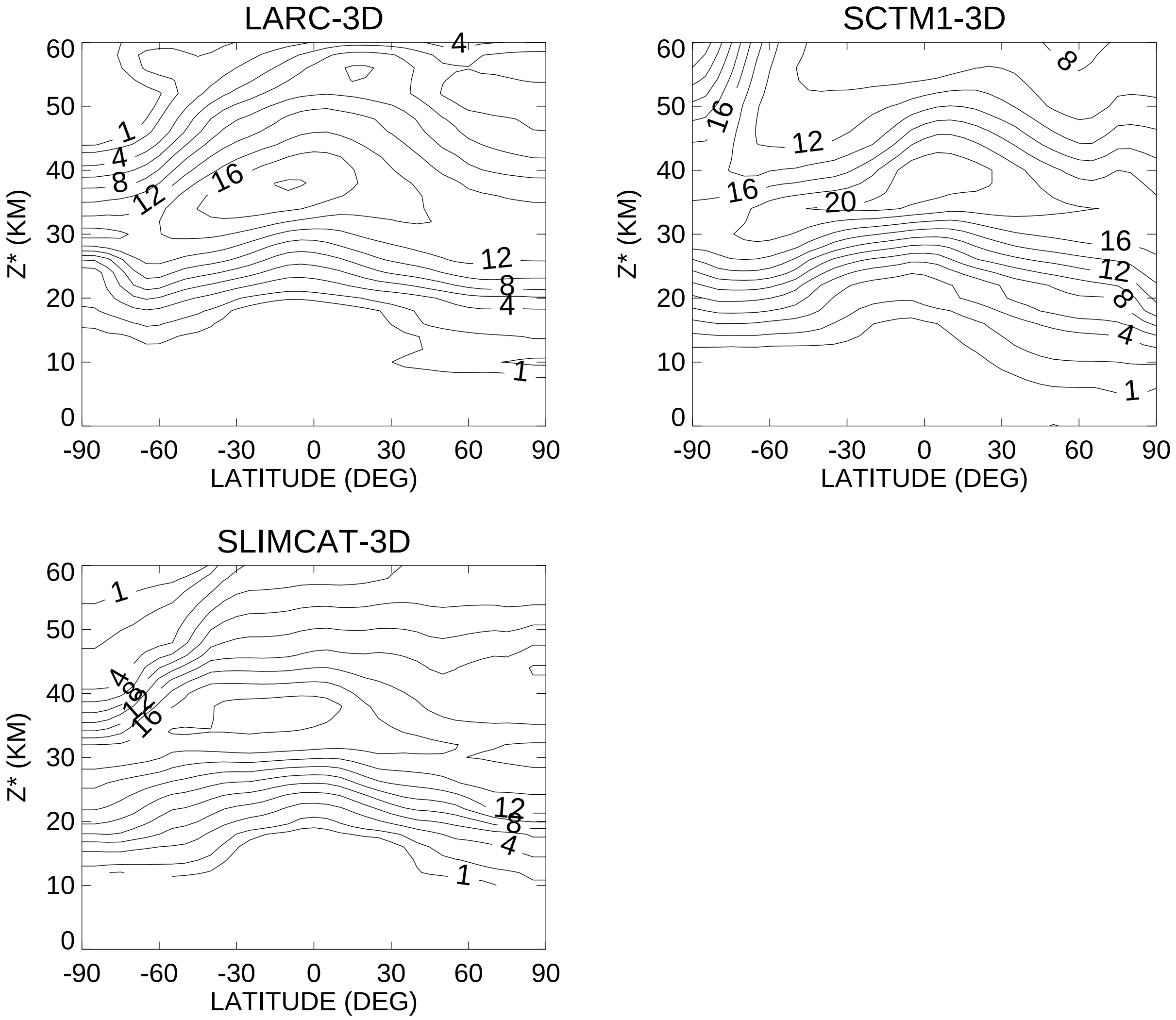

Figure 3.13: continued

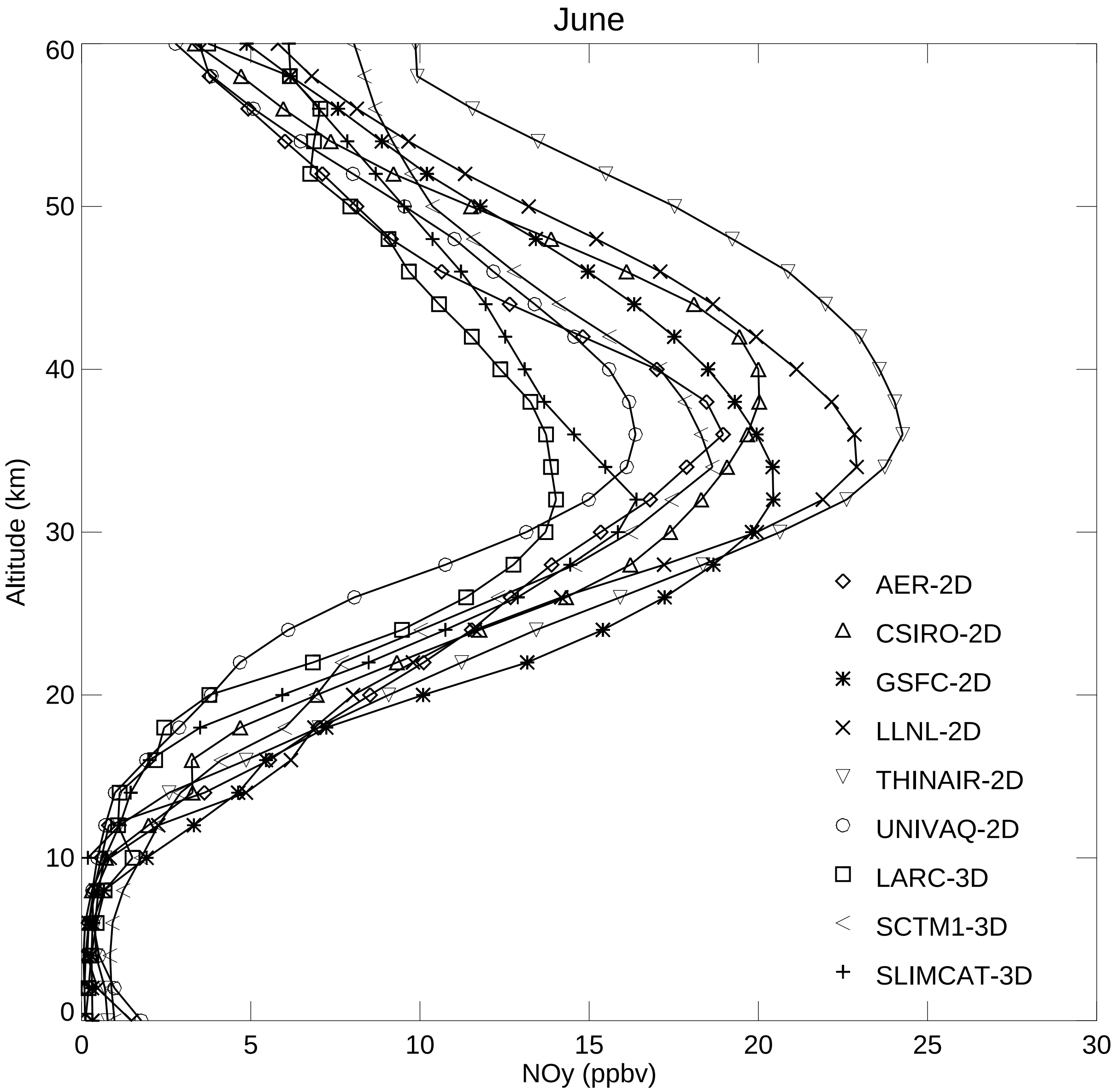

Figure 3.14: Calculated NO_y concentration (ppbv) as a function of altitude for Scenario D at 45^{o}N in June.

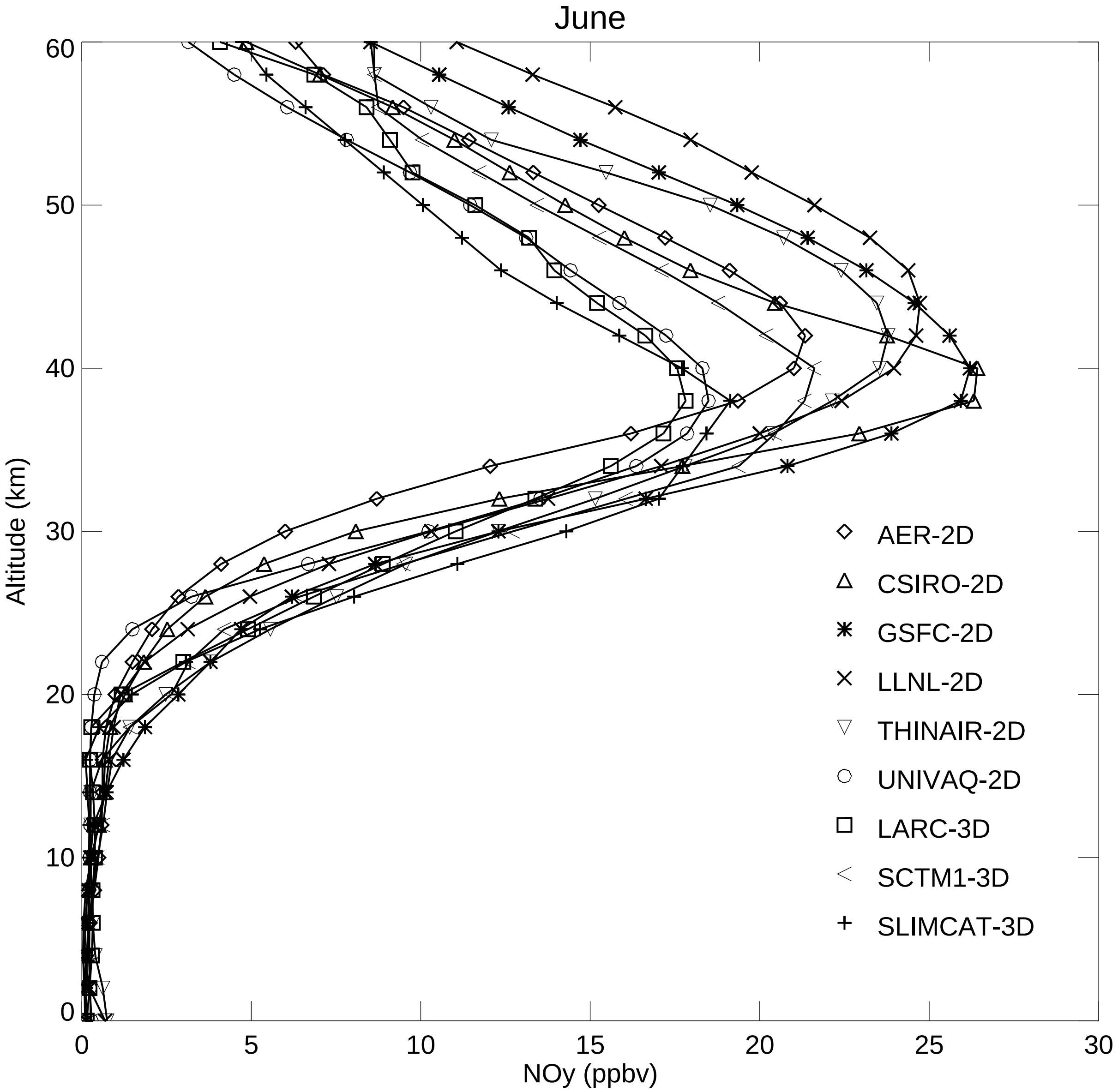

Figure 3.15: Calculated NO_y concentration (ppbv) as a function of altitude for Scenario D at the equator in June.

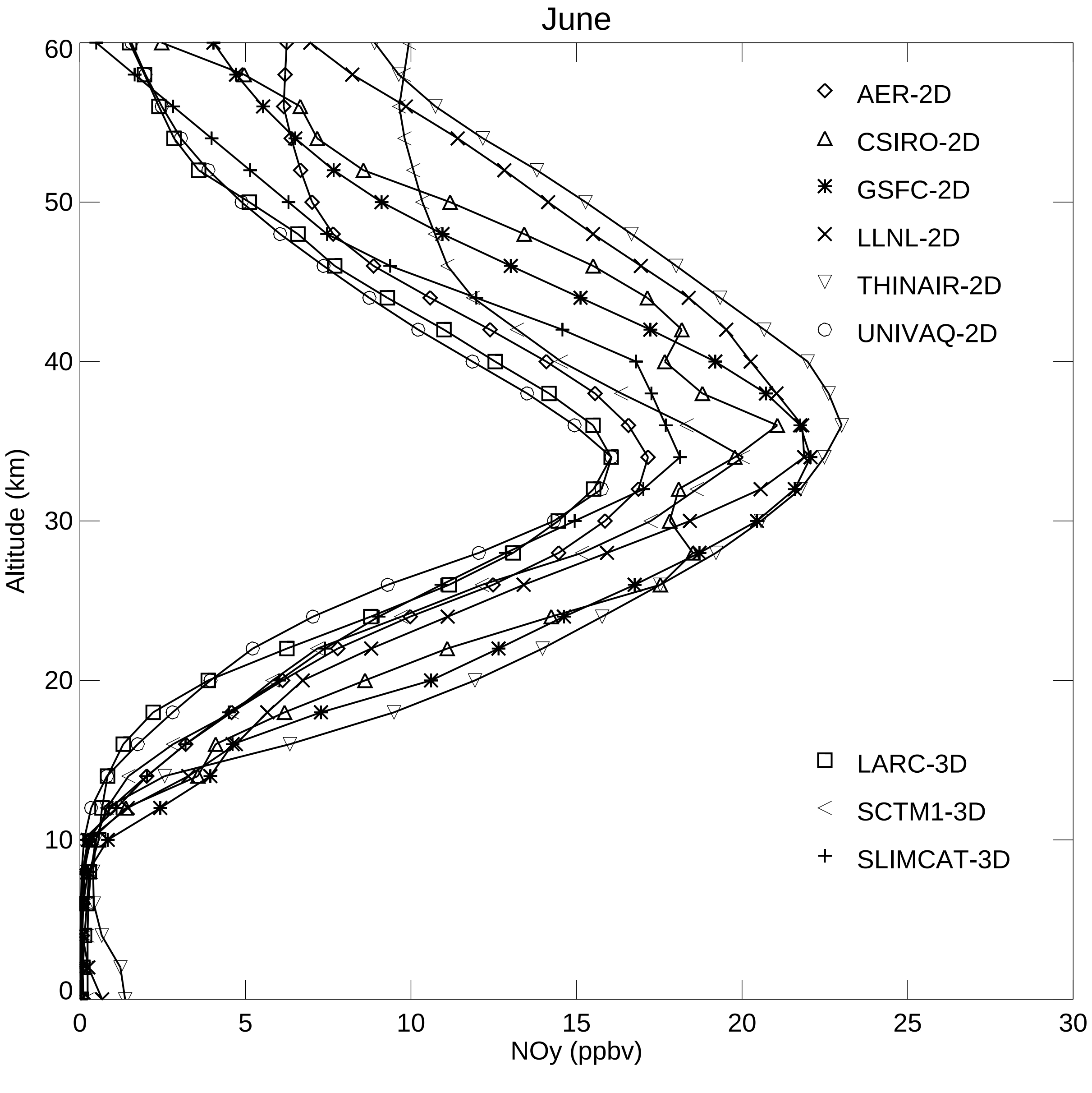

Figure 3.16: Calculated NO_y concentration (ppbv) as a function of altitude for Scenario D at 45^{o}S in June.

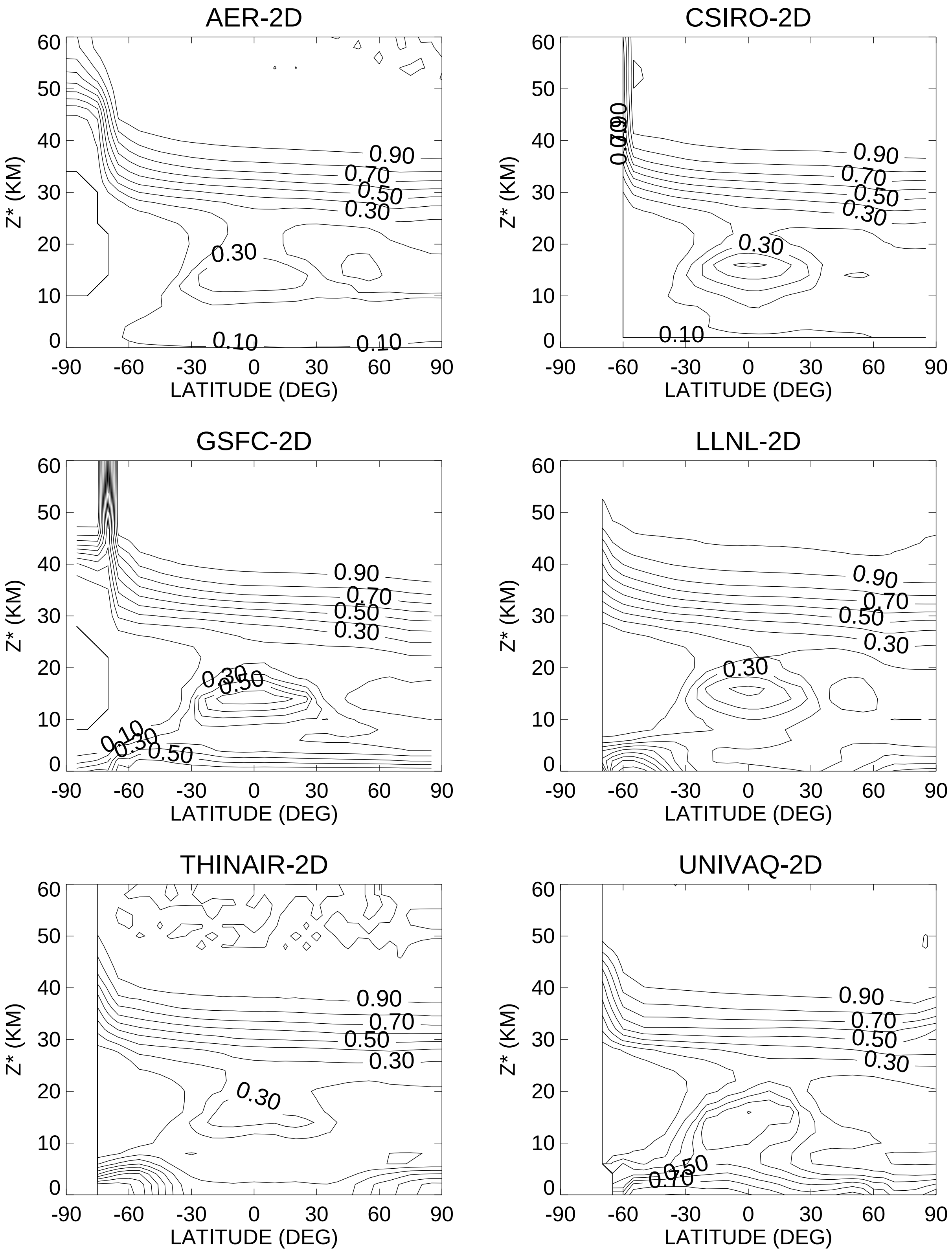

Figure 3.17: Calculated NO_x(=NO+NO_2)/NO_y ratio as a function of latitude and altitude for Scenario D in June of 2015. Contour interval is 0.1.

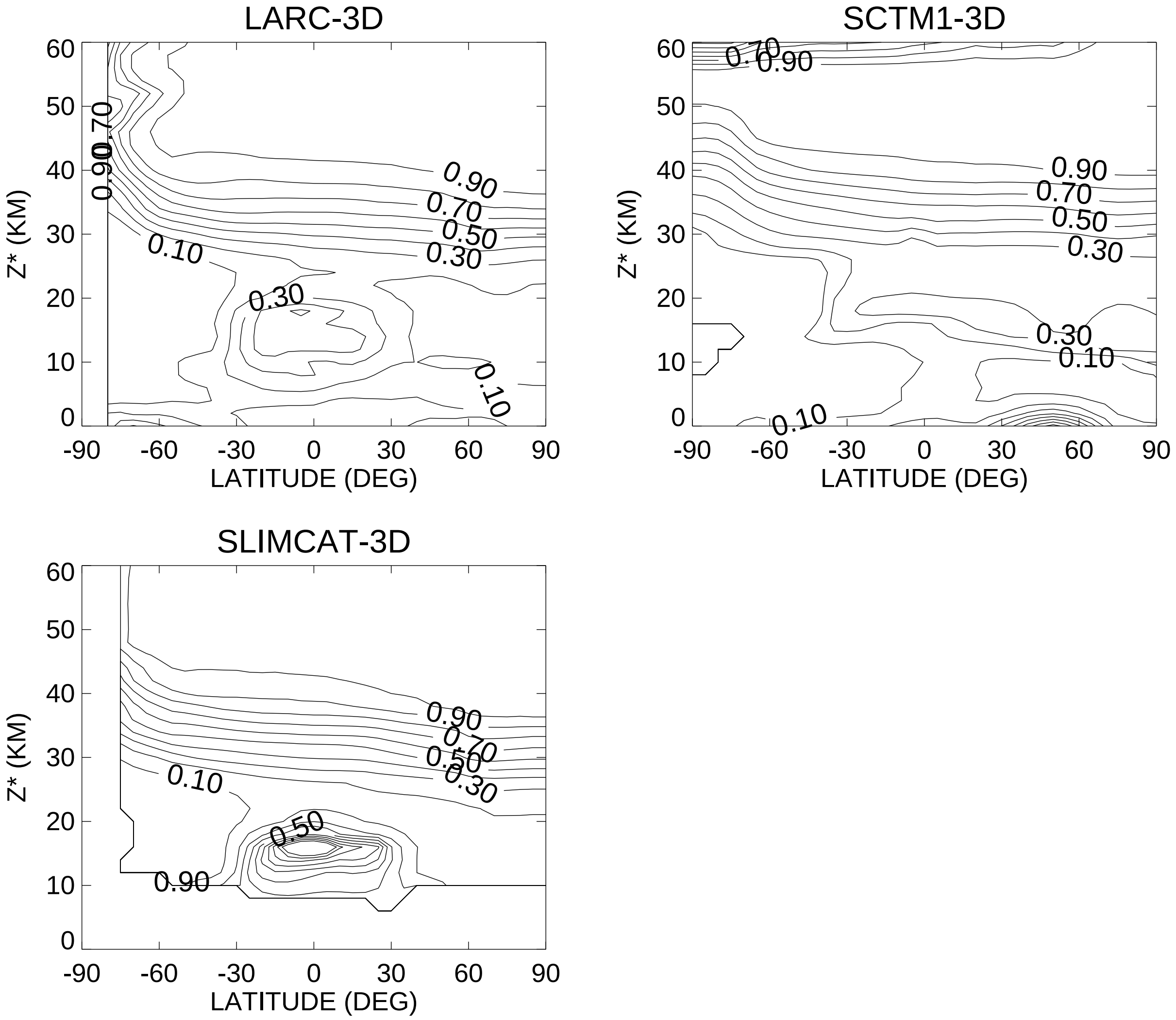

Figure 3.17: continued

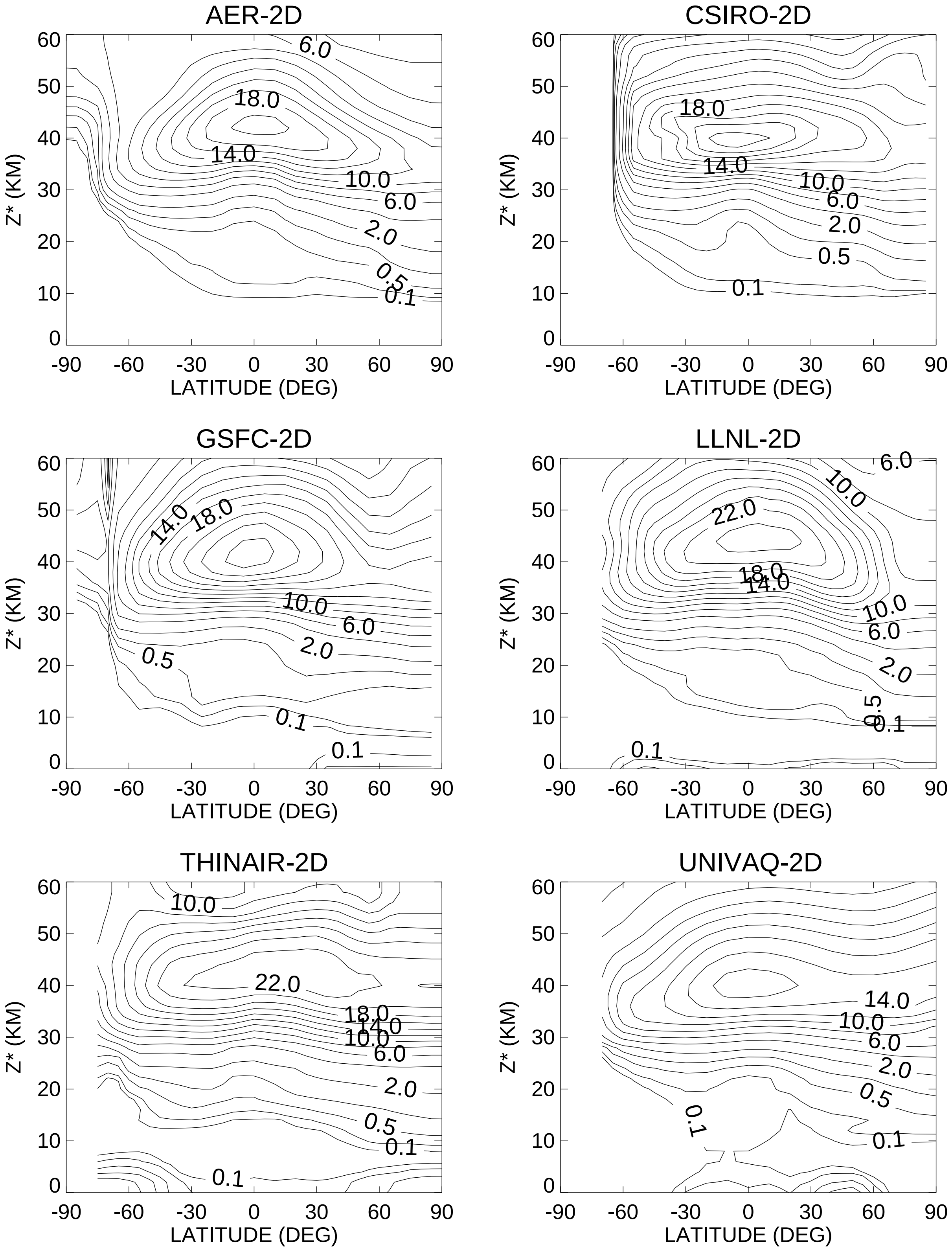

Figure 3.18: Calculated NO_x (=NO+NO_2) mixing ratios (ppbv) as a function of latitude and altitude for Scenario D in June of 2015. Daytime averages are shown for 2-D models, 24-hour averages for 3-D models. Contours are 0.1, 0.2, 0.5, 1, and 2 to 24 by 2 ppbv.

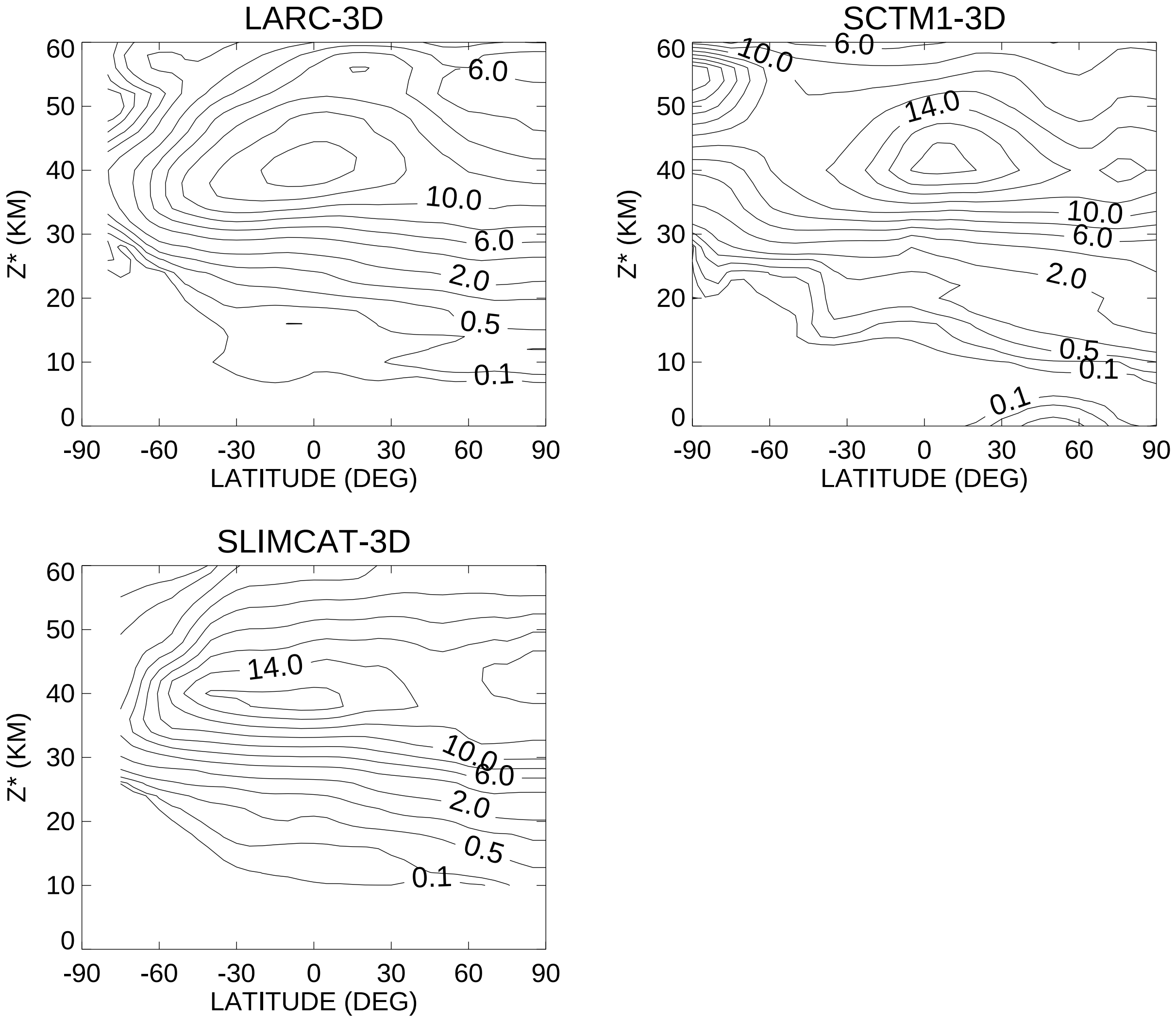

Figure 3.18: continued

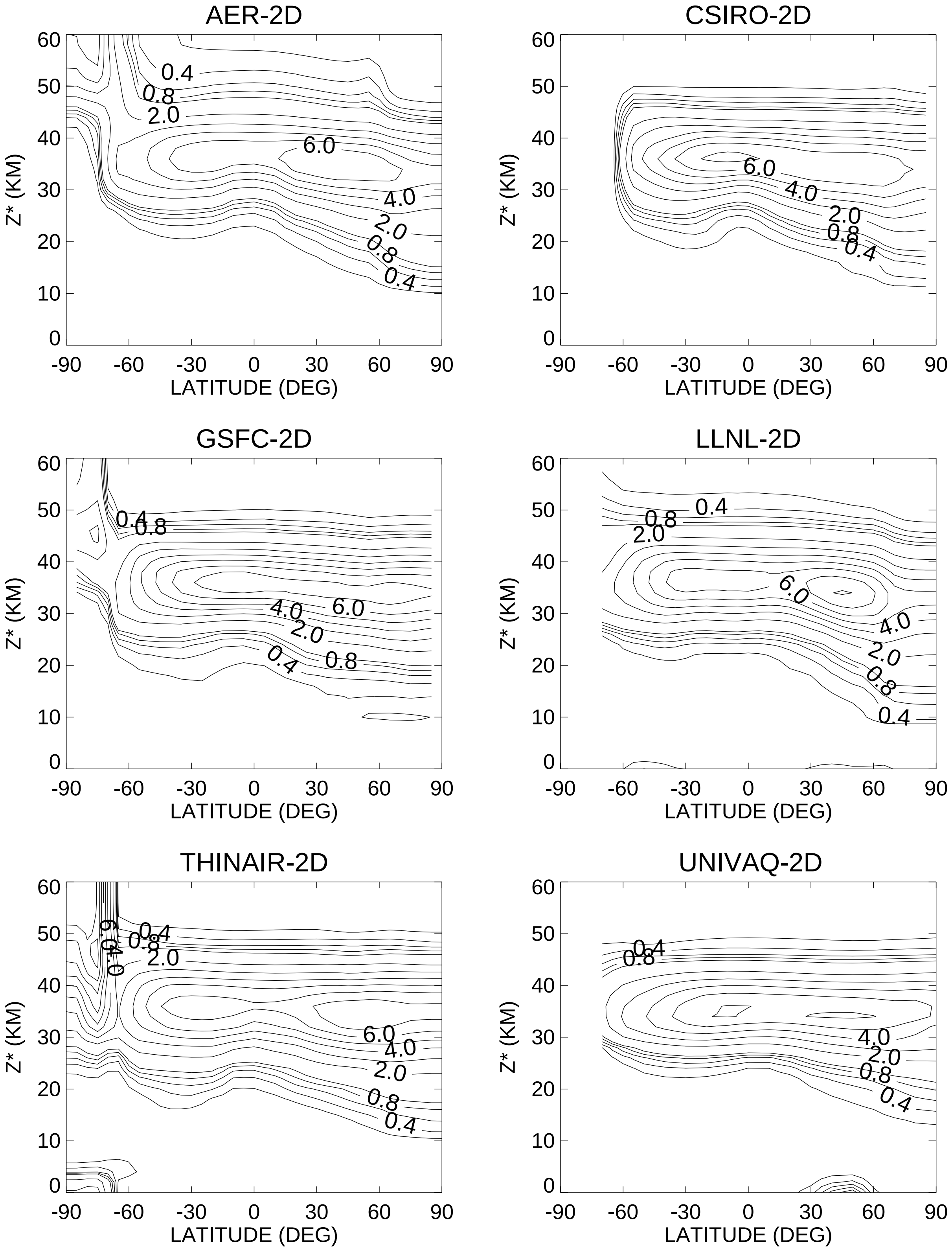

Figure 3.19: Calculated NO_2 mixing ratios (ppbv) as a function of latitude and altitude for Scenario D in June of 2015. Daytime averages are shown for 2-D models, 24-hour averages for 3-D models. Contours are .2, .4, .6, .8, and 1 to 10 by 1 ppbv.

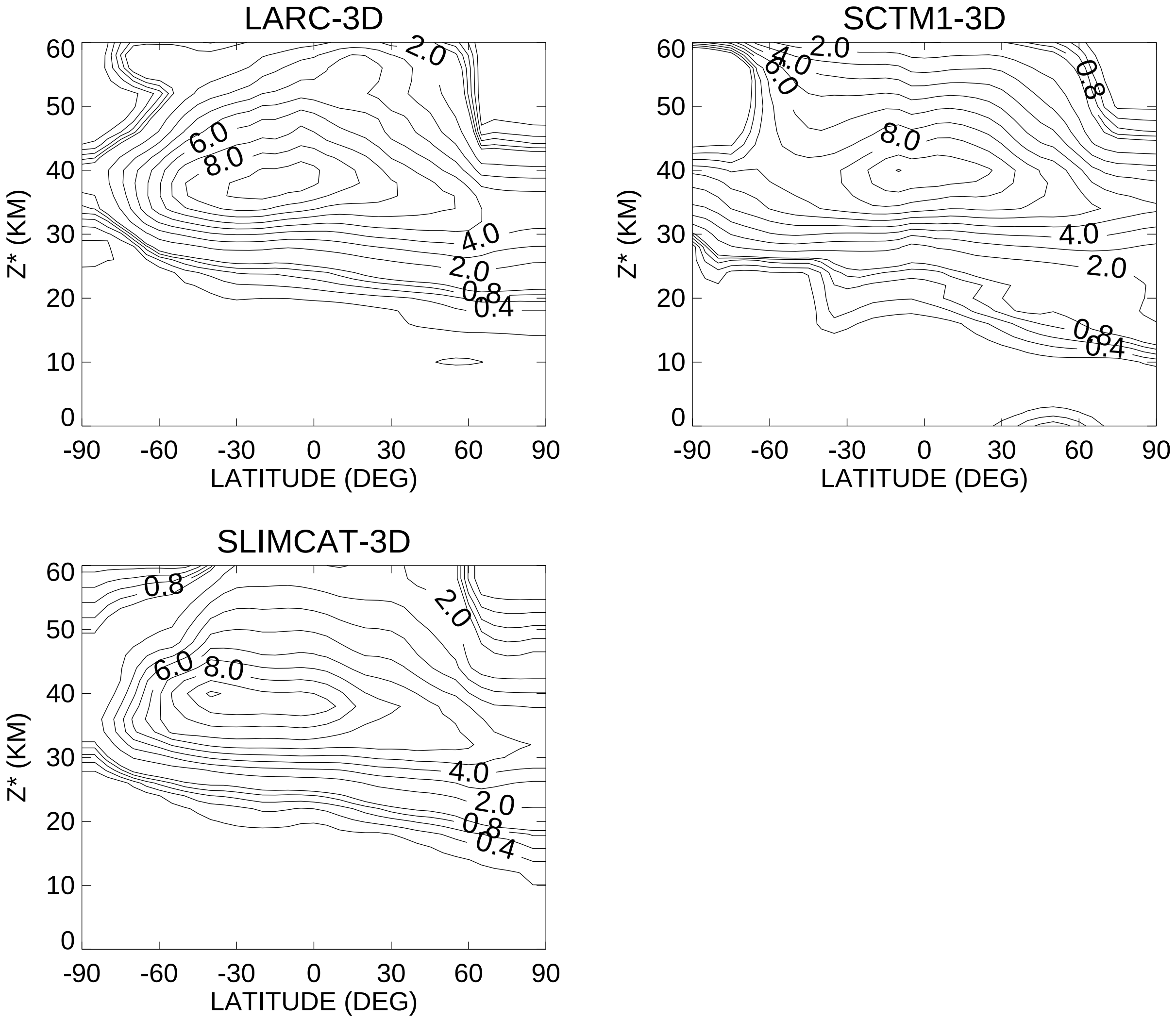

Figure 3.19: continued

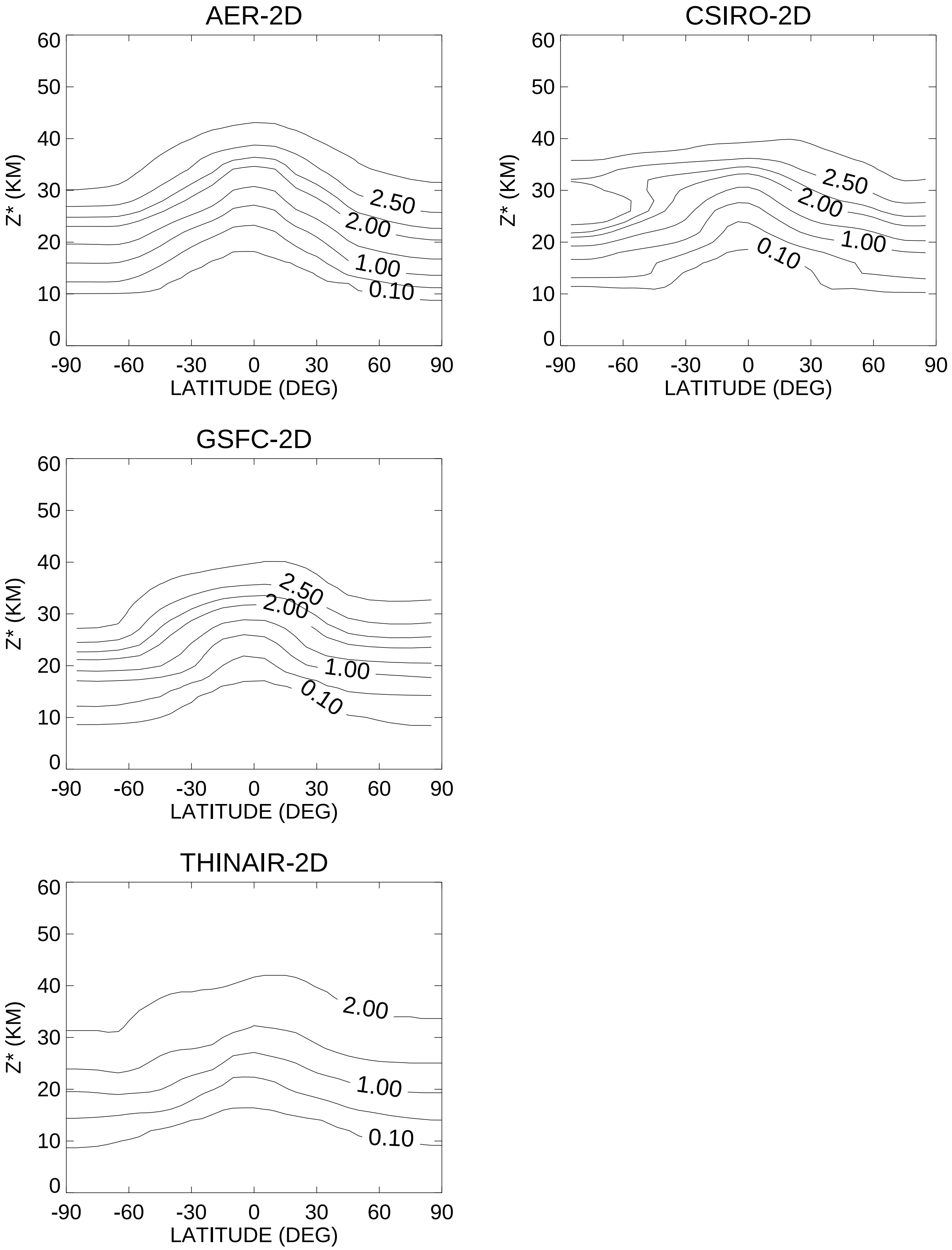

Figure 3.20: Calculated Cl_y mixing ratios (ppbv) as a function of latitude and altitude for Scenario D in June of 2015. Contours are .1, .5, 1, 1.5, 2, 2.25, 2.5, 2.75 ppbv.

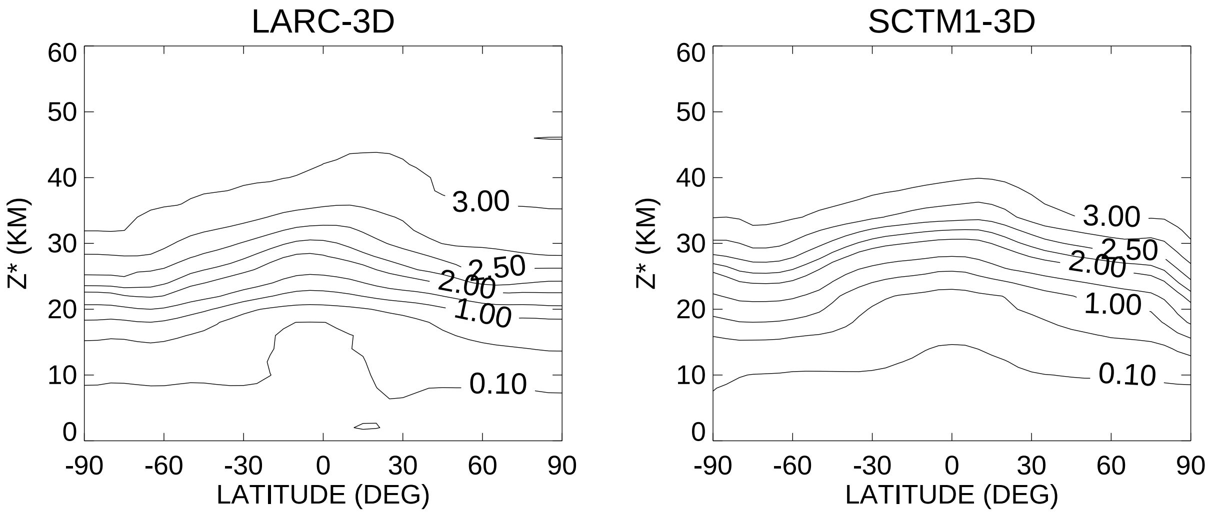

Figure 3.20: continued

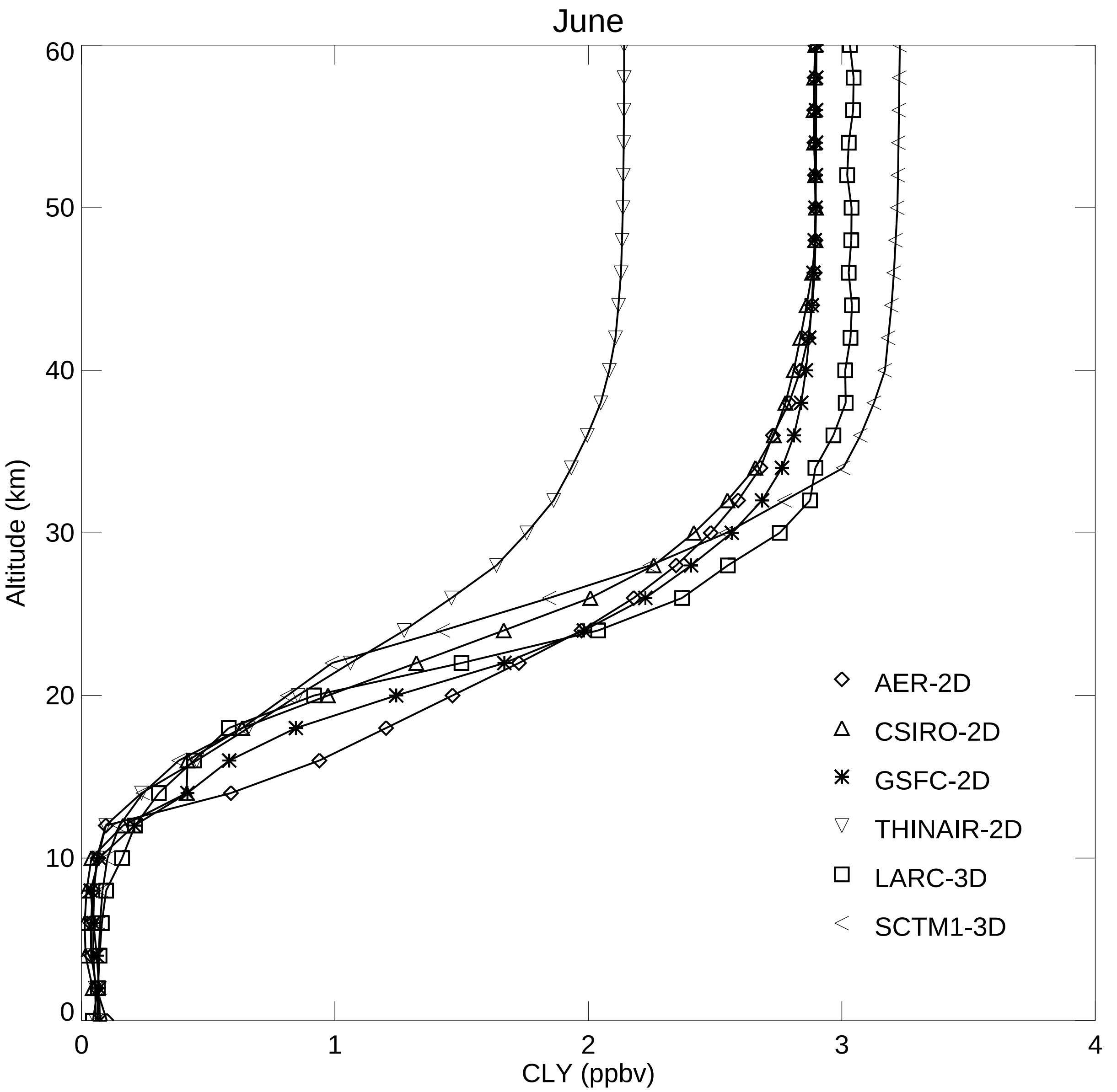

Figure 3.21: Calculated Cl_y concentration (ppbv) as a function of altitude for Scenario D at 45^{o}N in June.

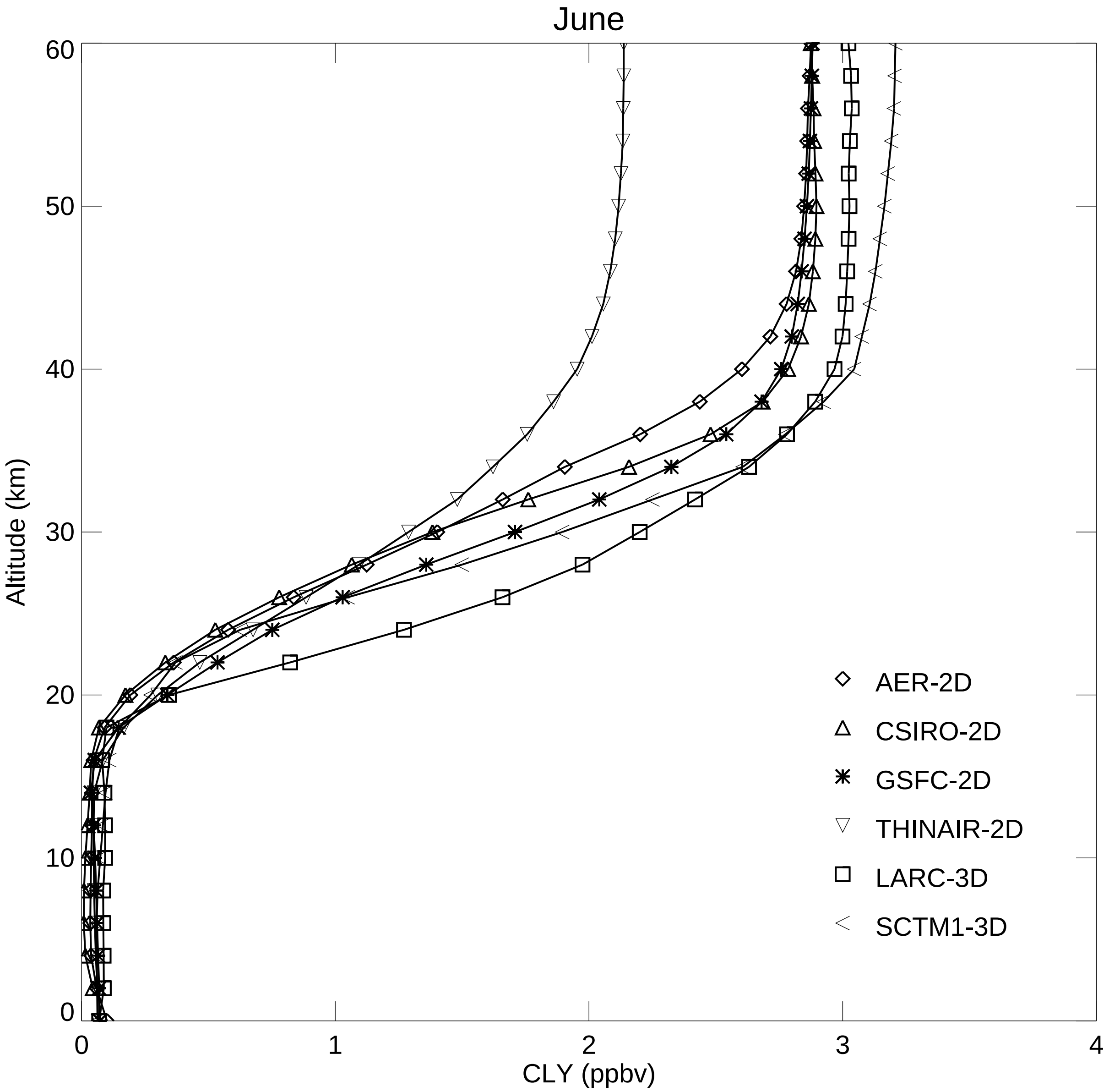

Figure 3.22: Calculated Cl_y concentration (ppbv) as a function of altitude for Scenario D at the equator in June.

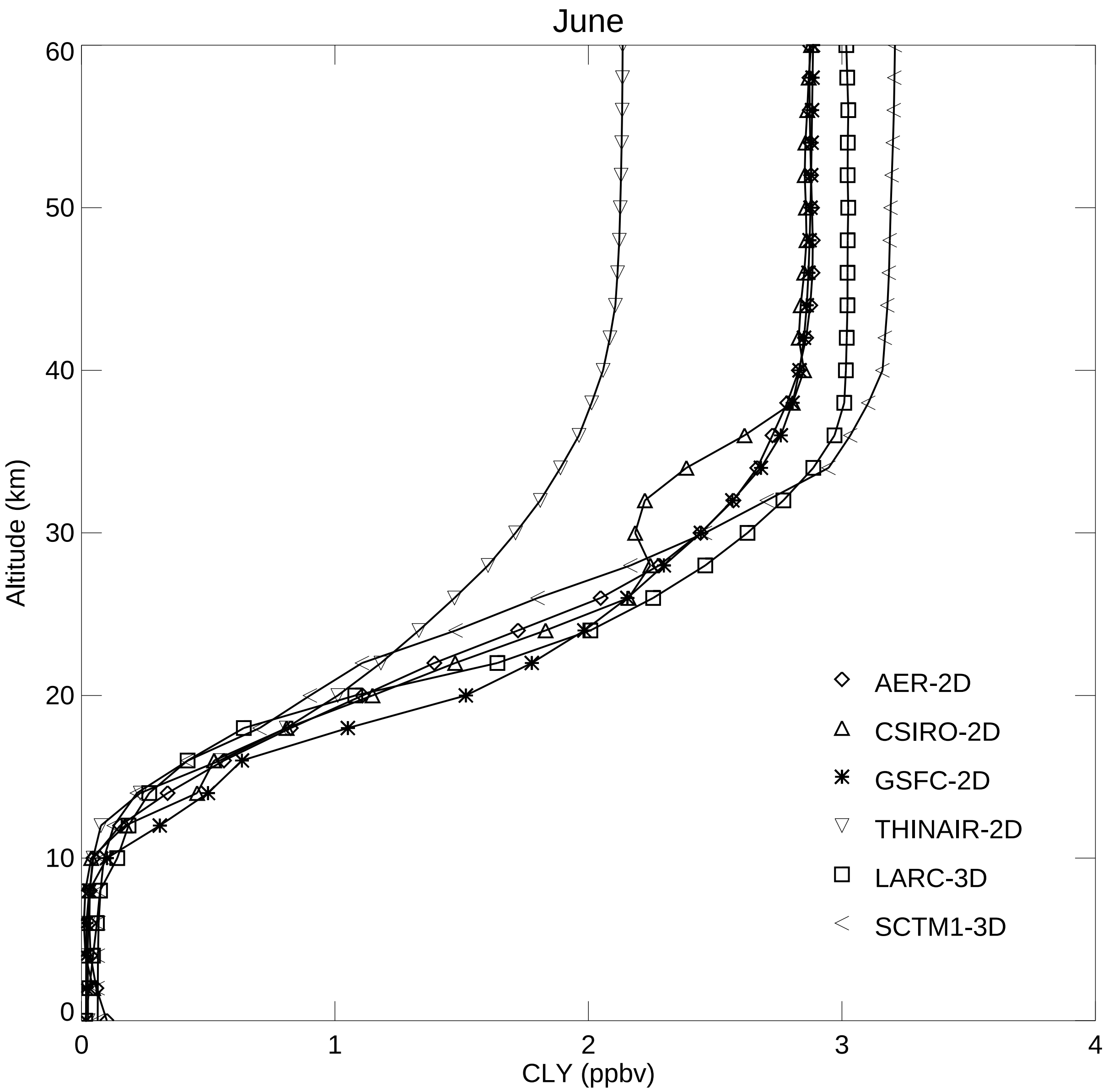

Figure 3.23: Calculated Cl_y concentration (ppbv) as a function of altitude for Scenario D at 45^oS in June.

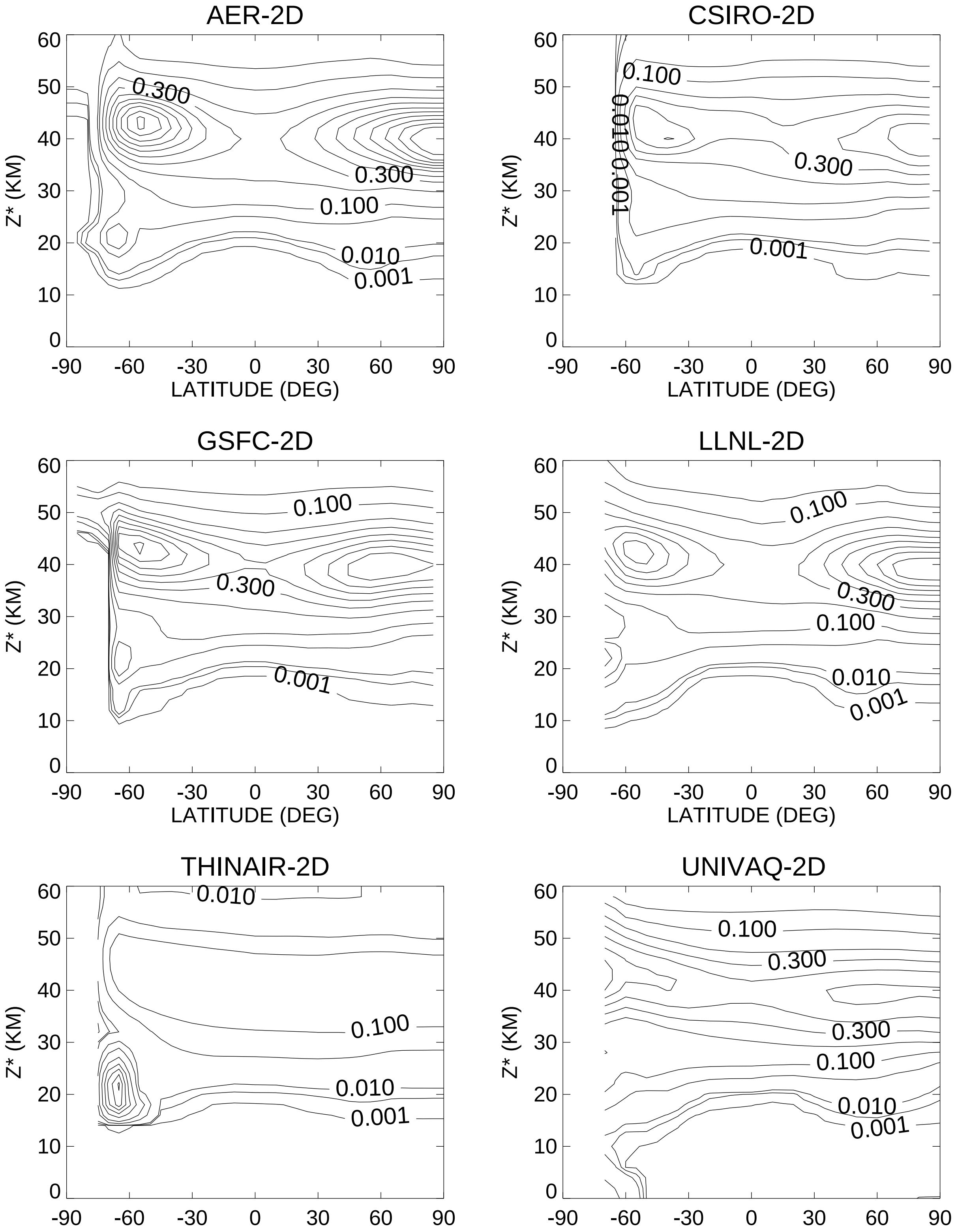

Figure 3.24: Calculated ClO mixing ratios (ppbv) as a function of latitude and altitude for Scenario D in June of 2015. Daytime averages are shown for 2-D models, 24-hour averages for 3-D models. Contours are .001, .005, .01, .05, and .1 to 1.0 by 0.1 ppbv.

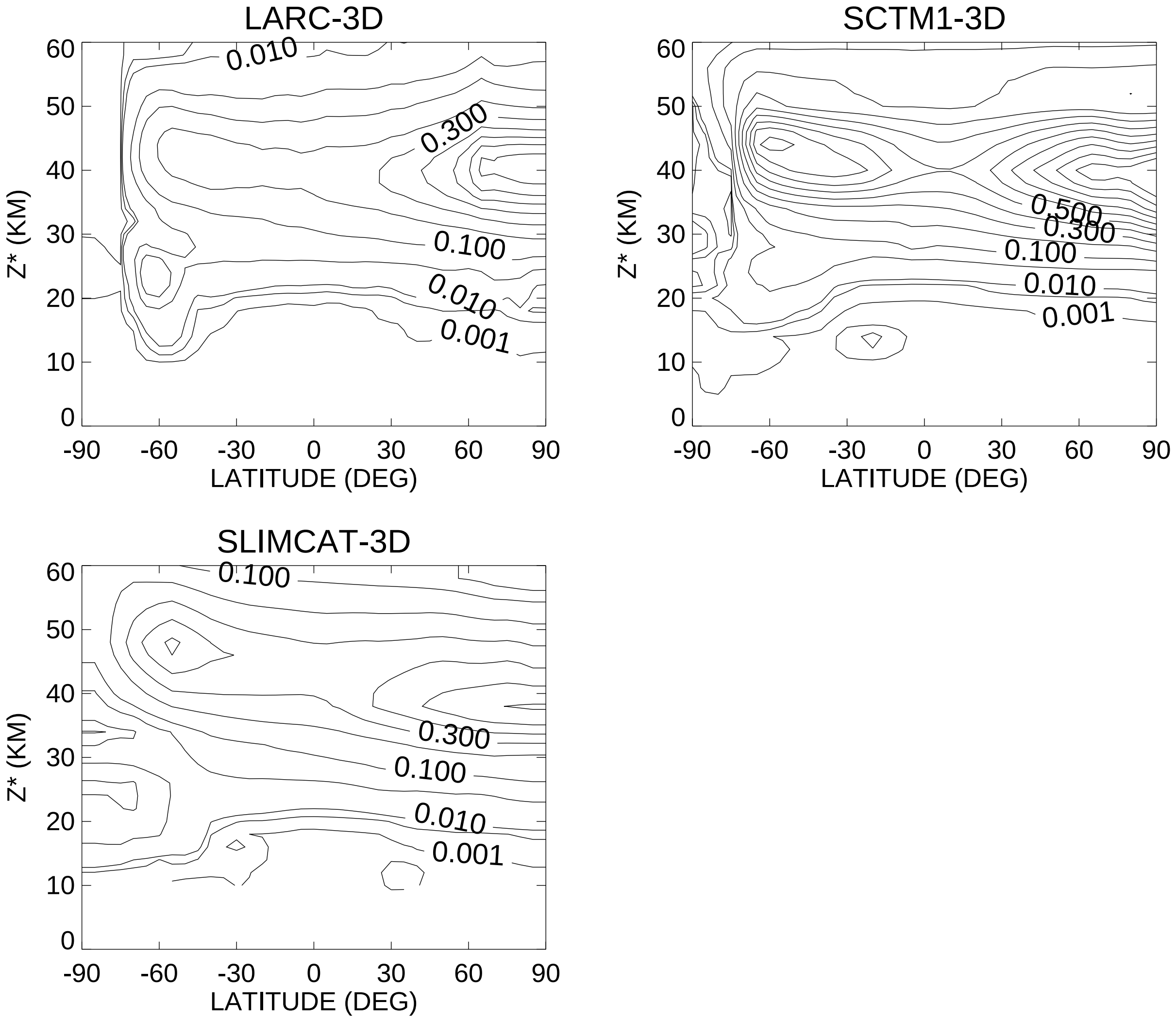

Figure 3.24: continued

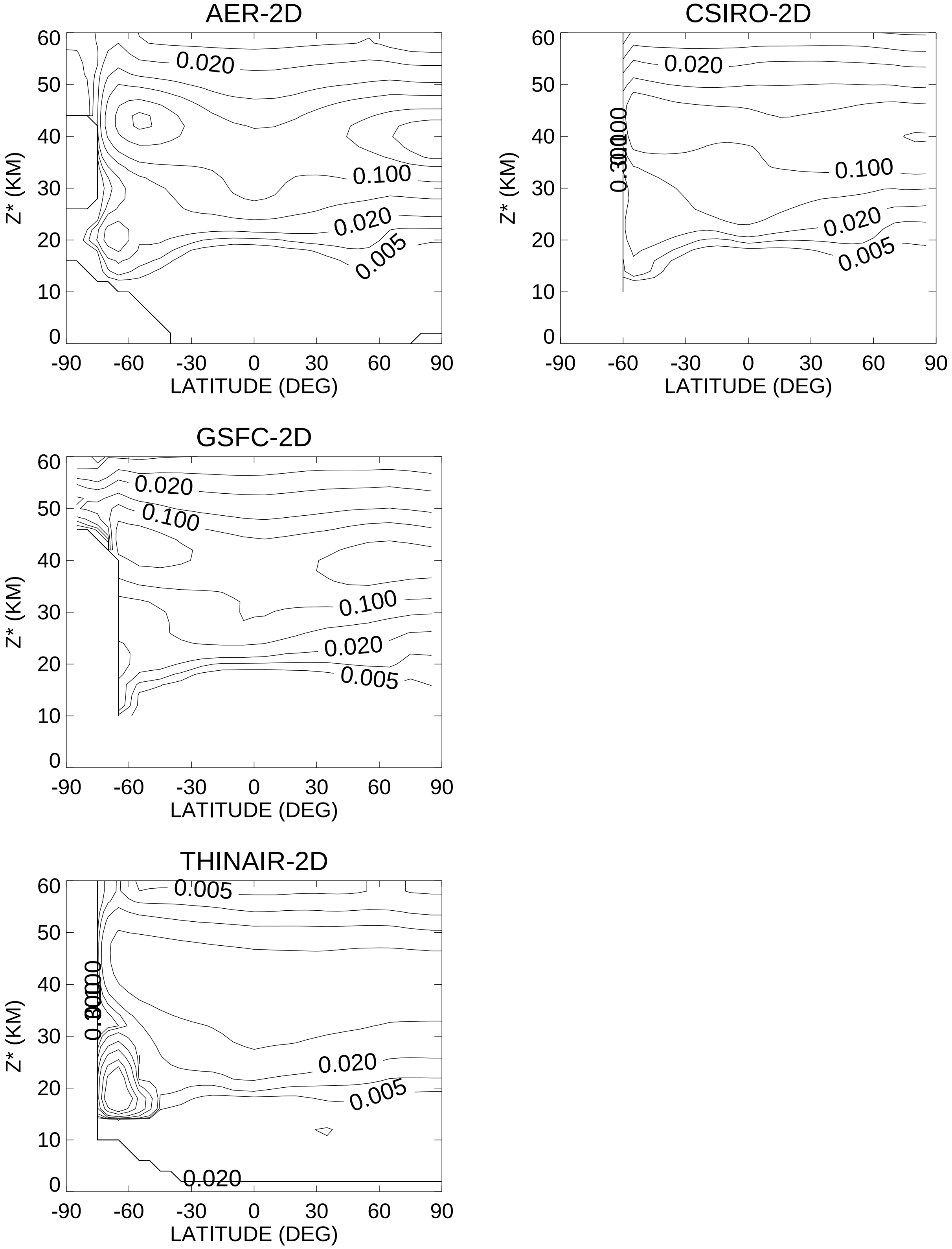

Figure 3.25: Calculated ClO/Cl_y ratio as a function of latitude and altitude for Scenario D in June of 2015. Contours are .005, .01, .02, .05, .1, .15, .2.

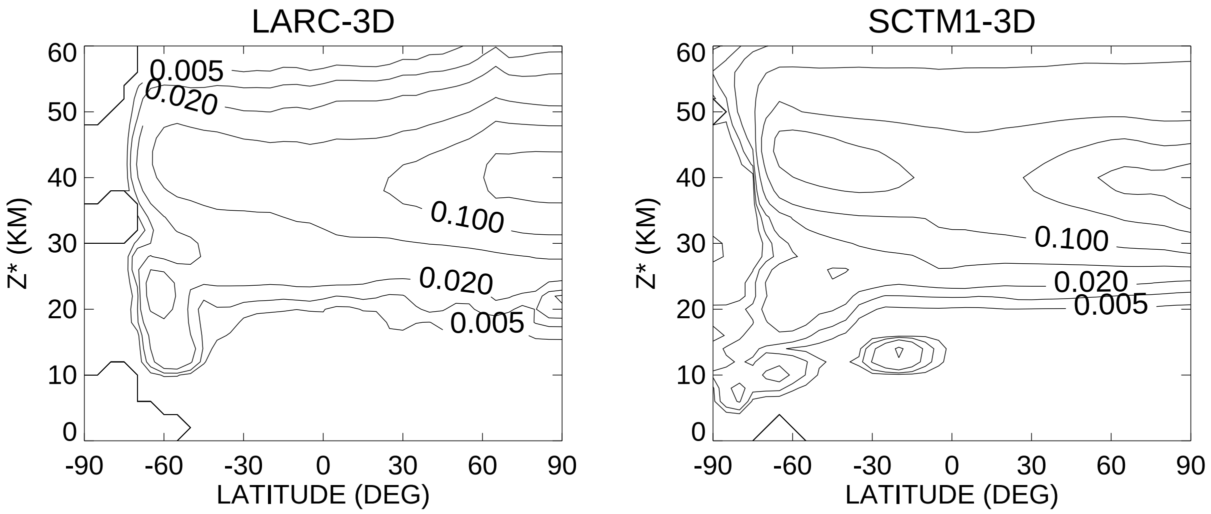

Figure 3.25: continued

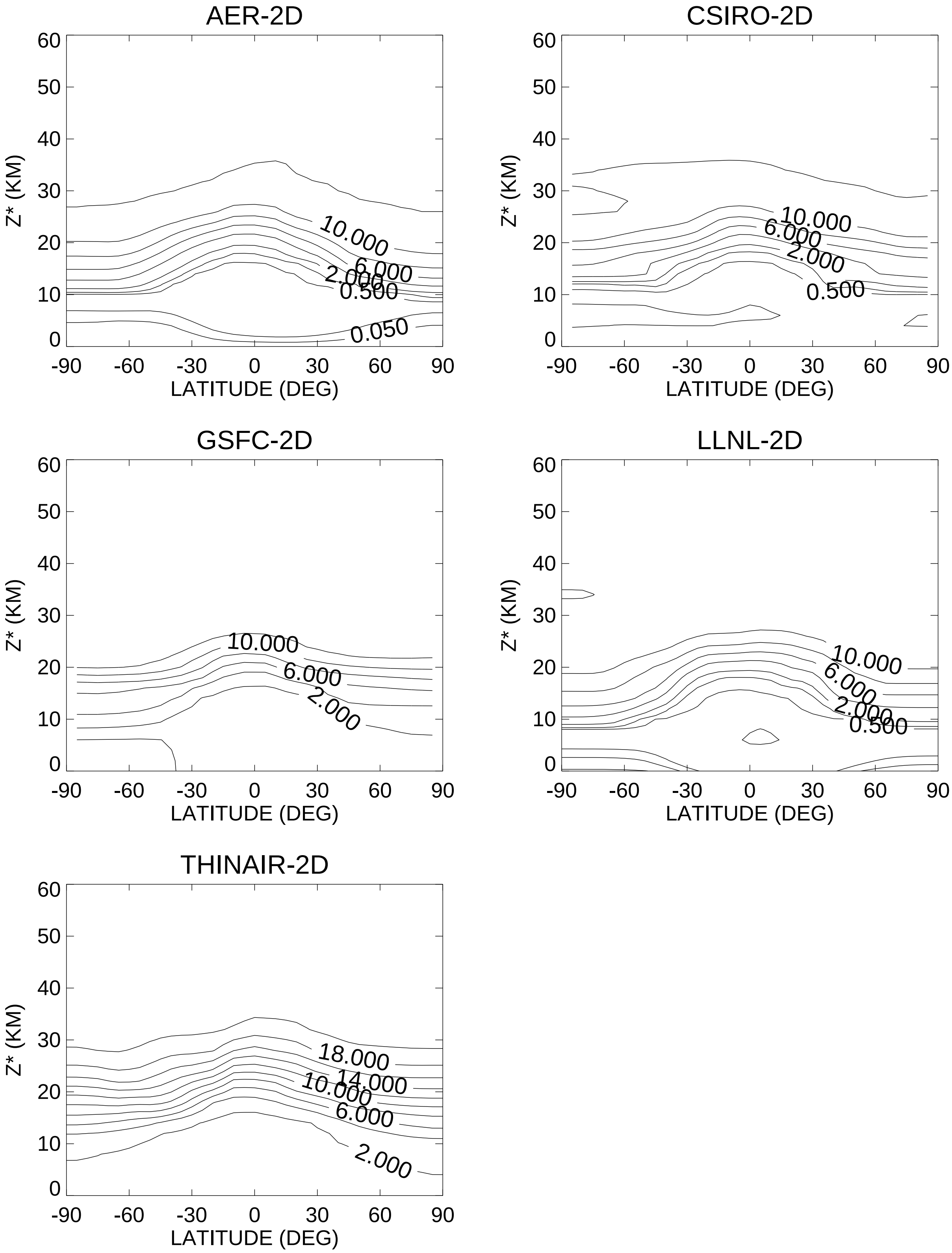

Figure 3.26: Calculated Br_y mixing ratios (pptv) as a function of latitude and altitude for Scenario D in June of 2015. Contours are .05, .01, .5, 1, and 2 to 20 by 2 pptv.

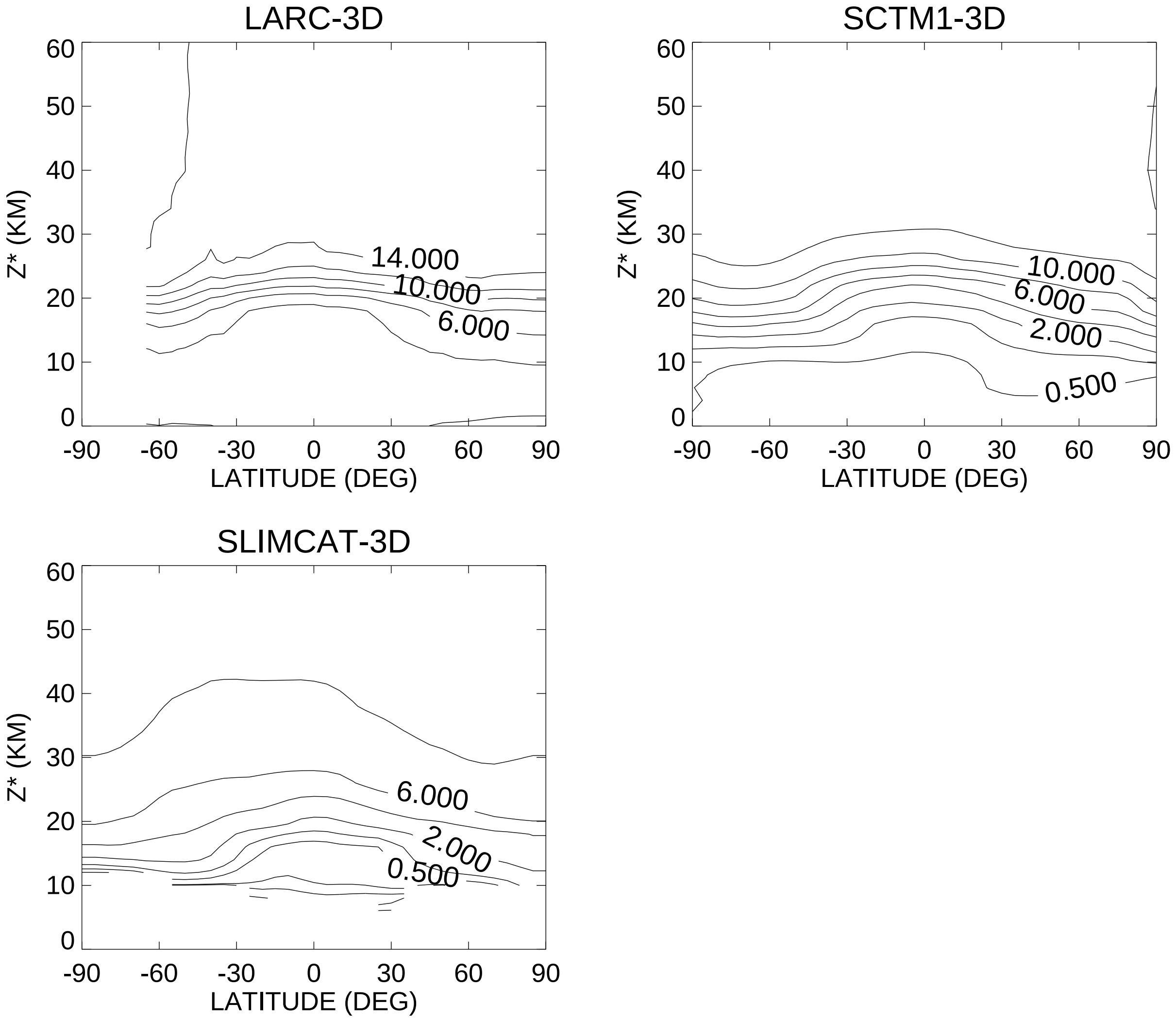

Figure 3.26: continued

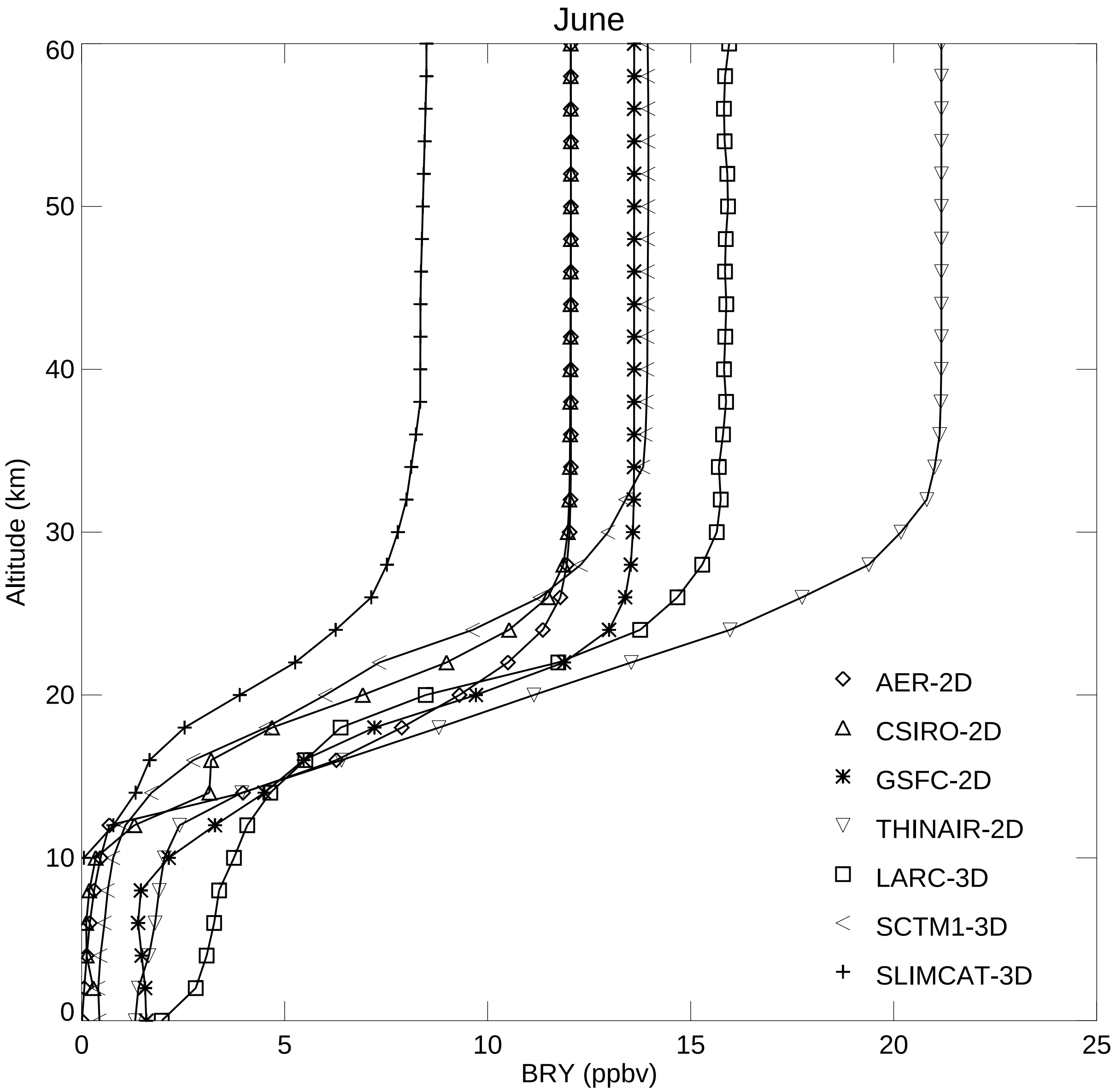

Figure 3.27: Calculated Br_y concentration (ppbv) as a function of altitude for Scenario D at 45^oN in June.

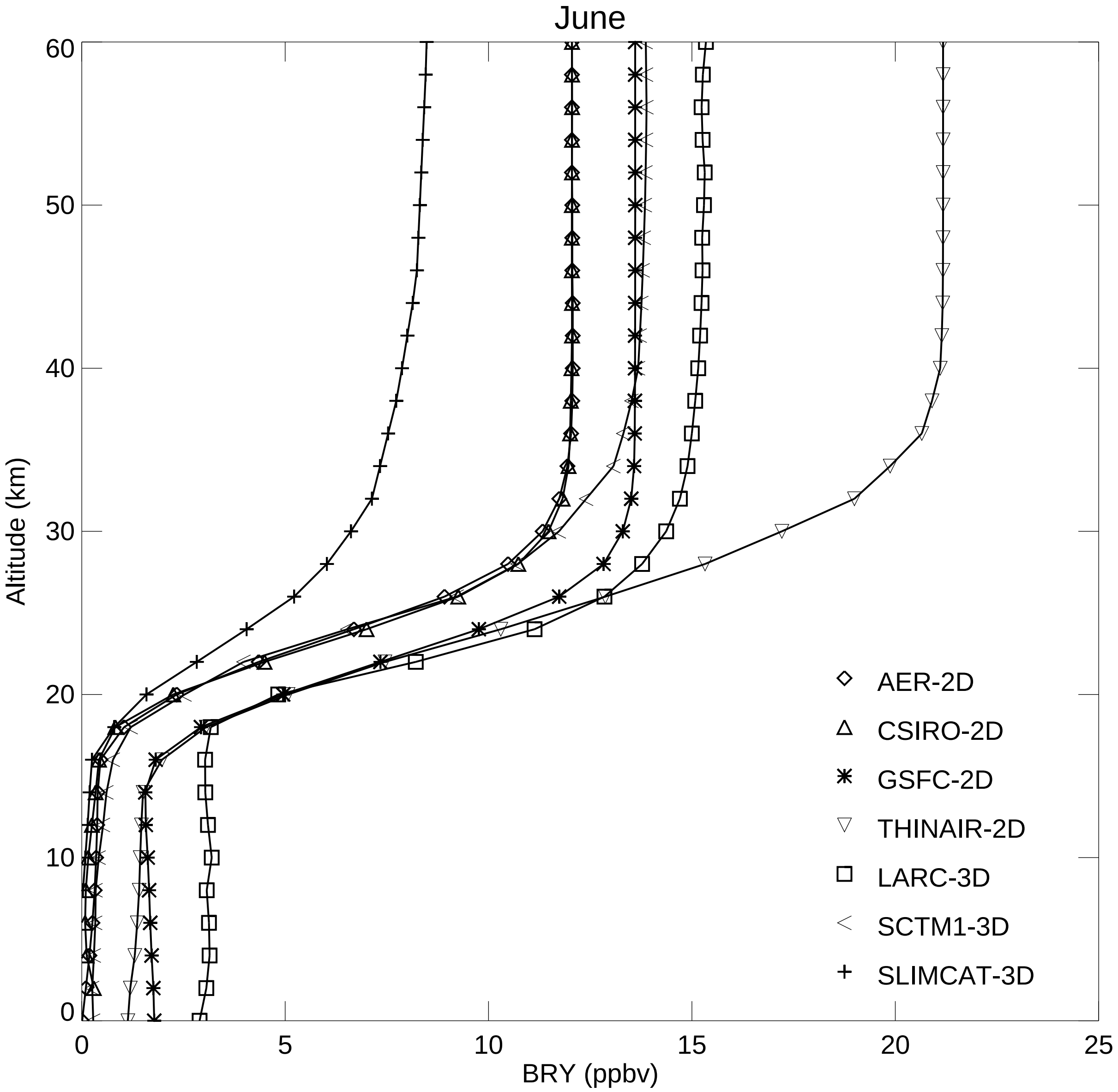

Figure 3.28: Calculated Br_y concentration (ppbv) as a function of altitude for Scenario D at the equator in June.

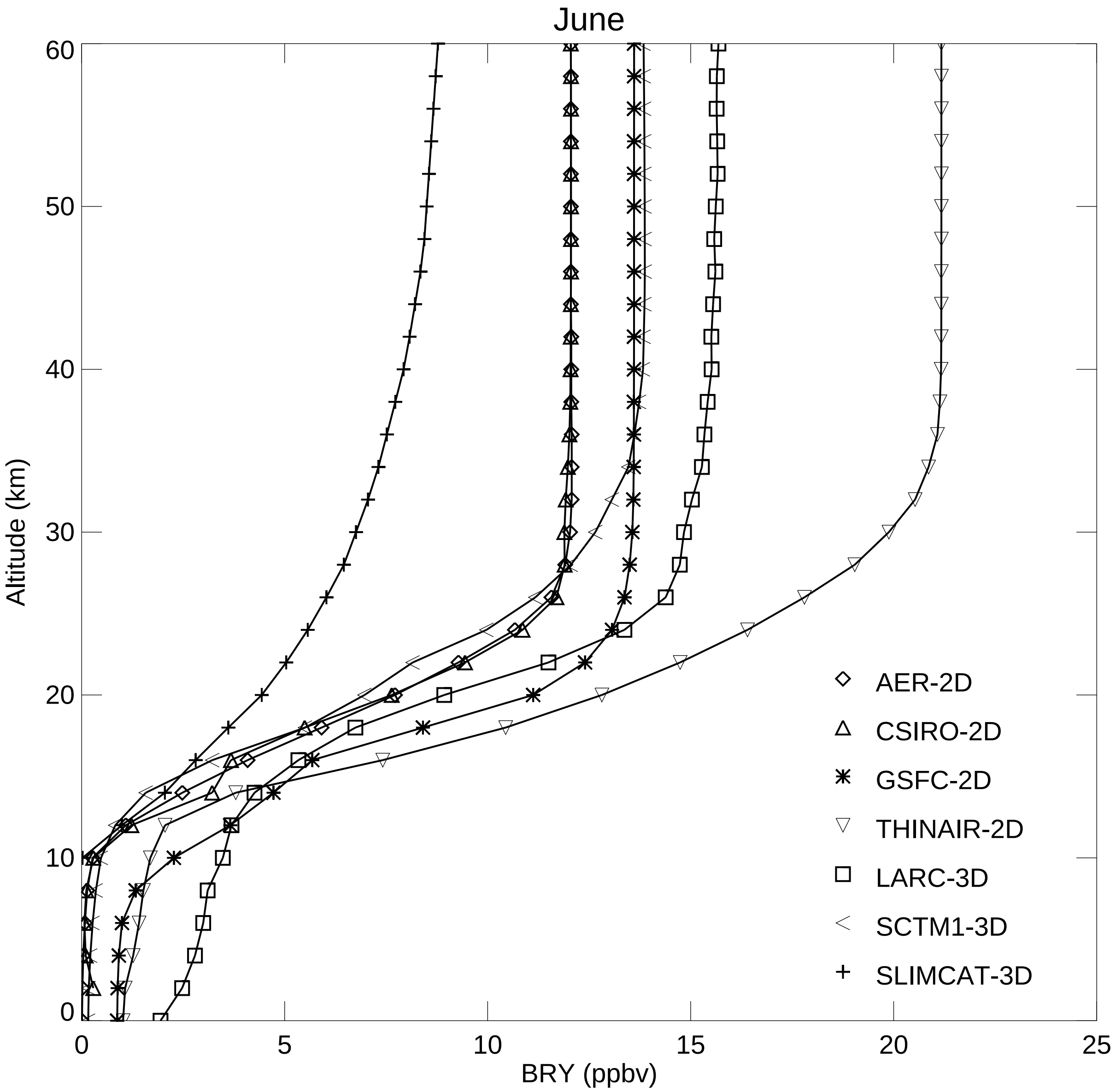

Figure 3.29: Calculated Br_y concentration (ppbv) as a function of altitude for Scenario D at 45^oS in June.

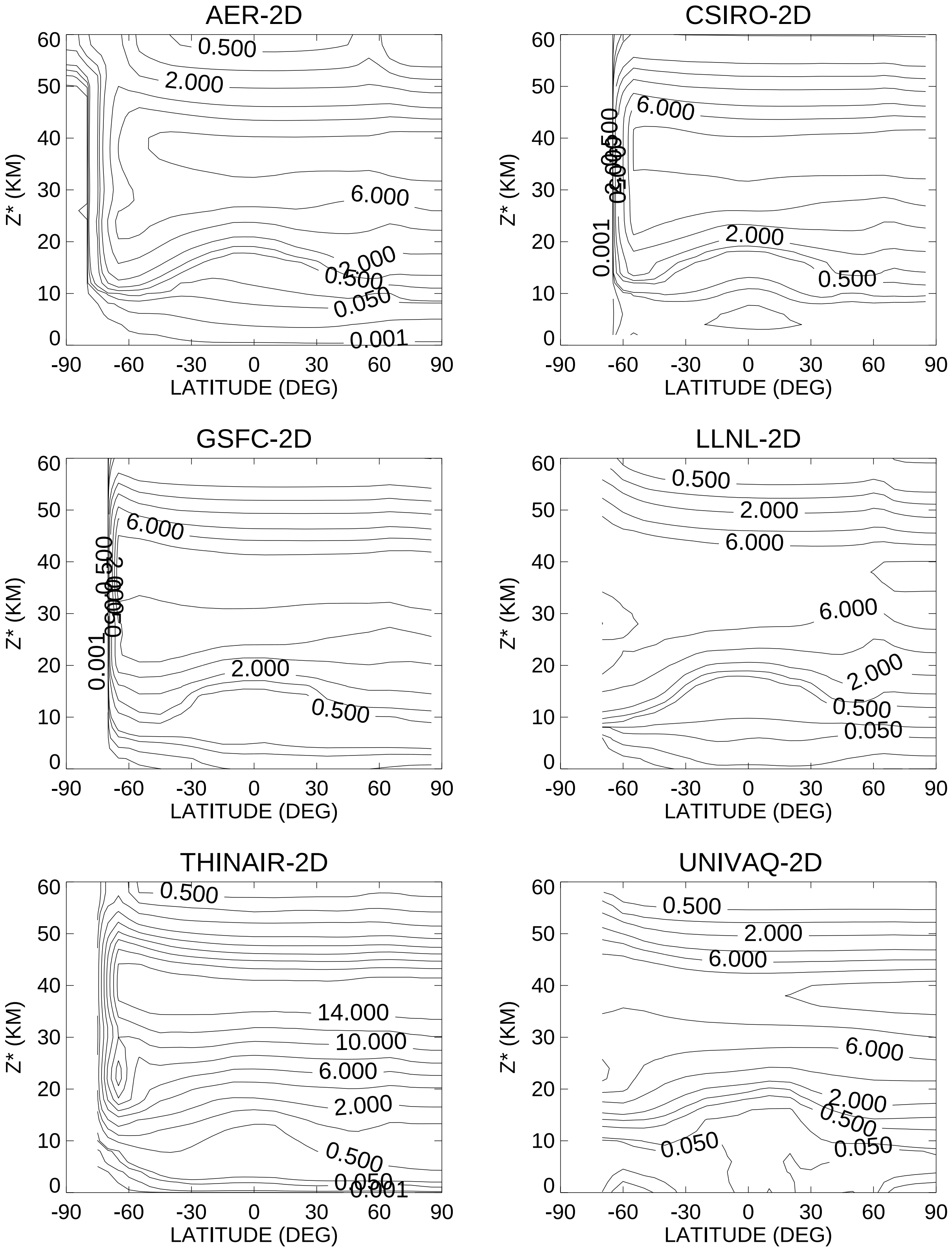

Figure 3.30: Calculated BrO mixing ratios (pptv) as a function of latitude and altitude for Scenario D in June of 2015. Daytime averages are shown for 2-D models, 24-hour averages for 3-D models. Contours are .001, .01, .05, .1, .5, 1, and 2 to 14 by 2 pptv.

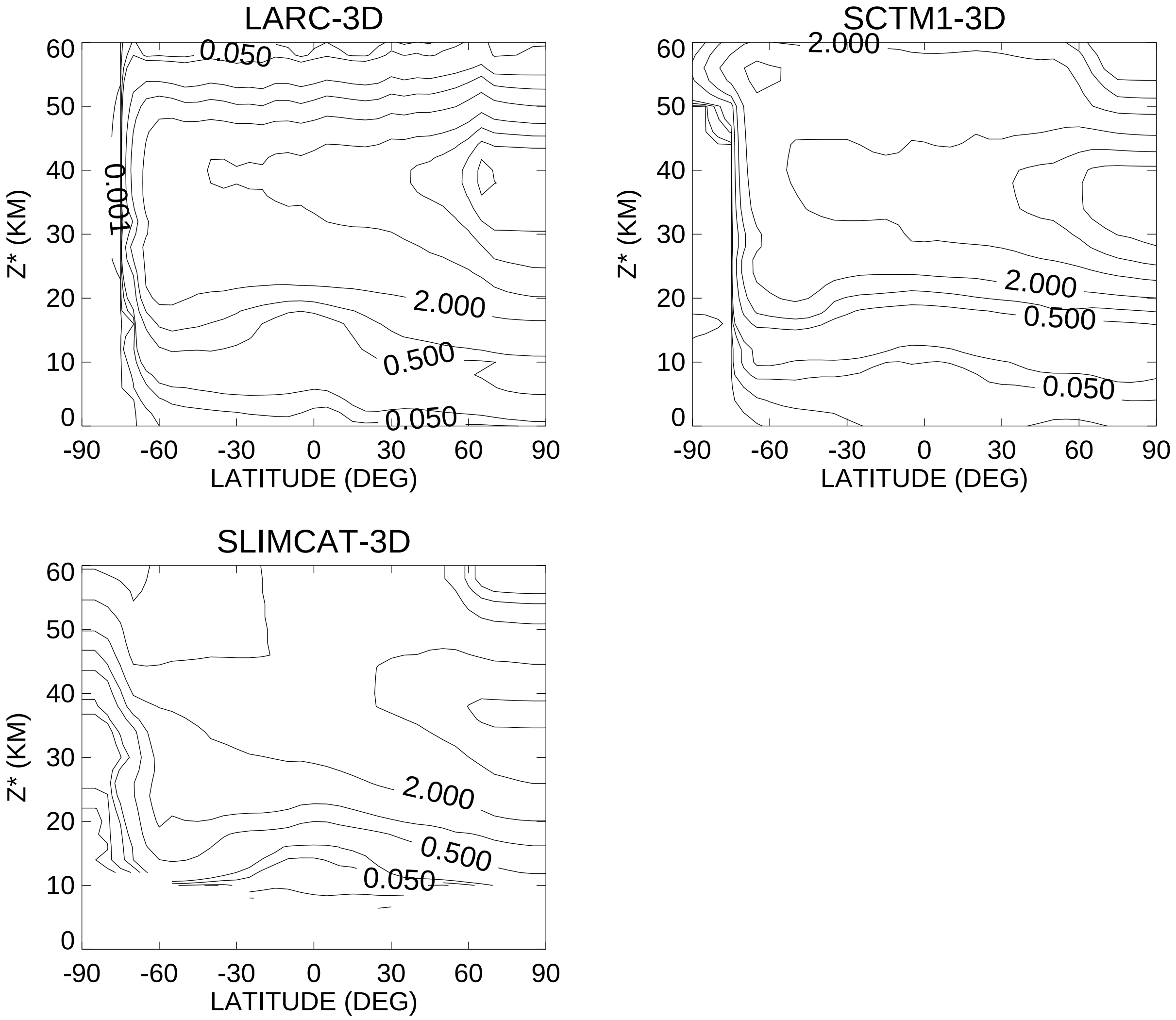

Figure 3.30: continued

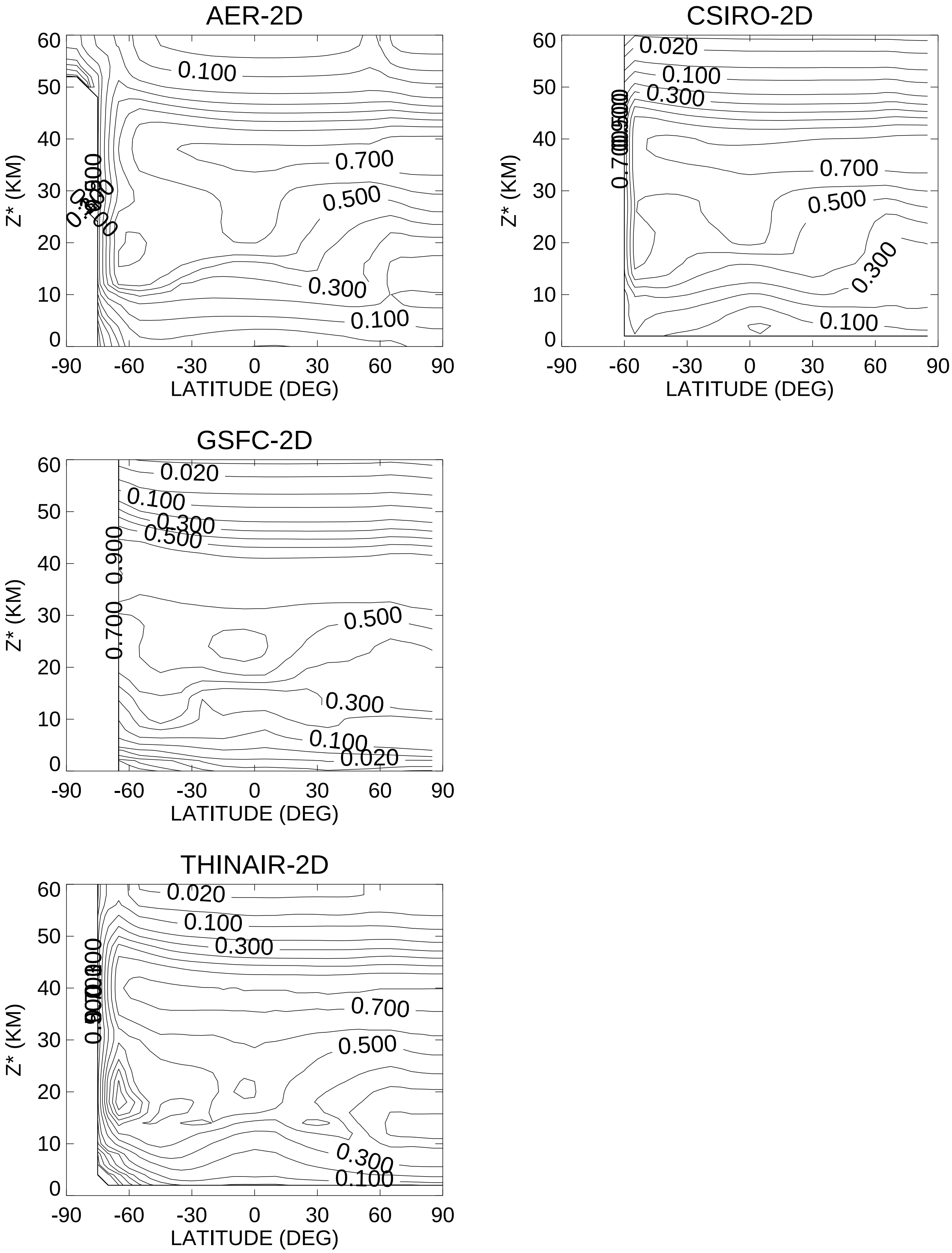

Figure 3.31: Calculated BrO/Br_y ratio as a function of latitude and altitude for Scenario D in June of 2015. Contours are .001, .002, .005, .01, .02, .05, and .1 to .7 by .1.

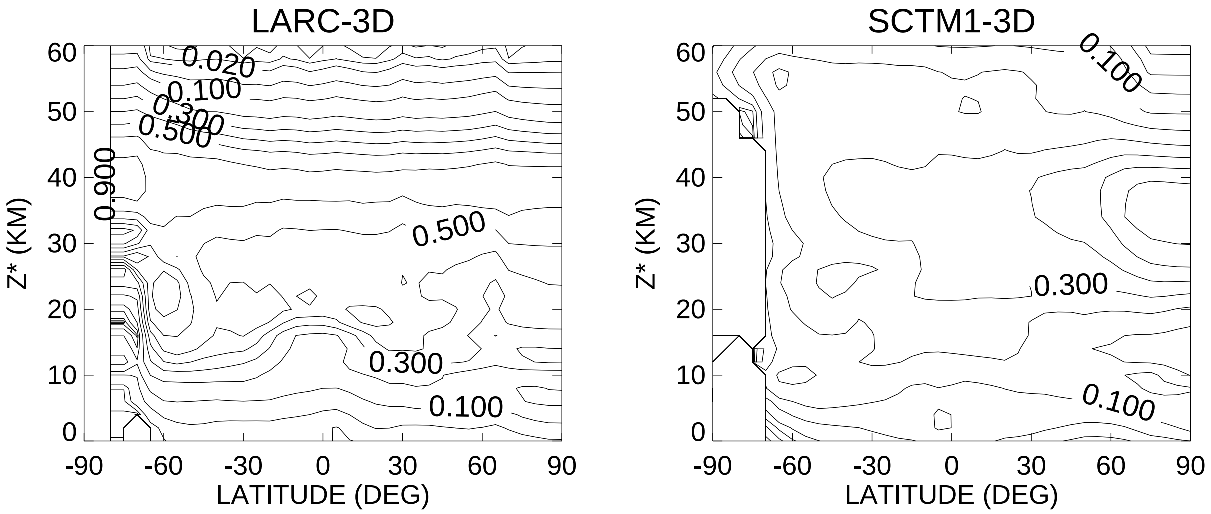

Figure 3.31: continued

3.2 Scenario D3 Results

Scenario D3 differs from Scenario D only in the aerosol SAD employed. Scenario D3 assumes an enhanced SAD due to volcanic eruptions of 4xSA0. The calculated values of total ozone column for this scenario are shown in Figure 3.32. The percent difference in ozone column between Scenario D3 and Scenario D is shown in Figure 3.33. Enhanced aerosol loading leads to reductions in ozone column of up to 3% in the AER model, 1% in the CSIRO model, 10% in the GSFC model, 15% in the LLNL model, and 4% in the UNIVAQ model. Ozone mixing ratios in June for Scenario D3 are shown in Figure 3.34. Changes in ozone mixing ratio relative to Scenario D are shown in Figure 3.35. All models show reductions in ozone below 20 km and increases from 20-30 km due to enhanced aerosol SAD.

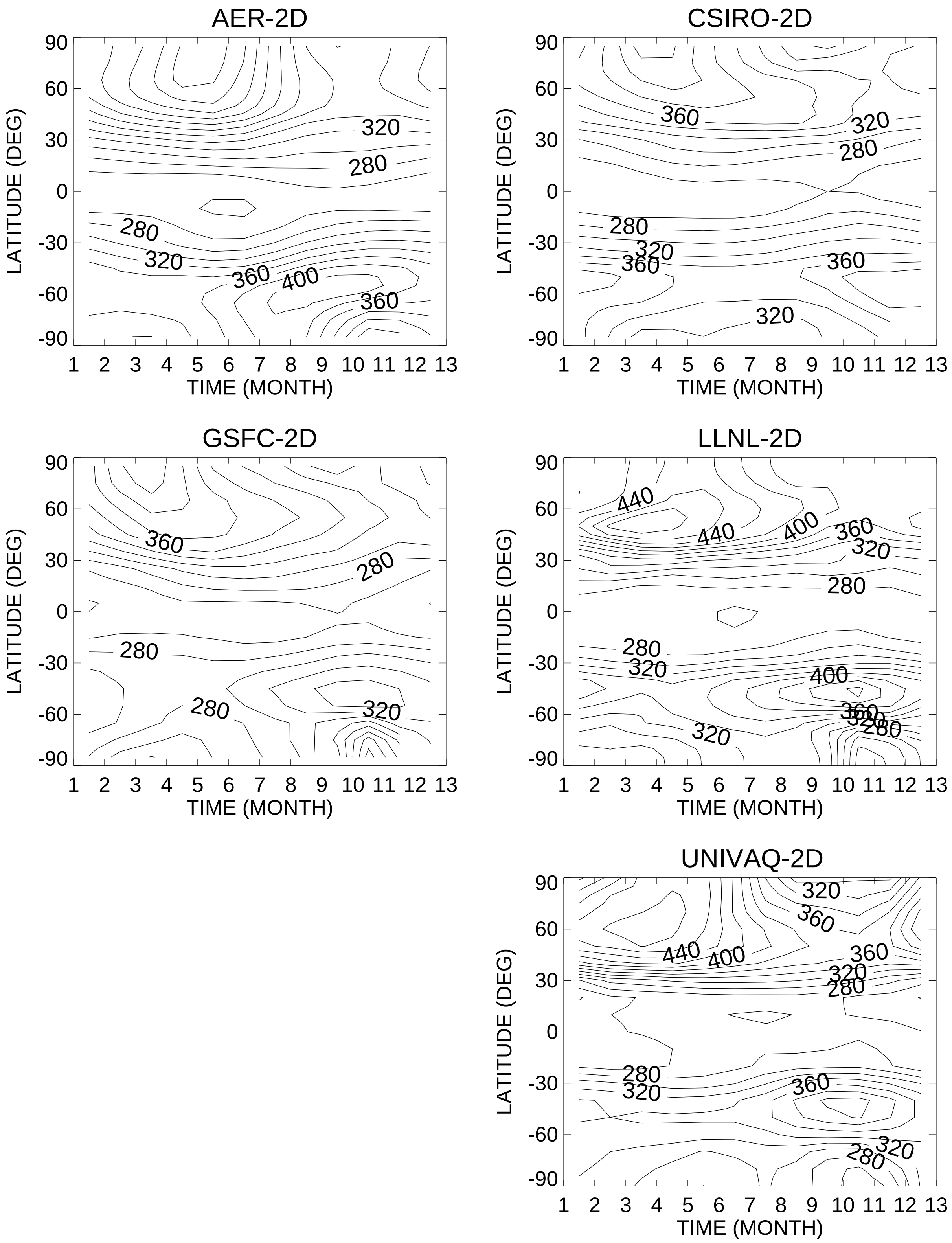

Figure 3.32: Total column ozone (Dobson Units) as a function of latitude and season as calculated by the models for Scenario D3, the 2015 background atmosphere with SAD=4xSA0 and with subsonic aircraft included. Contour interval is 20 DU.

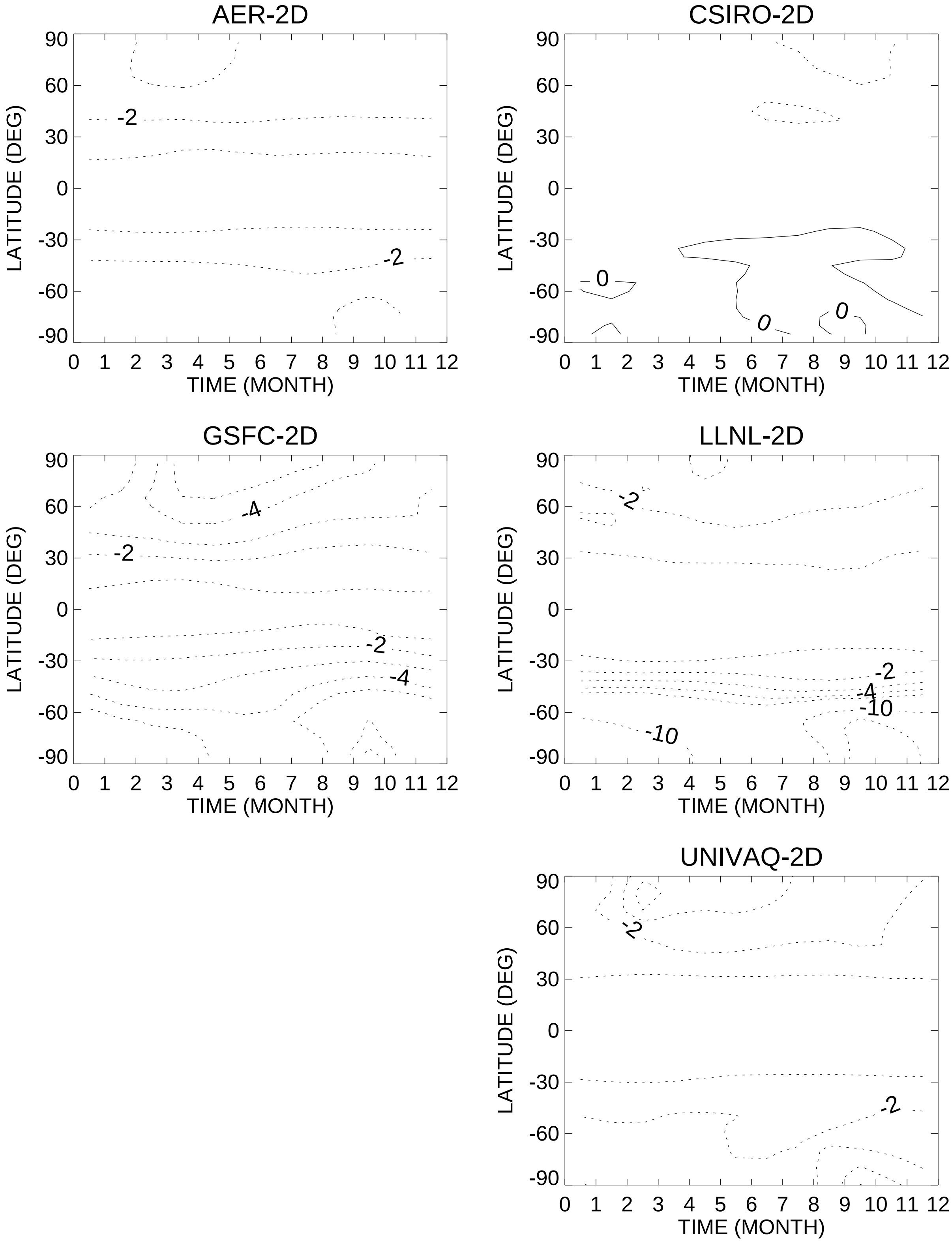

Figure 3.33: Percent change in total column ozone between Scenarios D3 and D. The difference in the scenarios is the background sulfate aerosol surface area density. Contours are -15, -10, -5, -4, -3, -2, -1, 0.

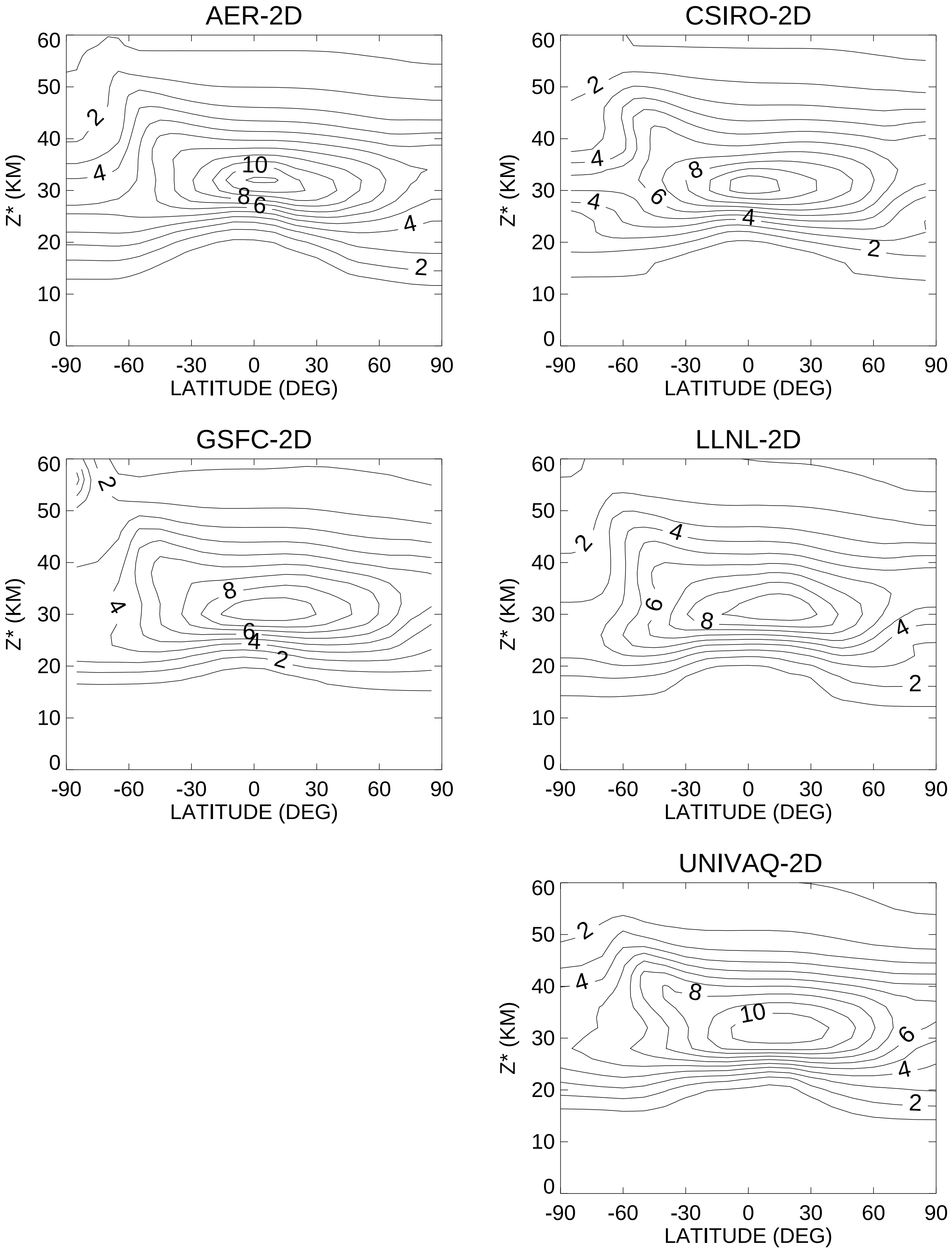

Figure 3.34: Calculated ozone mixing ratios (ppmv) as a function of latitude and altitude for Scenario D3 in June of 2015. The contour interval is 1 ppmv.

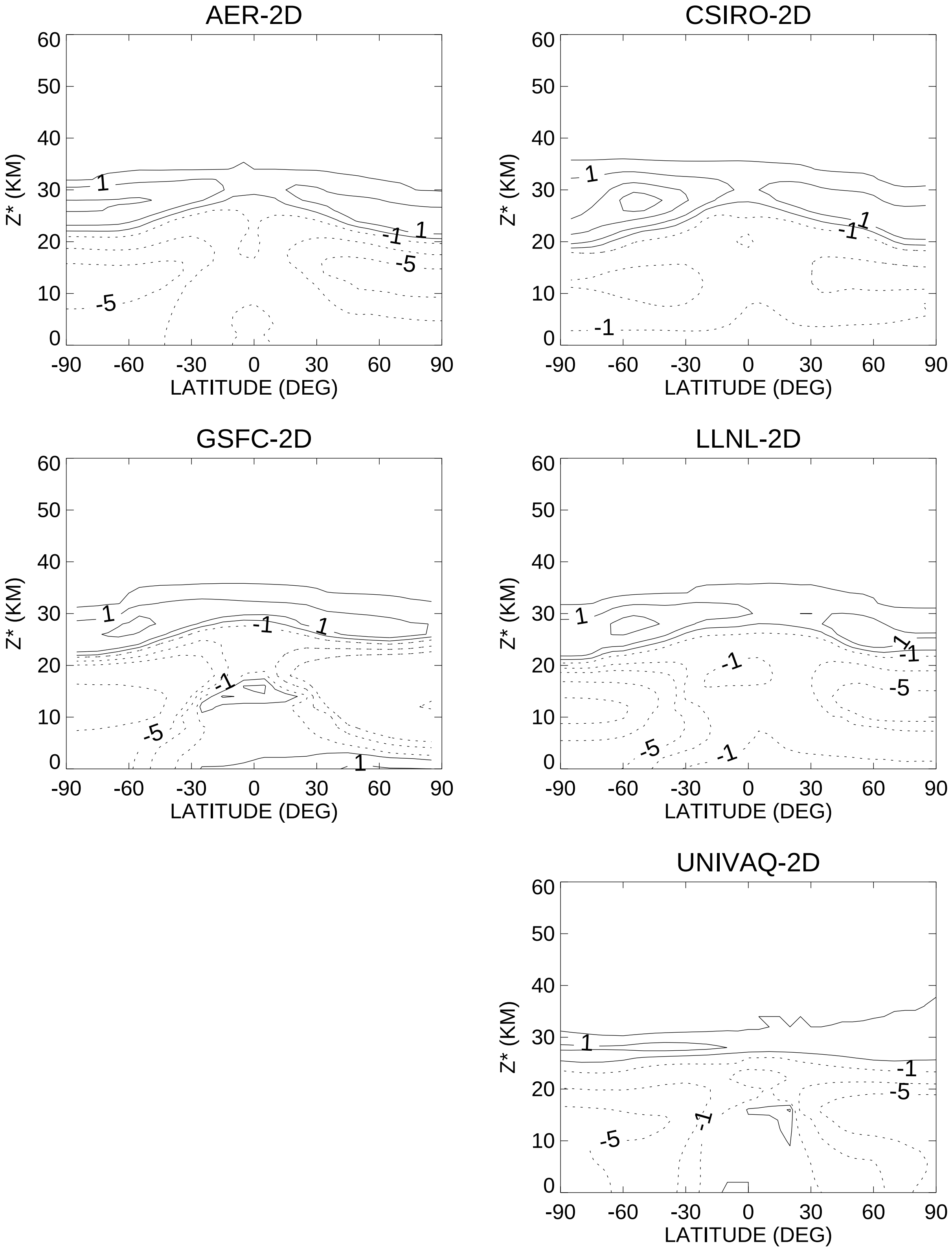

Figure 3.35: Percent change in ozone concentration between Scenarios D3 and D in June of 2015. The difference in the scenarios is the background sulfate aerosol surface area density. Contours are -15, -10, -5, -3, -1, 0, 1, 2, 3%.

3.3 Scenario D4 Results

Scenario D4 differs from Scenario D in that the PSC representation was removed from the models. Note that the CSIRO model did not include a PSC representation in any of its calculations. Therefore Scenarios D and D4 are identical for CSIRO and difference plots between D and D4 for this model are not shown. Figure 3.36 shows total ozone columns calculated by the models for Scenario D4. As seen in Figures 3.37, ozone column is increased by removing the PSC representation. In the AER model, the effect is 2% in the northern springtime polar region and 5% in the southern springtime polar region. The UNIVAQ model shows a 1% effect in the NH and a 3% effect in the SH. The GSFC model shows no effect in the northern hemisphere, but a very large effect (>30%) in the southern hemisphere. Ozone mixing ratios for June from Scenario D4 are shown in Figure 3.38. Differences in ozone mixing ratio between Scenarios D4 and D for March, June, and October are shown in Figures 3.39, 3.40, and 3.41, respectively. June differences are small for all but the GSFC model, which shows southern hemisphere differences in the lower stratosphere of up to 45%.

Differences in H_2O due to omission of the model PSC parameterization are shown in Figure 3.42 for June conditions. Southern hemisphere increases in H_2O are seen for all three models, extending to 60^{o}S in the AER and GSFC models and to 30^{o}S in the UNIVAQ model. The GSFC model also shows a small impact of PSCs from 30 to 40 km in the northern high latitudes. Differences in NO_y are shown in Figure 3.43. NO_y concentrations increase without model PSCs, ie. denitrification leads to reductions in NO_y when PSCs are included in the models. Maximum denitrification is 60% in the AER model, 80% in the GSFC model, and 97% in the UNIVAQ model southern polar region (60-90^{o}N). The UNIVAQ model shows modest denitrification in the lower stratosphere for both hemispheres in June, and the GSFC model shows some denitrification at all southern latitudes. ClO differences are shown in Figure 3.44 and show lower levels of ClO without PSCs in the southern hemisphere. The UNIVAQ model in addition shows reduced ClO in the northern hemisphere. The GSFC model also shows increased ClO in the southern midlatitudes below 15 km in June.

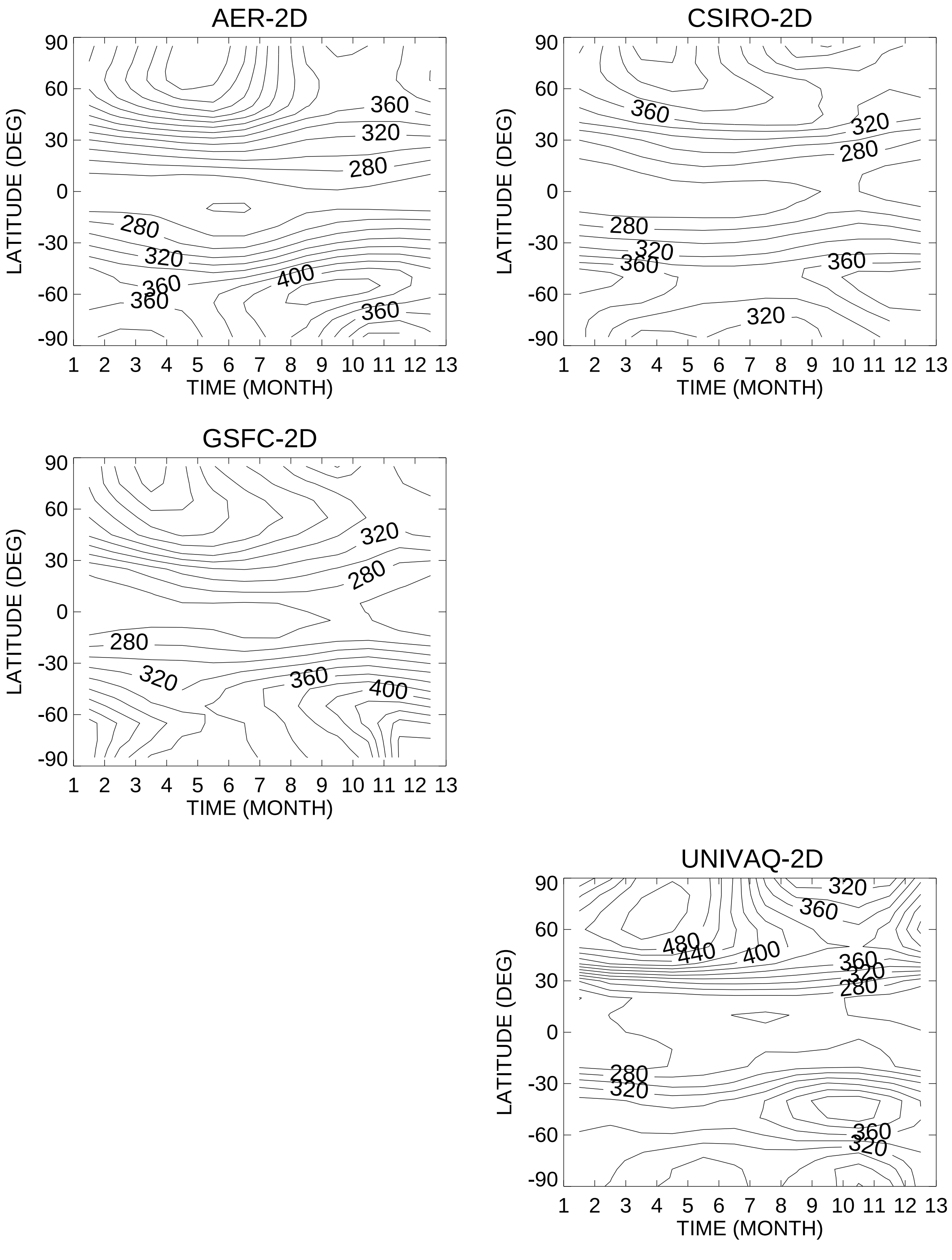

Figure 3.36: Total column ozone (Dobson Units) as a function of latitude and season as calculated by the models for Scenario D4, the 2015 background atmosphere with the model PSC representation removed. Contour interval is 20 DU.

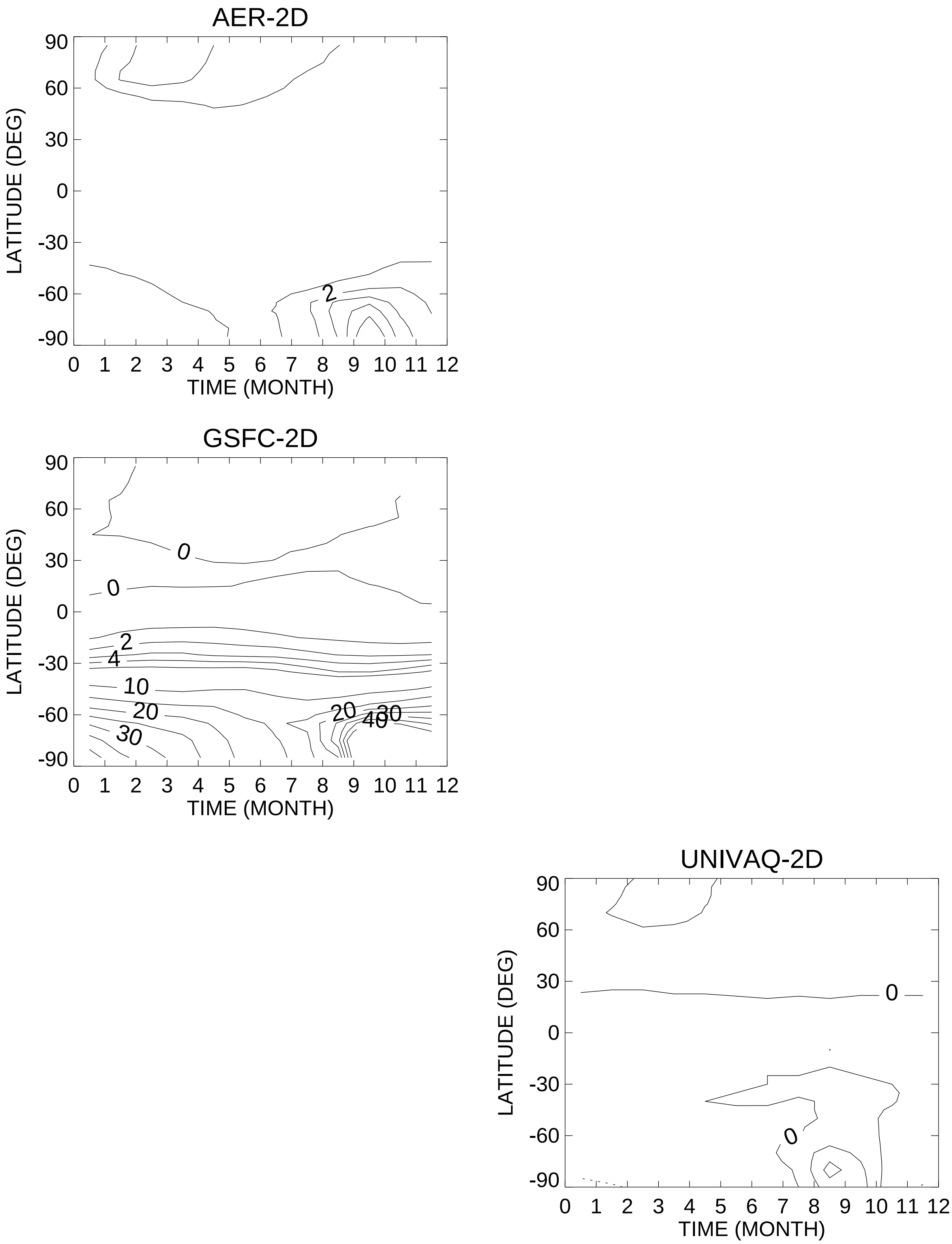

Figure 3.37: Percent change in total ozone column between Scenarios D4 and D. The difference in the scenarios is that the PSC representation is removed in Scenario D4. Contours are -1 to 5 by 1 and 10 to 30 by 5.

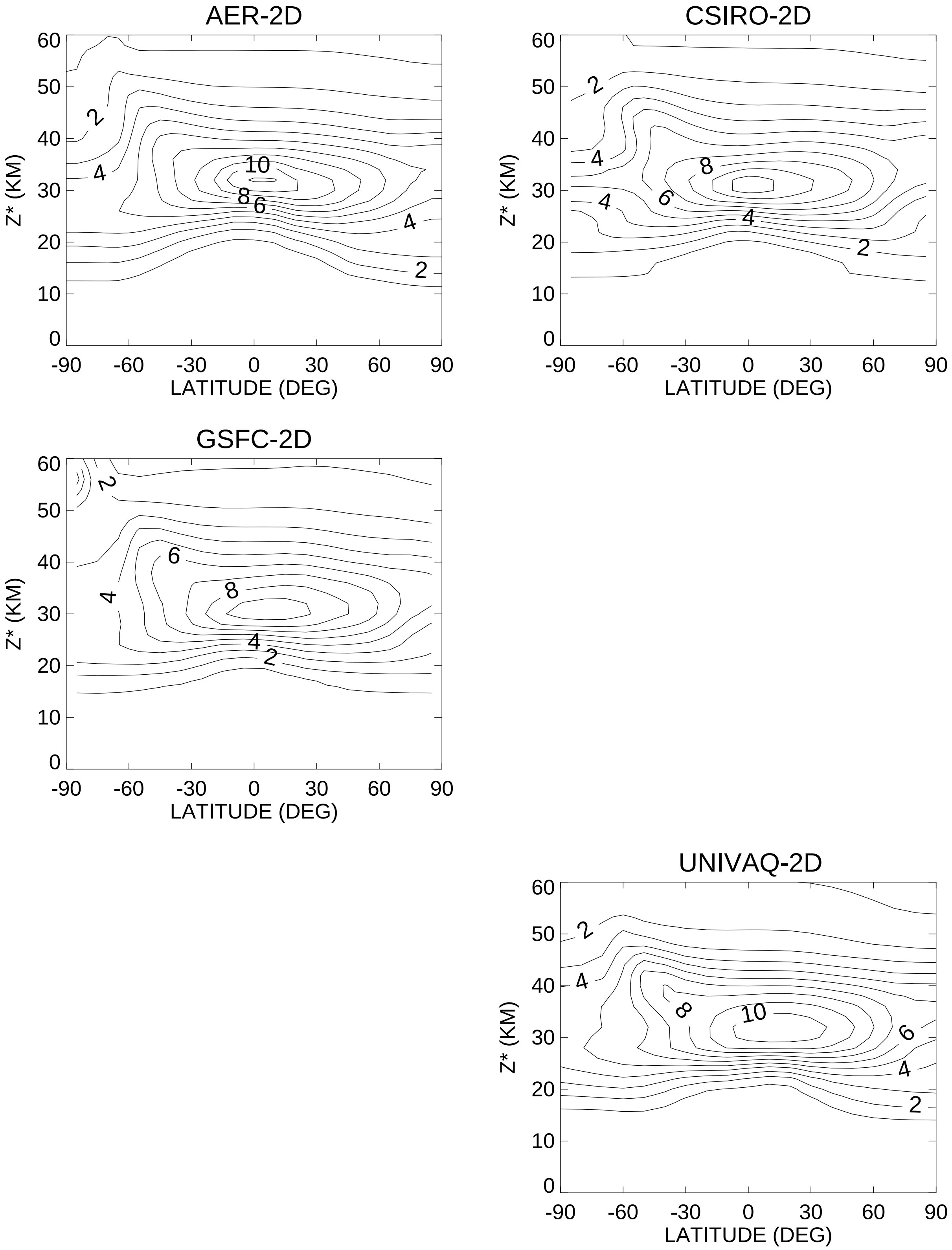

Figure 3.38: Calculated ozone mixing ratios (ppmv) as a function of latitude and altitude for Scenario D4 in June of 2015. The contour interval is 1 ppmv.

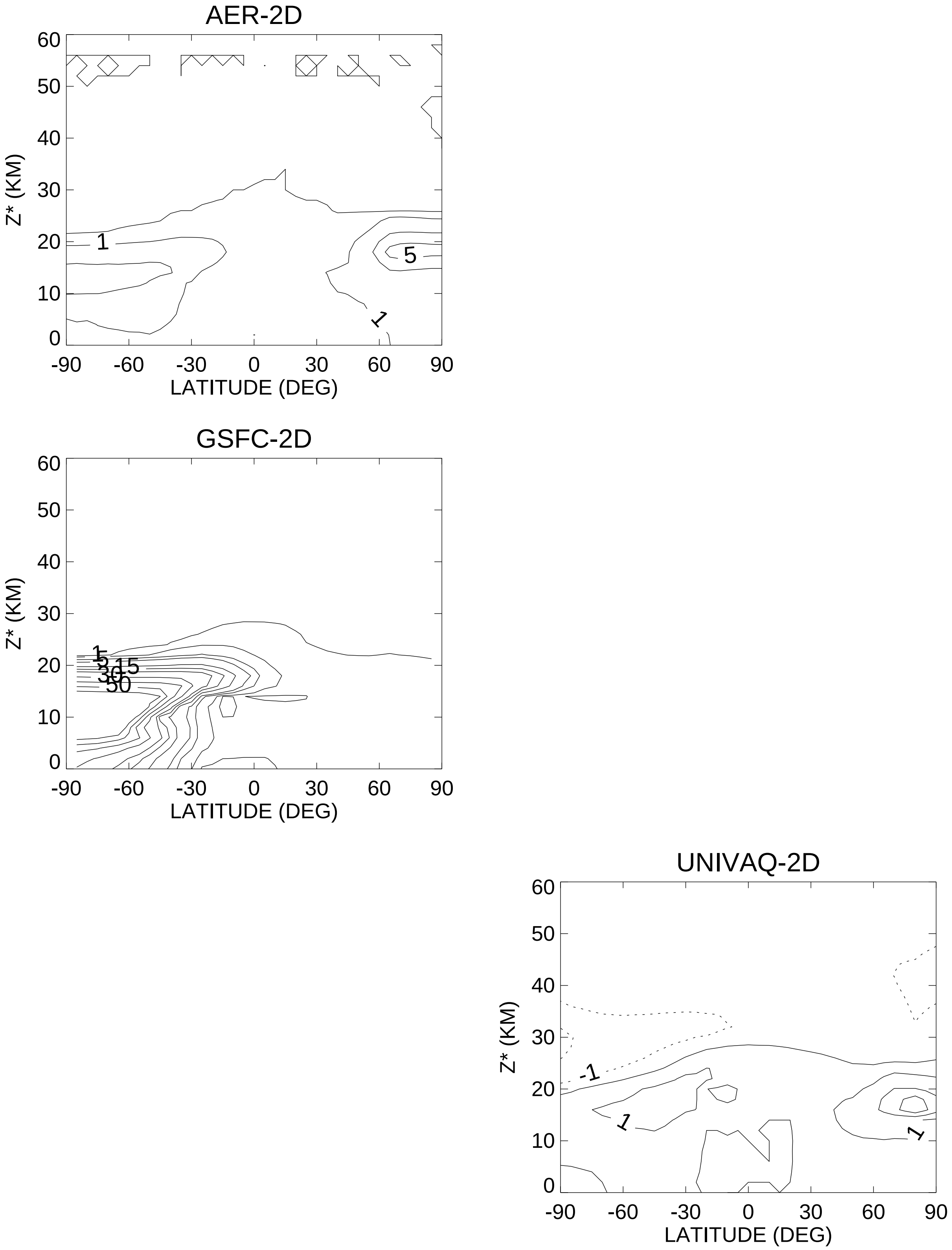

Figure 3.39: Percent change in ozone concentration between Scenarios D4 and D in March of 2015. The difference in the scenarios is that the PSC representation is removed in Scenario D4. Contours are -1, 0, 1, 3, 5, 10, 15, and 20 to 60 by 10.

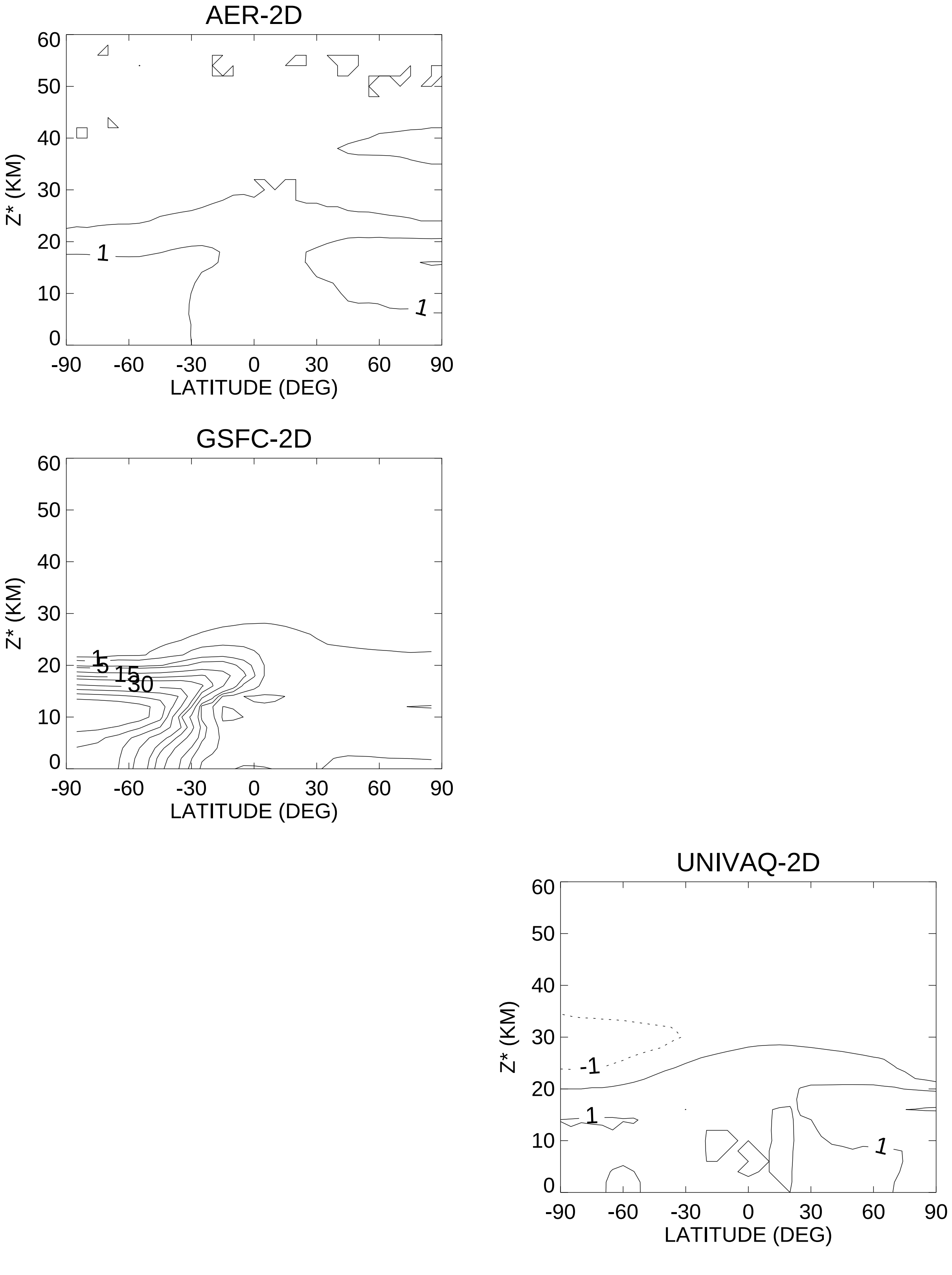

Figure 3.40: Percent change in ozone concentration between Scenarios D4 and D in June of 2015. The difference in the scenarios is that the PSC representation is removed in Scenario D4. Contours are -1, 0, 1, 3, 5, 10, 15, and 20 to 60 by 10.

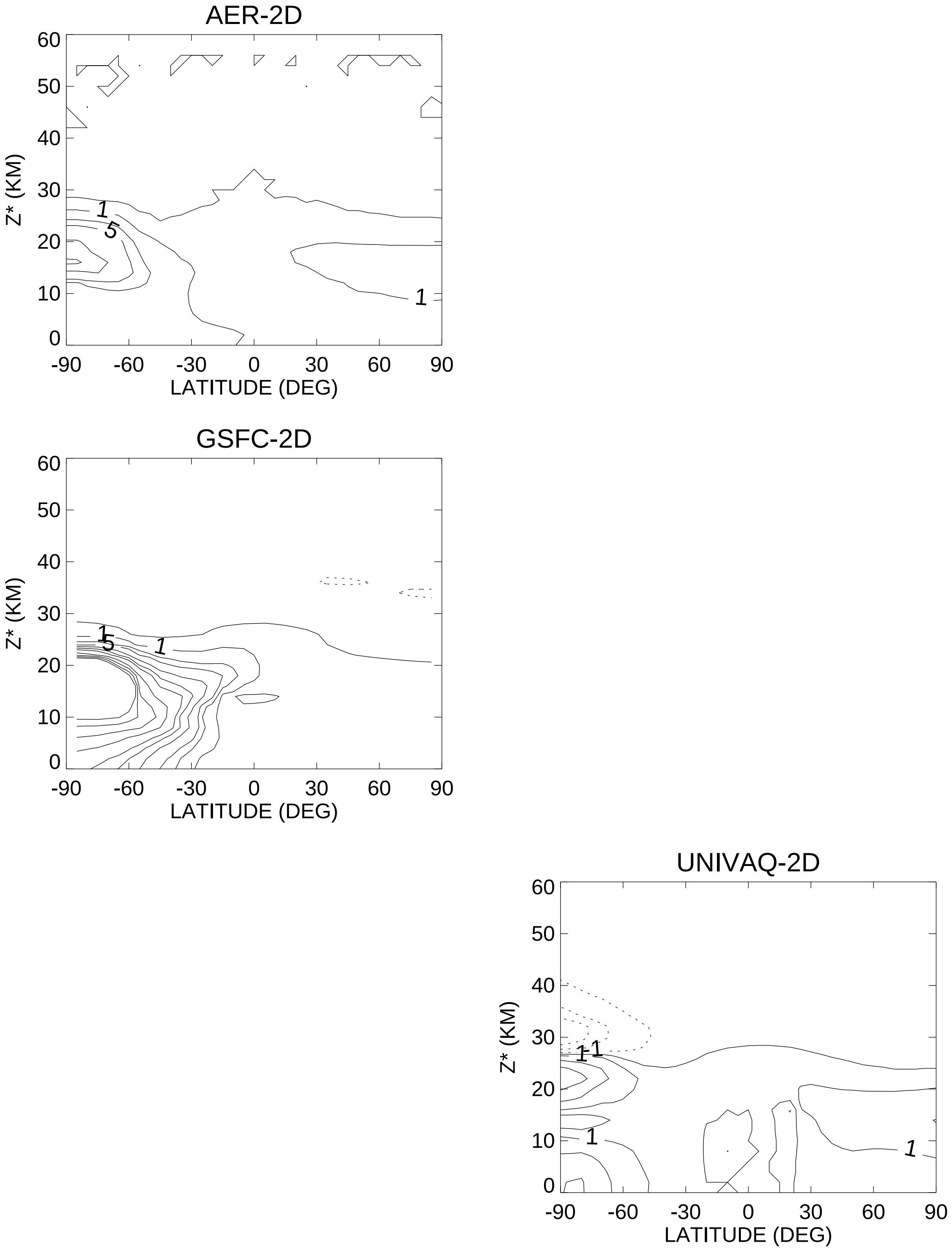

Figure 3.41: Percent change in ozone concentration between Scenarios D4 and D in October of 2015. The difference in the scenarios is that the PSC representation is removed in Scenario D4. Contours are -1, 0, 1, 3, 5, 10, 15, and 20 to 60 by 10.

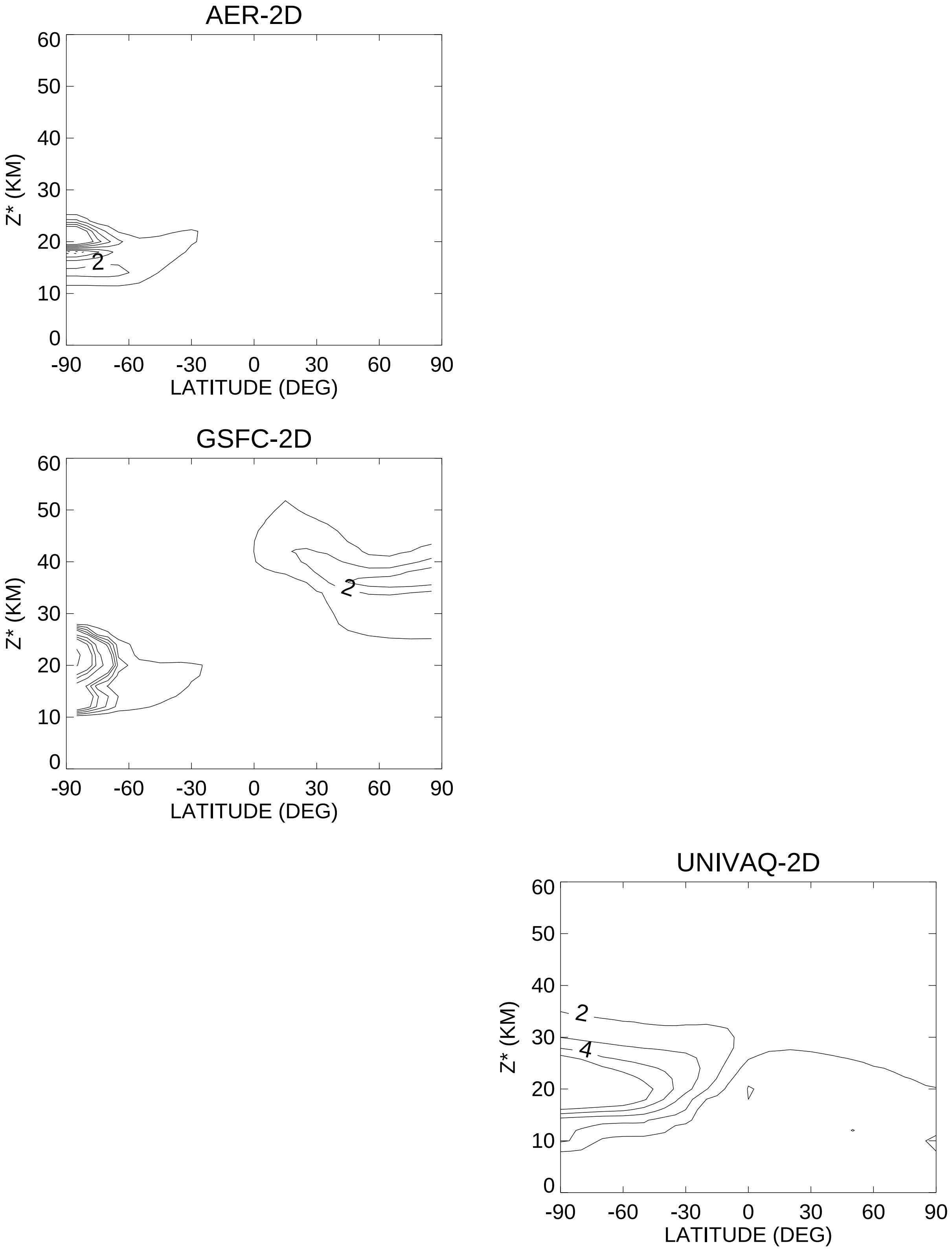

Figure 3.42: Percent change in H_2O concentration between Scenarios D4 and D in June of 2015. The difference in the scenarios is that the PSC representation is removed in Scenario D4. Contours are 1 to 5 by 1 and 10, 15, 20, 30, 40.

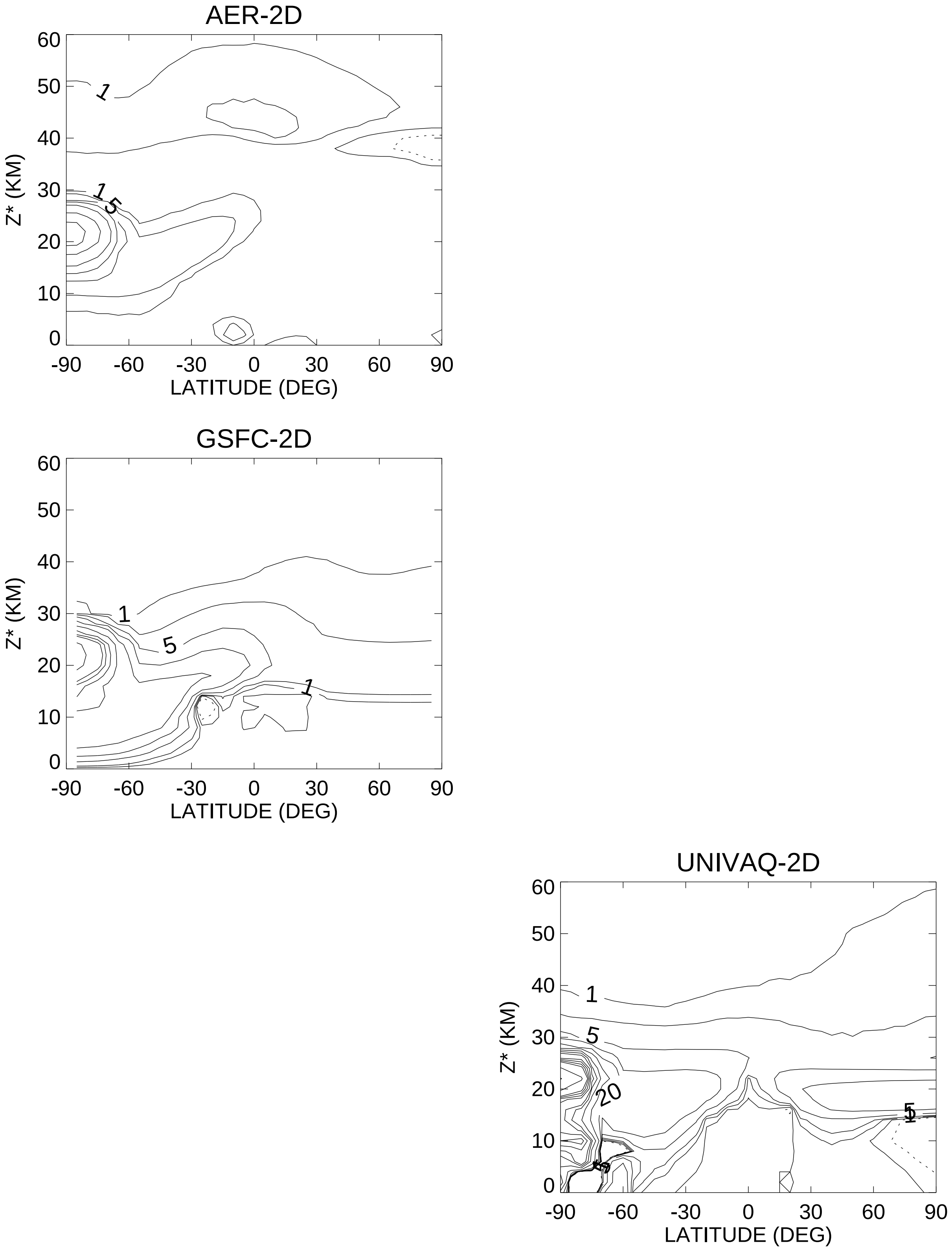

Figure 3.43: Percent change in NO_y concentration between Scenarios D4 and D in June of 2015. The difference in the scenarios is that the PSC representation is removed in Scenario D4. Contours are -1, 0, 1 2, 5, 10, 20, 50, 100, 150, 200, 400, 600, 800, 1000, 2000, 4000.

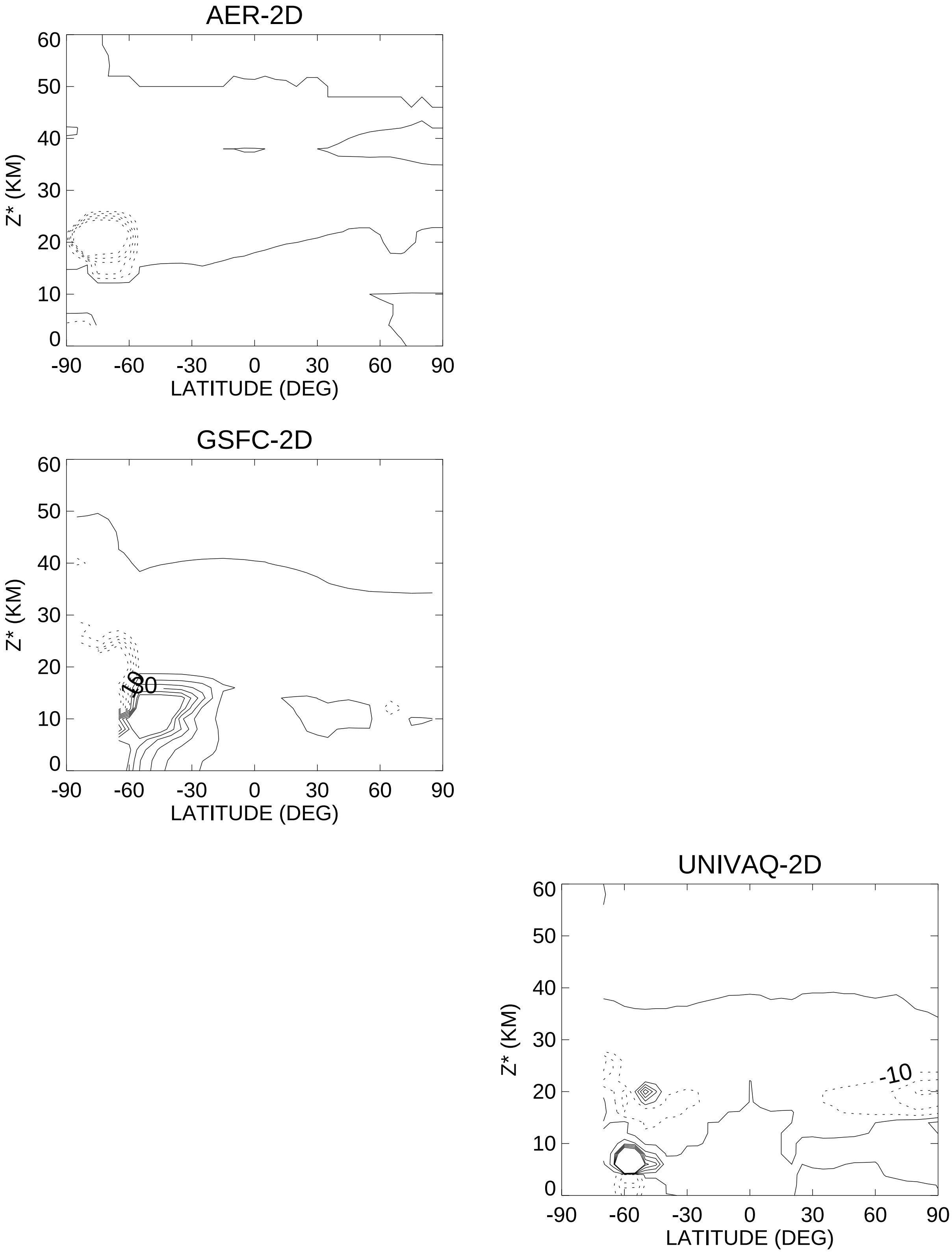

Figure 3.44: Percent change in ClO concentration between Scenarios D4 and D in June of 2015. The difference in the scenarios is that the PSC representation is removed in Scenario D4. Contours are -50 to 50 by 10.

3.4 Scenario D5 Results

Scenario D5 differs from Scenario D in the total odd chlorine loading. Boundary conditions of organic chlorine species were modified to produce approximately 1 ppbv of inorganic chlorine in the upper stratosphere. This scenario, along with D6, is used to test the sensitivity of the HSCT impact on ozone to background Cl_y concentrations. Cl_y mixing ratios as a function of latitude and altitude for June are shown in Figure 3.45. The AER model has just under 1 ppbv of Cl_y in the upper stratosphere and the GSFC model just over 1 ppbv.

Total ozone column fields for Scenario D5 are shown in Figure 3.46. Differences in total ozone between Scenarios D5 and D are shown in Figure 3.47. Ozone columns are greater with reduced Cl_y concentrations. All models show a 2% increase in tropical ozone due to reduced Cl_y. The AER model shows a 5% increase at northern high latitudes and a 5-15% increase at high southern latitudes. The GSFC model shows a 5% northern high latitude increases and greater than 30% increases at southern high latitude. The UNIVAQ model shows a 5% increases at high latitudes in both hemispheres. The GSFC changes due to reduced Cl_y are consistent with ozone change caused by removal of the PSC parameterization. Figure 3.48 shows ozone mixing ratios as a function of latitude and altitude for June from Scenario D5. Figure 3.49 shows changes in ozone mixing ratio relative to Scenario D. Large changes (15-30%) are found in the stratosphere above 30 km. The GSFC model also has large changes in the southern hemisphere lower stratosphere and troposphere due to the effects of heterogeneous chemistry.

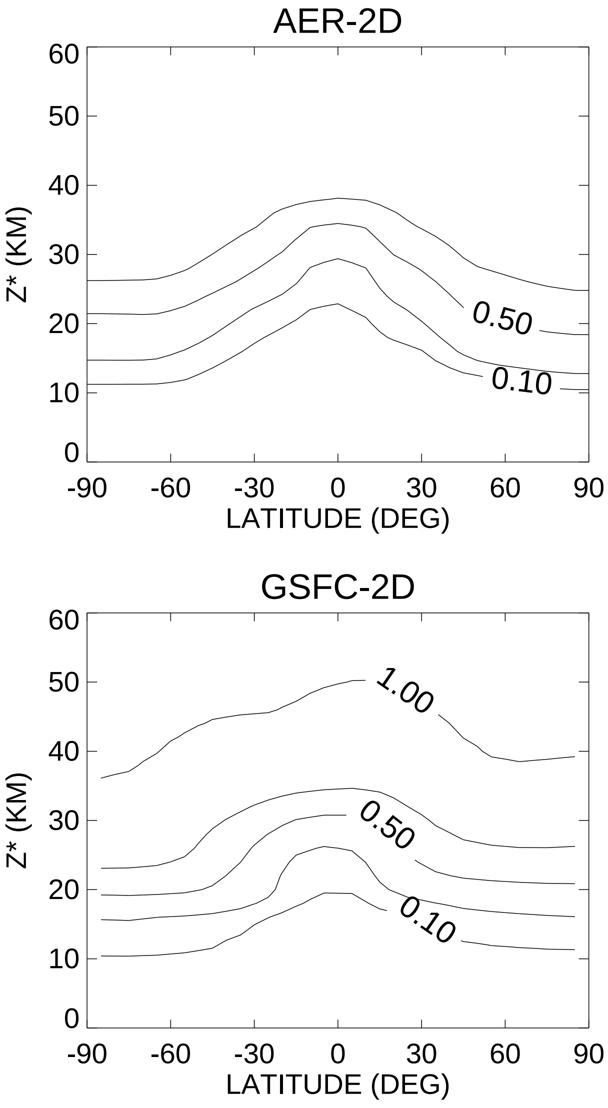

Figure 3.45: Calculated Cl_y mixing ratio (ppbv) in June for Scenario D5, the 2015 background atmosphere including subsonic aircraft and with organic chlorine boundary conditions adjusted to produce approximately 1 ppbv of inorganic chlorine. Contours are 0.1, 0.25, 0.5, 0.75 and 1.0 ppbv.

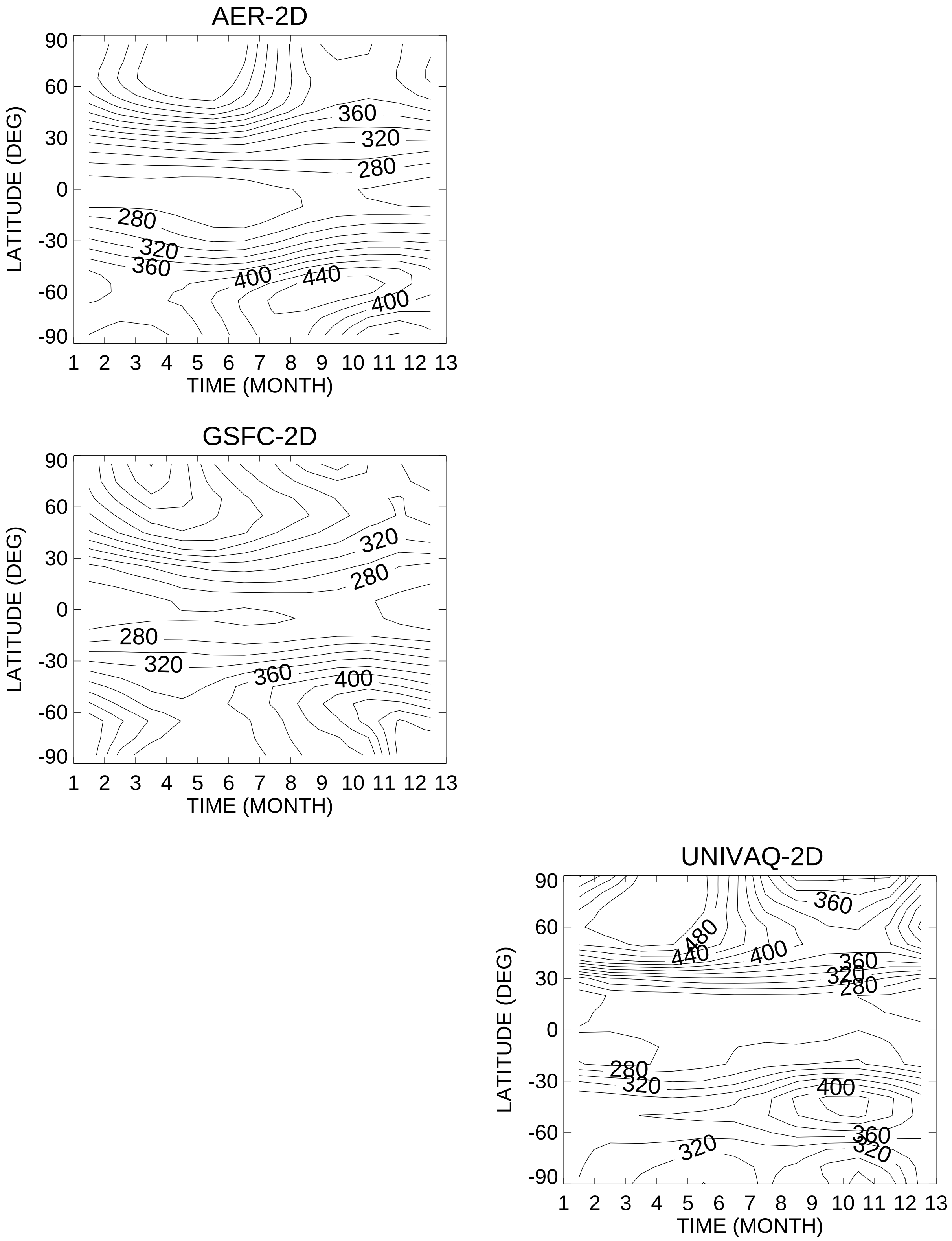

Figure 3.46: Total column ozone (Dobson Units) as a function of latitude and season as calculated by the models for Scenario D5, the 2015 background atmosphere with organic chlorine boundary conditions adjusted to produce approximately 1 ppbv of inorganic chlorine. Contour interval is 20 DU.

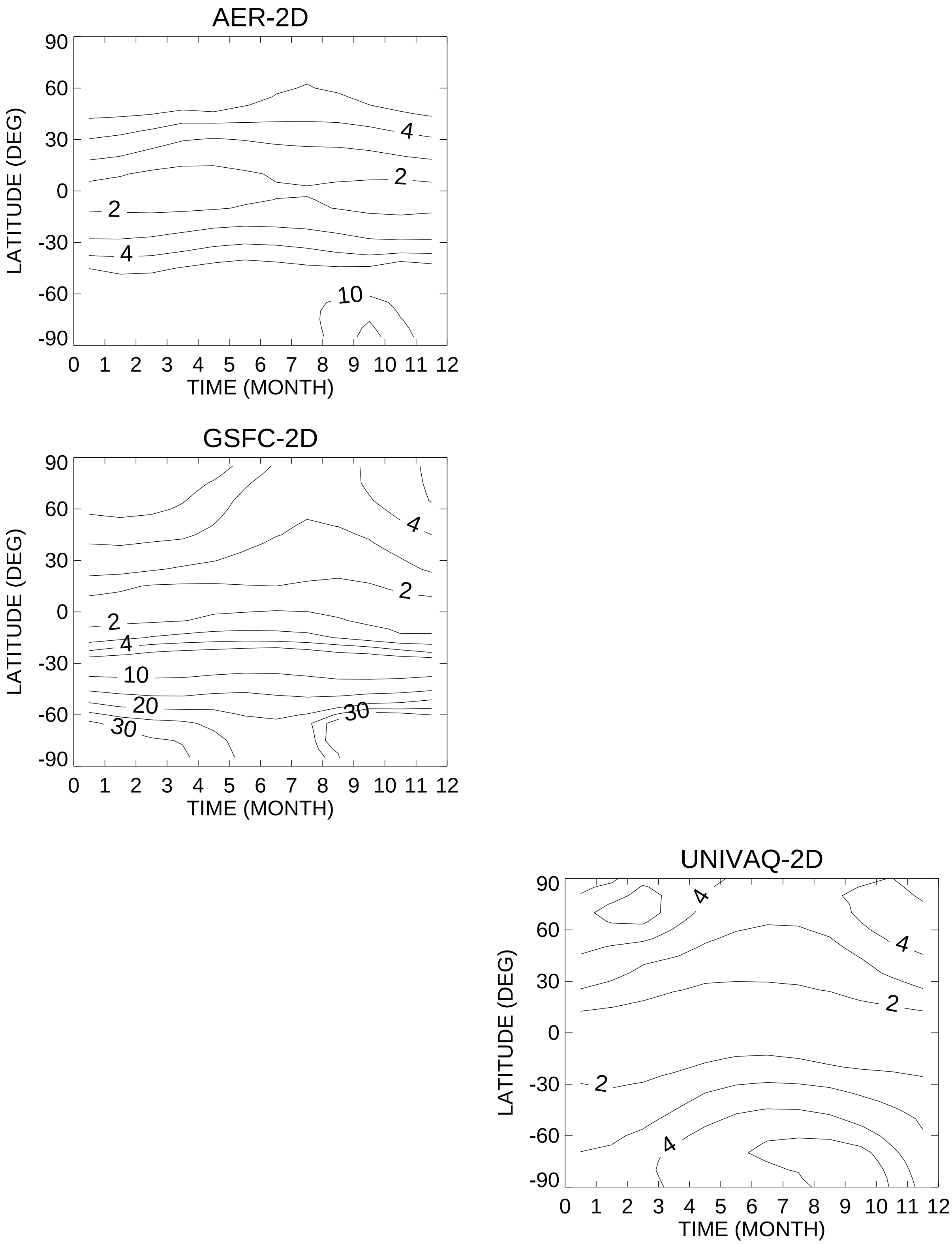

Figure 3.47: Percent change in total ozone column between Scenarios D5 and D. The difference in the scenarios is that D5 contains 1 ppbv of Cl_y and D contain 3 ppbv of Cl_y. Contours are 2, 3, 4, 5 and 10 to 30 by 5.

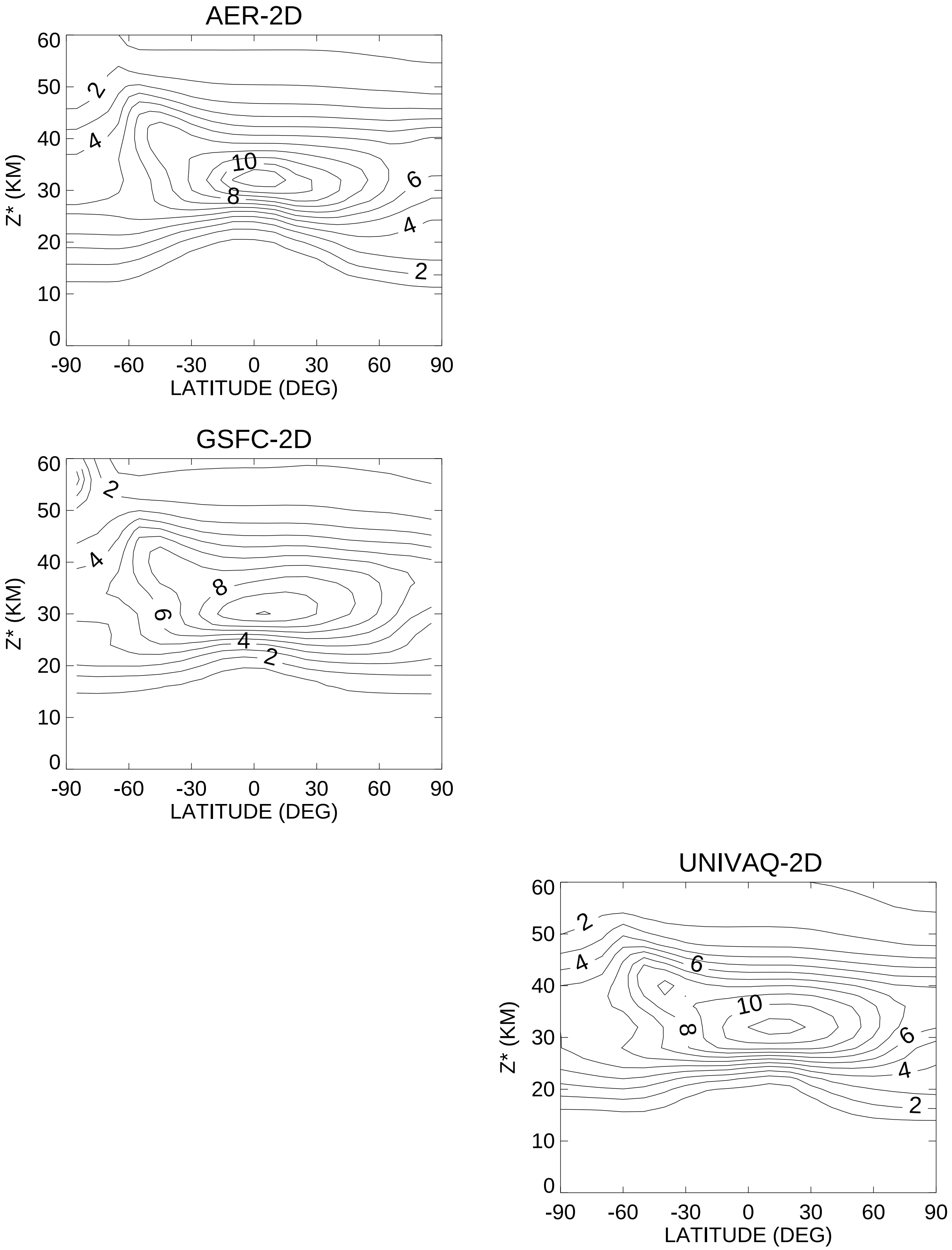

Figure 3.48: Calculated ozone mixing ratios (ppmv) as a function of latitude and altitude for Scenario D5 in June of 2015. The inorganic chlorine loading is 1 ppbv. The contour interval is 1 ppmv.

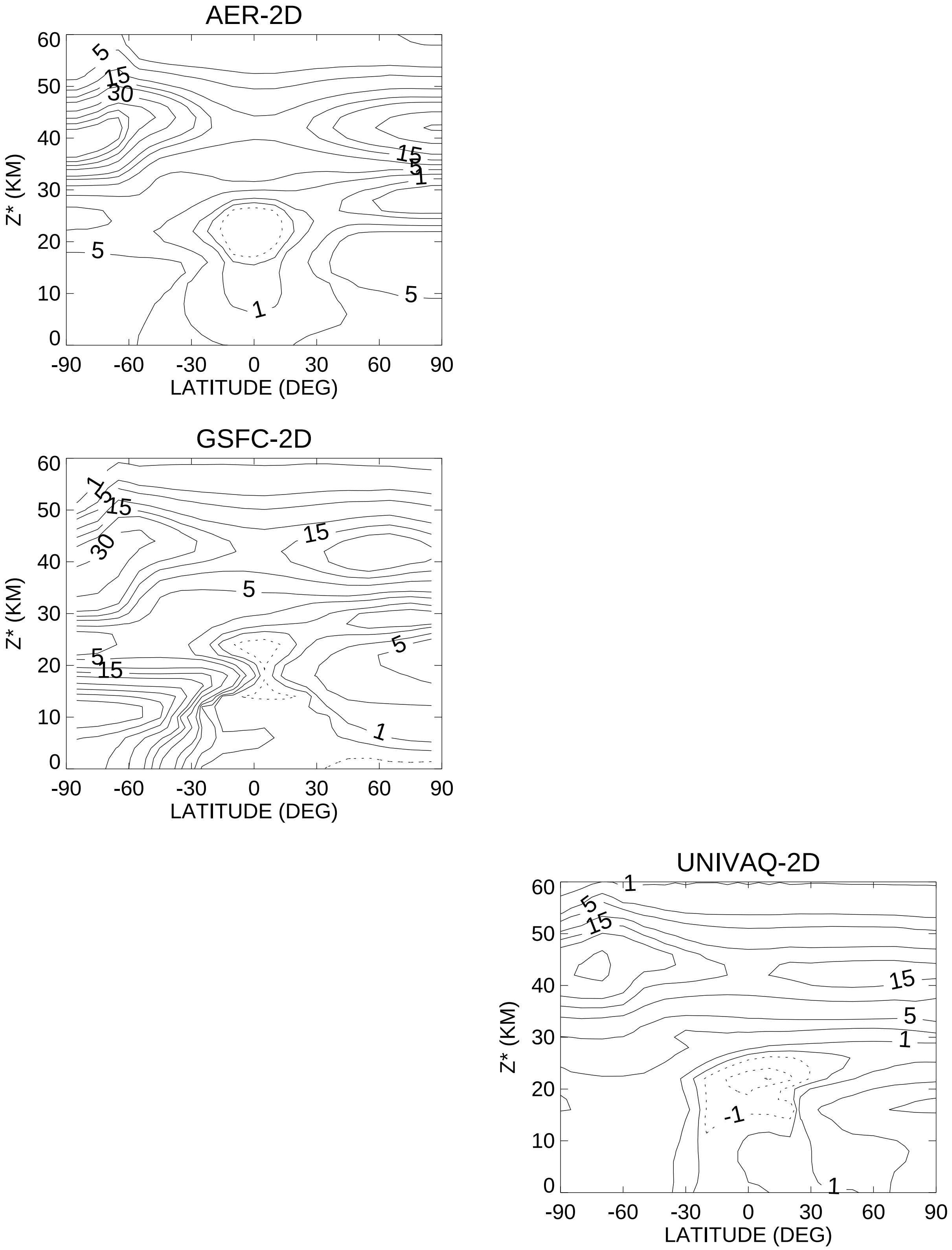

Figure 3.49: Percent change in ozone concentration between Scenarios D5 and D in June of 2015. The difference in the scenarios is that D5 contains 1 ppbv of Cl_y and D contain 3 ppbv of Cl_y. Contours are -1, 0, 1, 3, 5, 10, 15, and 20 to 60 by 10.

3.5 Scenario D6 Results

Scenario D6 contains a total odd chlorine loading of 4 ppbv. This scenario is also used to test the sensitivity of the HSCT impact on ozone to background Cl_y concentrations. Boundary conditions of organic chlorine species were modified to produce approximately 4 ppbv of inorganic chlorine in the upper stratosphere. Cl_y mixing ratios as a function of latitude and altitude for June are shown in Figure 3.50. The GSFC model has more Cl_y in the lower stratosphere than the AER model.

Total ozone column fields for Scenario D6 are shown in Figure 3.51. Differences in total ozone between Scenarios D6 and D are shown in Figure 3.52. Reduced ozone columns are calculated with larger Cl_y concentrations in the AER and GSFC models, but the UNIVAQ model shows little change between 4 ppbv of Cl_y and 3 ppbv of Cl_y. Figure 3.53 shows ozone mixing ratio for June for Scenario D6. Changes in June ozone mixing ratio relative to Scenario D are shown in Figure 3.54. Ozone is reduced above 30 km in all models due to the increase in Cl_y from 3 to 4 ppbv. The GSFC model also shows reduced ozone in the southern hemisphere lower stratosphere and troposphere, while the AER model shows some ozone reduction in the northern hemisphere lower stratosphere. In the UNIVAQ model, lower stratospheric ozone increases compensate for ozone reduction above 30 km.

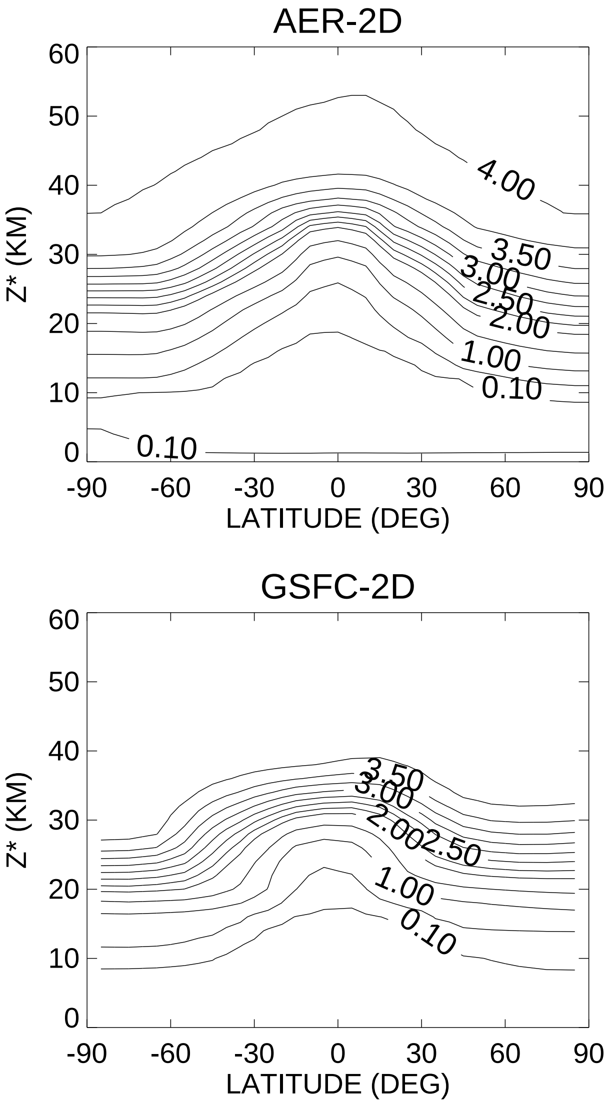

Figure 3.50: Calculated Cl_y mixing ratios (ppbv) in June for Scenario D6, the 2015 background atmosphere including subsonic aircraft and with organic chlorine boundary conditions adjusted to produce approximately 4 ppbv of inorganic chlorine. Contours are 0.1, 0.5, 1.0, 1.5, and 2.0 to 4.0 by 0.25 ppbv.

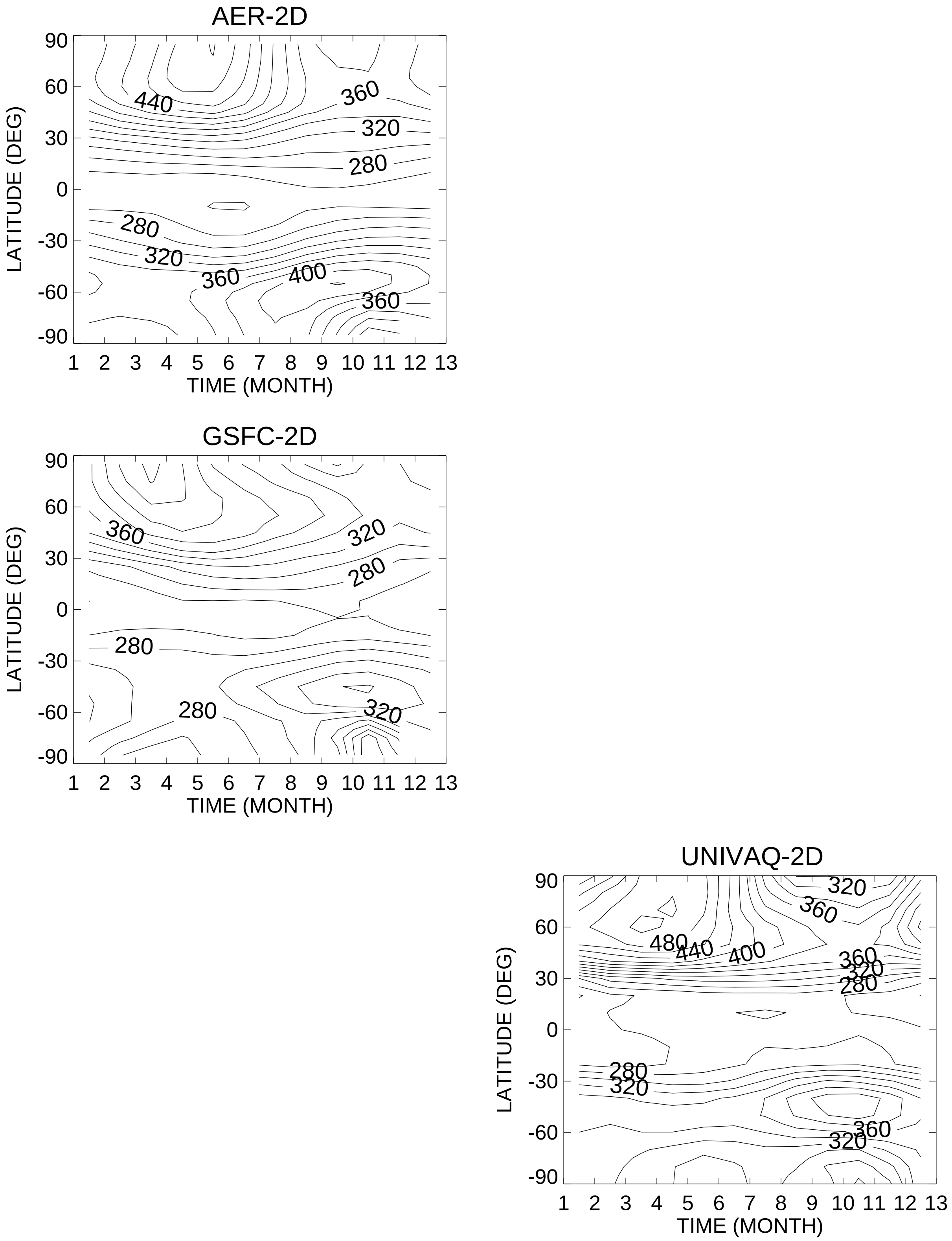

Figure 3.51: Total column ozone (Dobson Units) as a function of latitude and season as calculated by the models for Scenario D6, the 2015 background atmosphere with organic chlorine boundary conditions adjusted to produce approximately 4 ppbv of inorganic chlorine. Contour interval is 20 DU.

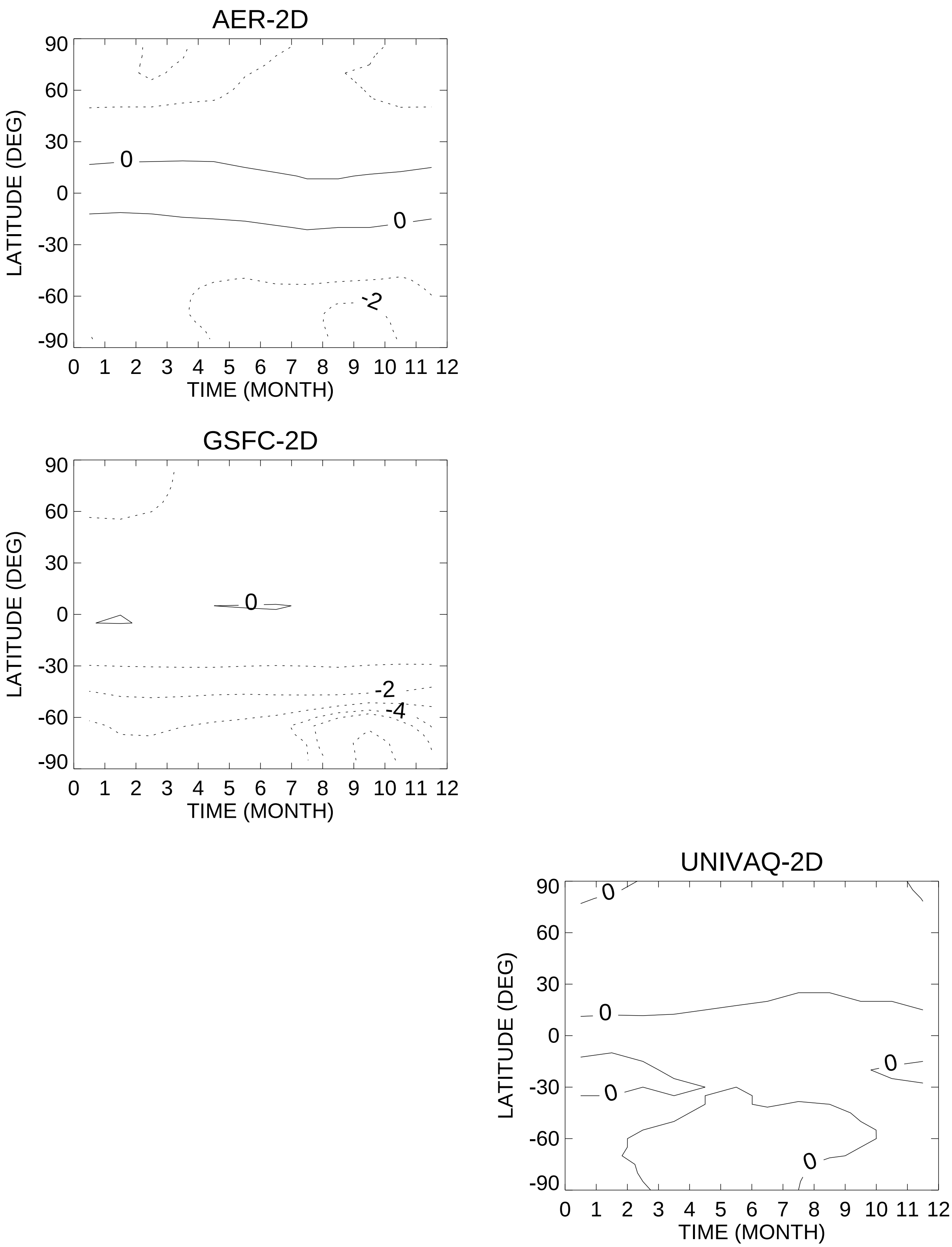

Figure 3.52: Percent change in total ozone column between Scenarios D6 and D. The difference in the scenarios is that D6 contains 4 ppbv of Cl_y and D contain 3 ppbv of Cl_y. Contours are -10, -5, -4, -3, -2, -1, 0.

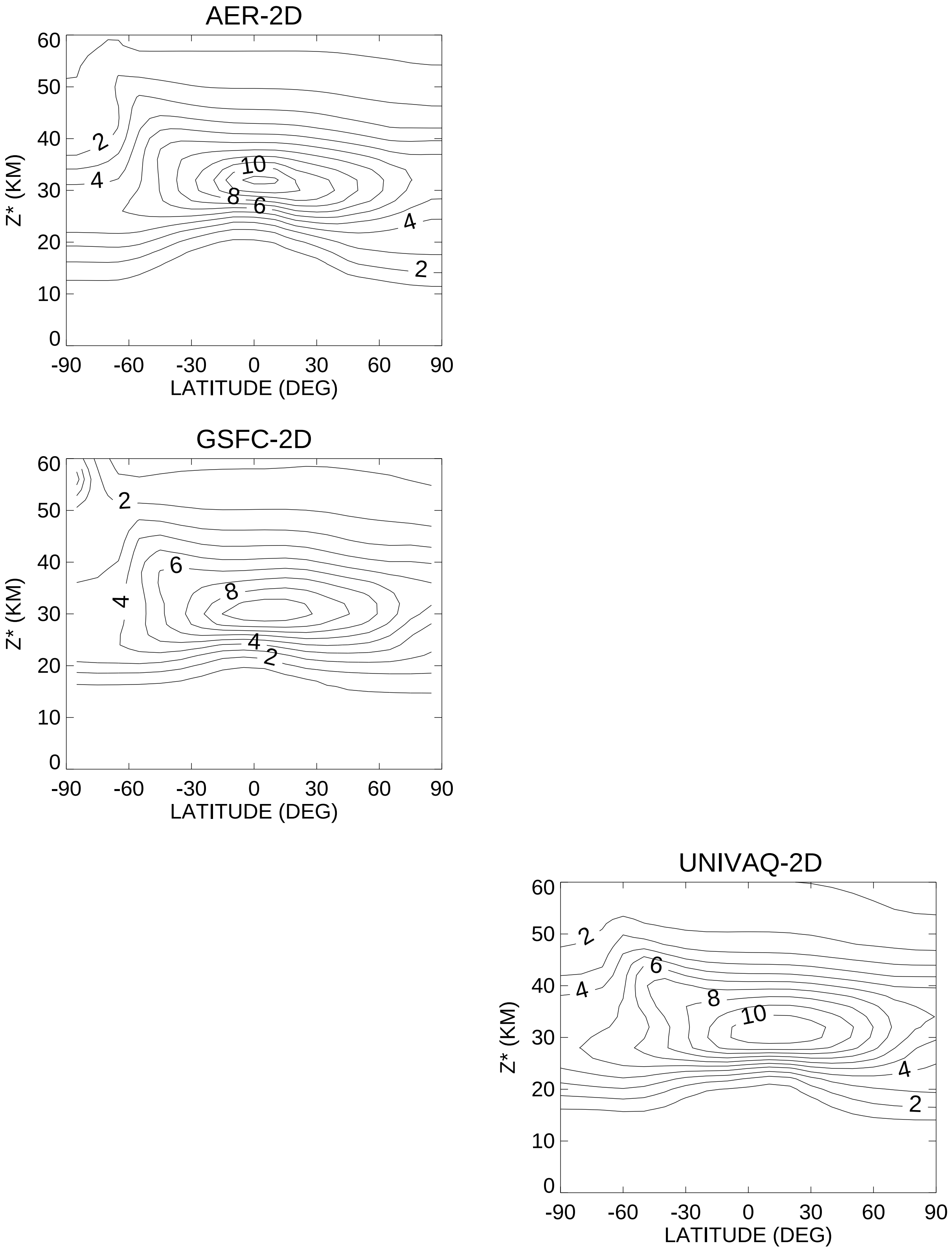

Figure 3.53: Calculated ozone mixing ratios (ppmv) as a function of latitude and altitude for Scenario D6 in June of 2015. The inorganic chlorine loading is 4 ppbv. The contour interval is 1 ppmv.

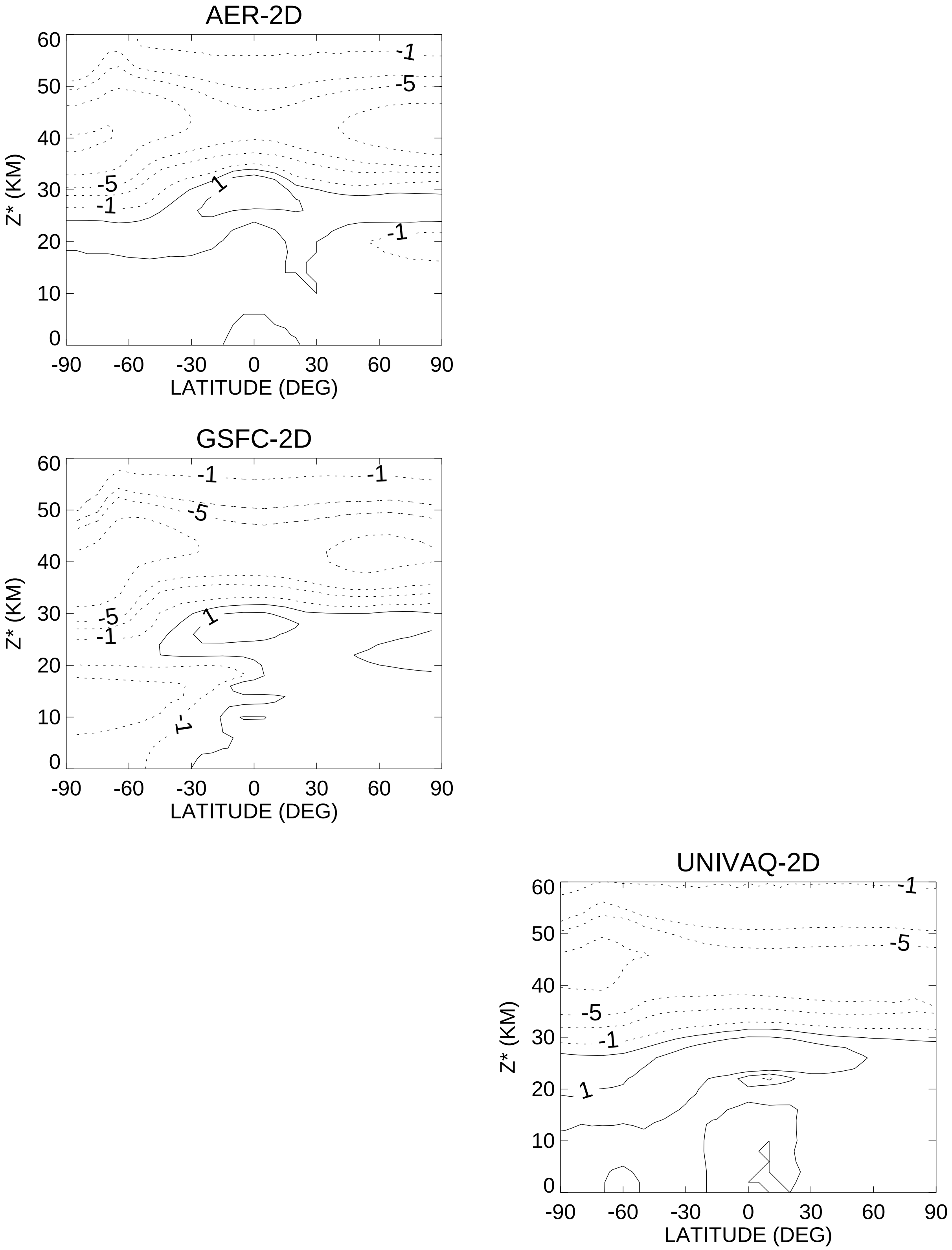

Figure 3.54: Percent change in ozone concentration between Scenarios D6 and D in June of 2015. The difference in the scenarios is that D6 contains 4 ppbv of Cl_y and D contain 3 ppbv of Cl_y. Contours are -15, -10, -5, -3, -1, 0, 1.

3.6 Scenario D7 Results

Scenario D7 did not employ the SA0 surface area density prescribed from WMO, but utilized interactive calculations of surface area density in the AER and UNIVAQ models. The UNIVAQ model included sulfur emissions for subsonic aircraft, assuming EI(SO_2)=0.4 and 50% SO_2 gas to particle conversion in the plume. The AER model did not consider sulfur emissions from subsonic aircraft and so employs a calculated non-volcanic background SAD. The SAD fields calculated by these models are shown in Figure 3.55. Note that the WMO SAD shown in Figure 3.1 includes no aerosols below 12 km. Modeling of tropospheric aerosols in 2-D models should be considered highly uncertain.

The calculated total ozone as a function of latitude and season for Scenario D7 is shown in Figure 3.56. The percent difference in total ozone relative to Scenario D is shown in Figure 3.57. Ozone column is increased by up to 1% in the AER model and up to 4% in the UNIVAQ model in the southern polar springtime due to the change in background aerosol SAD. Figure 3.58 shows ozone mixing ratios for June for this scenario. Changes in June ozone relative to Scenario D are shown in Figure 3.59. The AER model shows reduced ozone relative to Scenario D in most of the troposphere in June, but an increase above 10 km at middle and high latitudes. The UNIVAQ model show increased ozone at middle and high latitudes below 10 km in June and an ozone decrease in the northern hemisphere lower stratosphere. These calculations are provided as sensitivity analysis for understanding the effects of changes in background aerosol SAD on ozone perturbations.

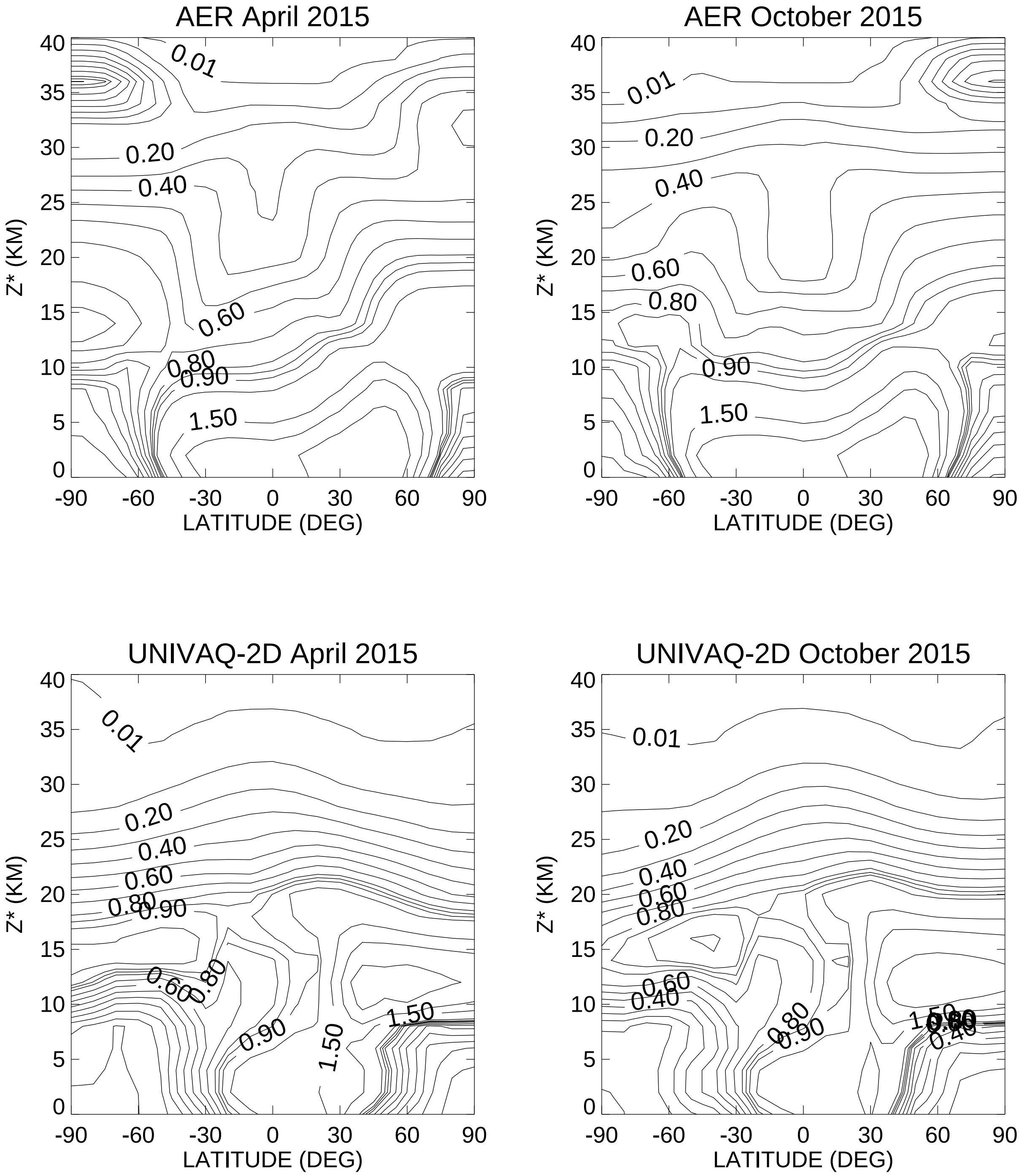

Figure 3.55: Aerosol surface area density ($\mu m^2/cm^3$) calculated by the AER and UNIVAQ models for Scenario D7, the 2015 background atmosphere including subsonic aircraft and interactive microphysics. The UNIVAQ model included sulfur emissions from subsonic aircraft assuming 50% SO_2 gas to particle conversion, while the AER model omitted subsonic sulfur. Contours are 0.01, 0.1 to 0.8 by 0.1, 0.85, 0.9, 1.0, 1.5, 2, 3.

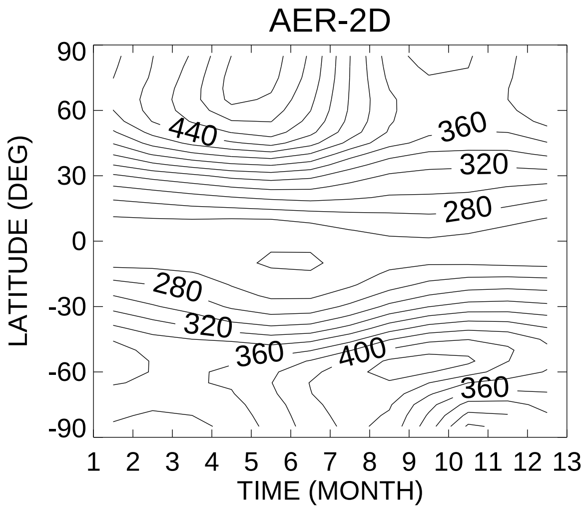

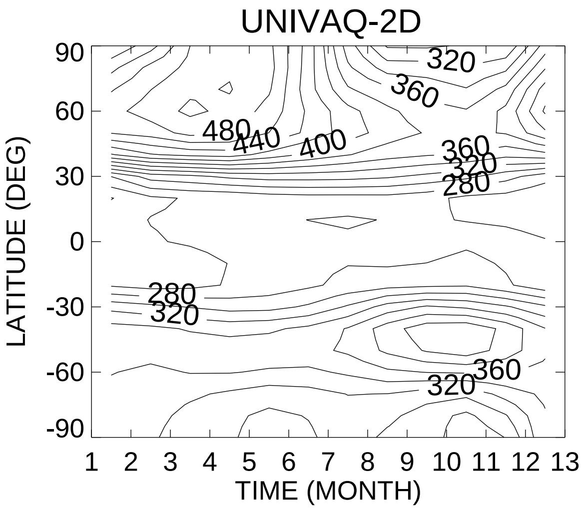

Figure 3.56: Total ozone column (Dobson Units) as a function of latitude and season as calculated by the models for Scenario D7, the 2015 background atmosphere including subsonic aircraft and interactive microphysics. The contour interval is 20 DU.

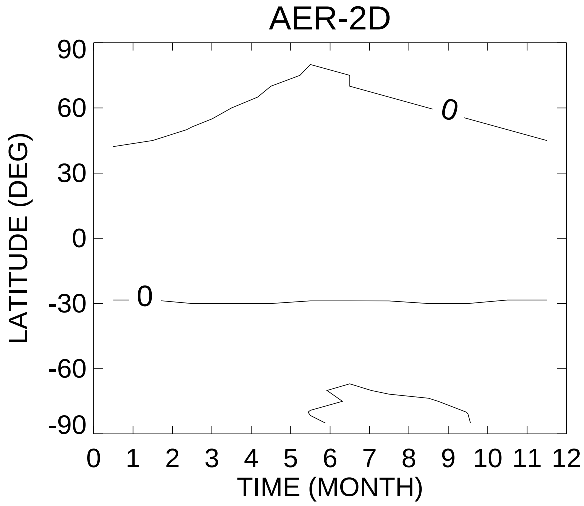

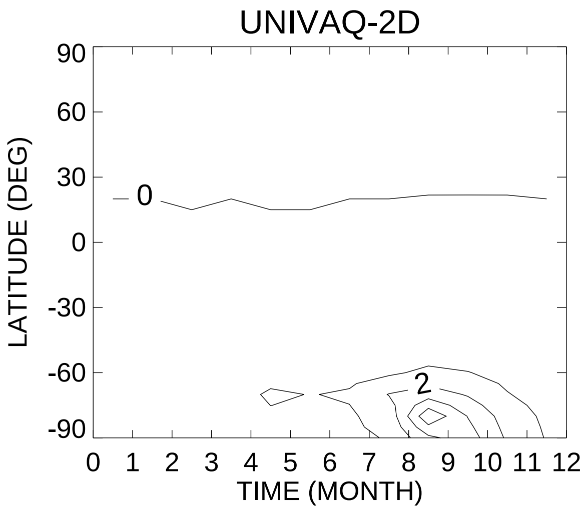

Figure 3.57: Percent change in total ozone column between Scenarios D7 and D. The difference in the scenarios is in the aerosol surface area density. Contours are 0, 1, 2, 3, 4.

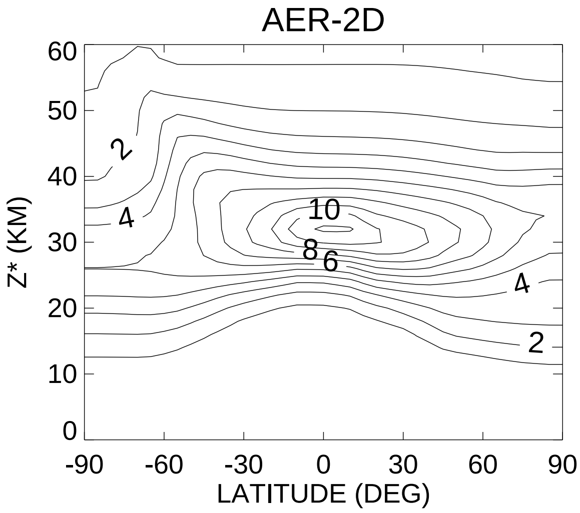

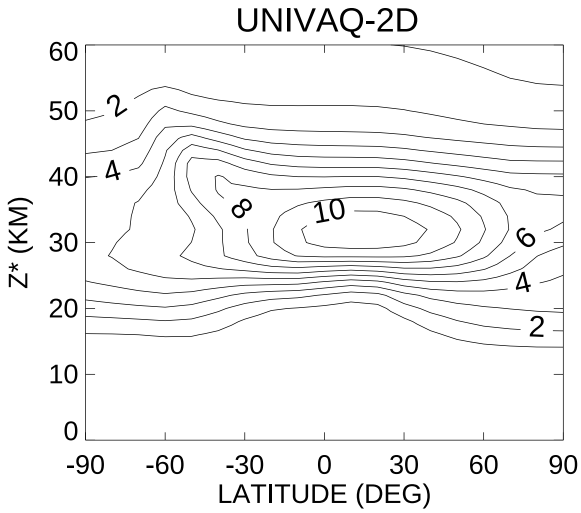

Figure 3.58: Calculated ozone mixing ratios (ppmv) as a function of latitude and altitude for Scenario D7 in June of 2015. Contour interval is 1 ppmv.

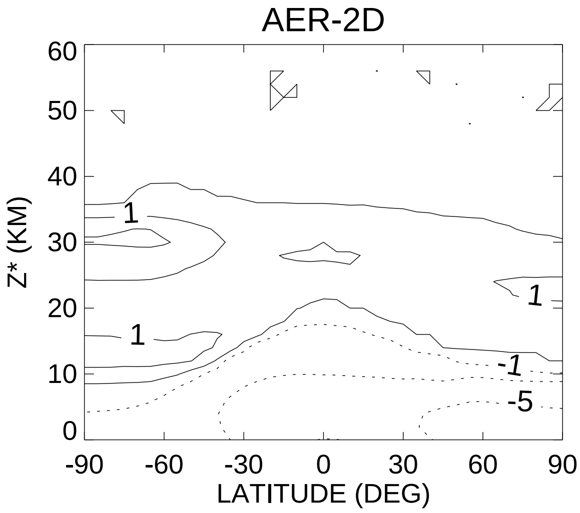

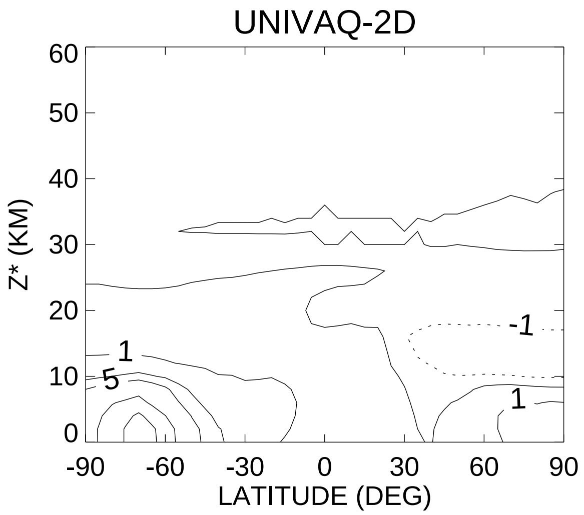

Figure 3.59: Percent change in ozone concentration between Scenarios D7 and D in June of 2015. The difference in the scenarios is in the aerosol surface area density. Contours are -5, -3, -1, 0, 1, 3, 5, 10, 15.

3.7 Scenario D8 Results

Scenario D8 is similar to Scenario D7 except that 100% SO_2 gas to particle conversion in the plume is assumed for subsonic aircraft emissions in the UNIVAQ model. The AER model did not consider sulfur emissions from subsonic aircraft, and so D7 and D8 are identical for the AER model. The SAD fields calculated for Scenario D8 are shown in Figure 3.60. Total ozone fields as a function of latitude and season are shown in Figure 3.61. Changes in total ozone relative to Scenario D are shown in Figure 3.62. Figure 3.63 shows ozone mixing ratios as a function of latitude and altitude for June, and Figure 3.64 shows changes in June ozone relative to Scenario D.

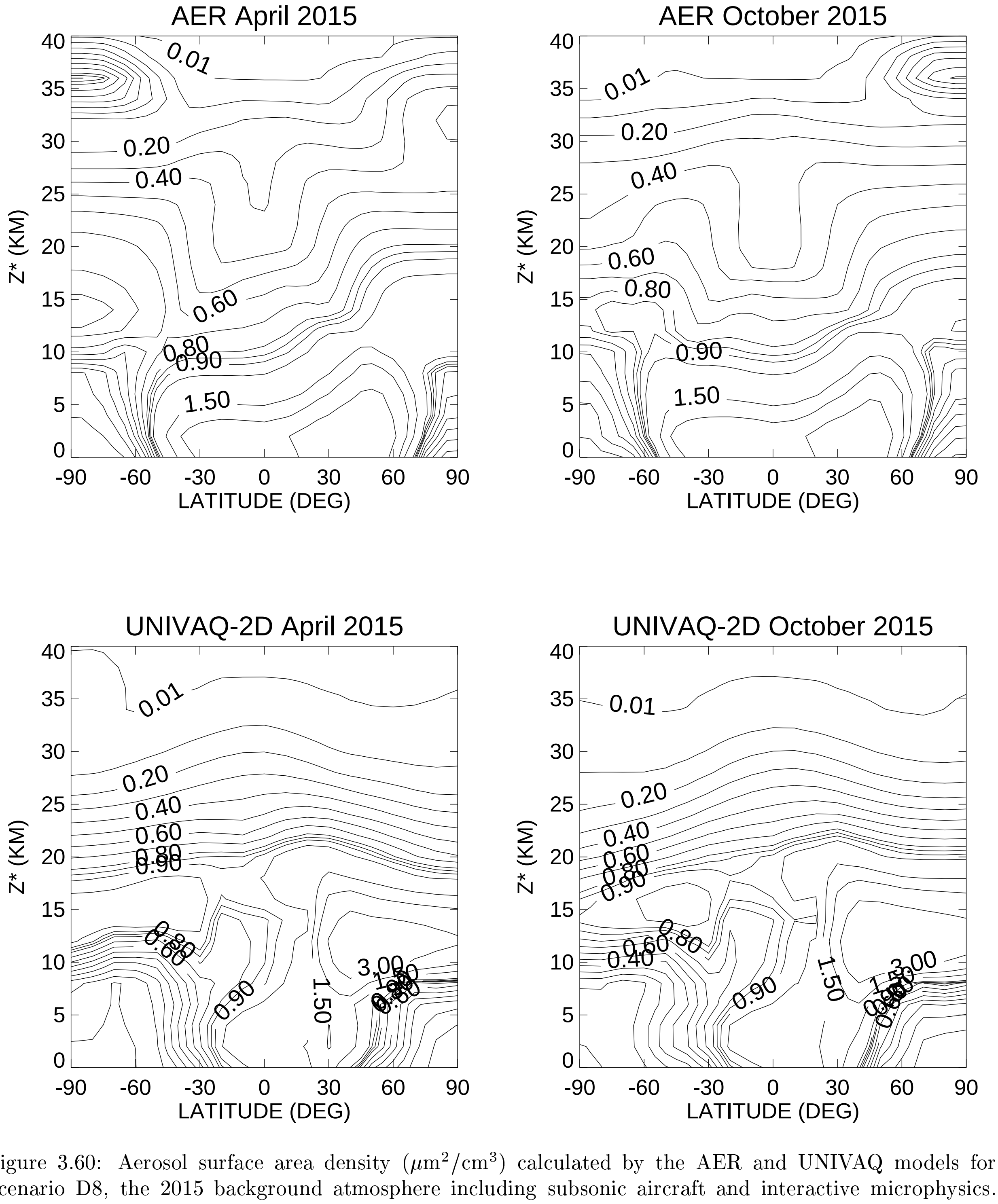

Figure 3.60: Aerosol surface area density ($\mu m^2/cm^3$) calculated by the AER and UNIVAQ models for Scenario D8, the 2015 background atmosphere including subsonic aircraft and interactive microphysics. The UNIVAQ model included sulfur emissions from subsonic aircraft assuming 100% SO_2 gas to particle conversion, while the AER model did not. Contours are 0.01, 0.1 to 0.8 by 0.1, 0.85, 0.9, 1.0, 1.5, 2, 3.

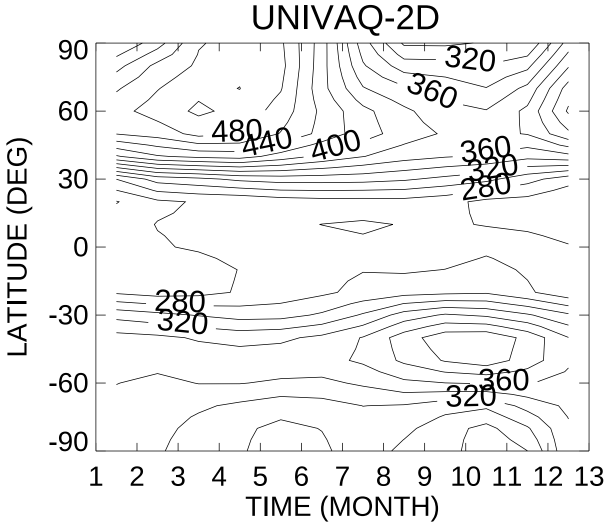

Figure 3.61: Total ozone column (Dobson Units) as a function of latitude and season as calculated by the UNIVAQ model for Scenario D8, the 2015 background atmosphere including subsonic aircraft and interactive microphysics. Contour interval is 20 DU.

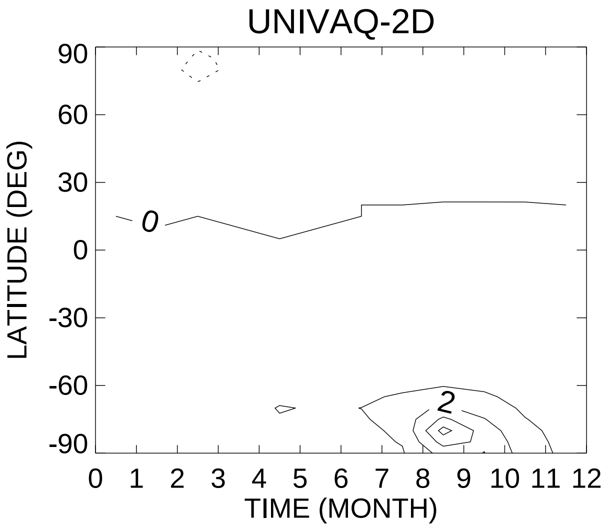

Figure 3.62: Percent change in total ozone column between Scenarios D8 and D. The difference in the scenarios is in the aerosol surface area density. Contours are 0, 1, 2, 3, 4.

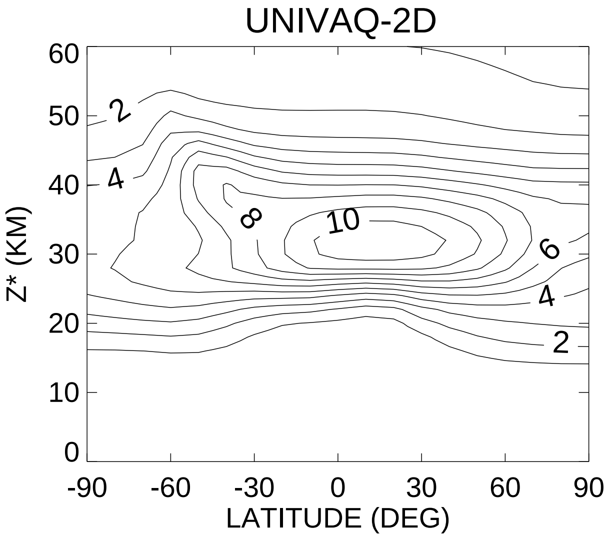

Figure 3.63: Ozone mixing ratio (ppmv) as a function of latitude and altitude as calculated by the UNIVAQ model for Scenario D8 in June on 2015. Contour interval is 1 ppmv.

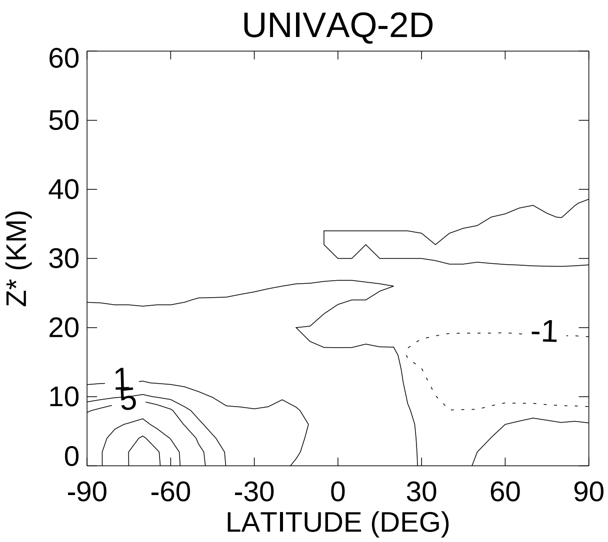

Figure 3.64: Percent change in ozone concentration between Scenarios D8 and D in June of 2015. The difference in the scenarios is in the aerosol surface area density. Contours are -1, 0, 1, 3, 5, 10, 15.

3.8 Scenario D9 Results

Scenario D9 represent the 2050 background atmosphere. Surface boundary conditions are described in Table 3.1. The nonvolcanic sulfate surface area density SA0 is used. The subsonic aircraft fleet is the same as that used in 2015. Calculated NO_y mixing ratios as a function of latitude and altitude for June are shown in Figure 3.65. The N_2O boundary condition for 2050 is 11% greater than for 2015, so NO_y concentrations are increased accordingly. Cl_y mixing ratios are shown in Figure 3.66 and Br_y fields in Figure 3.67. The surface boundary conditions provide for 2.0 ppbv of Cl_y and 11 pptv of Br_y.

Total column ozone as a function of latitude and season is shown in Figure 3.68 for Scenario D9. Figure 3.69 shows changes in total ozone relative to Scenario D, the 2015 background atmosphere. Ozone columns are larger in 2050 than in 2015 due to the reduced concentration of Cl_y and Br_y. The GSFC and LLNL models calculate total ozone increases of 10-30% in the southern hemisphere high latitudes, while the AER, CSIRO, and UNIVAQ model calculate much smaller changes. Figure 3.70 shows ozone mixing ratios for June for Scenario D9. Changes in June ozone concentration relative to Scenario D are shown in Figure 3.71. All models show significant ozone increases between 35 and 50 km. The GSFC and LLNL models also show significant ozone increases in the southern hemisphere lower stratosphere, due to the importance of PSC processes in those models.

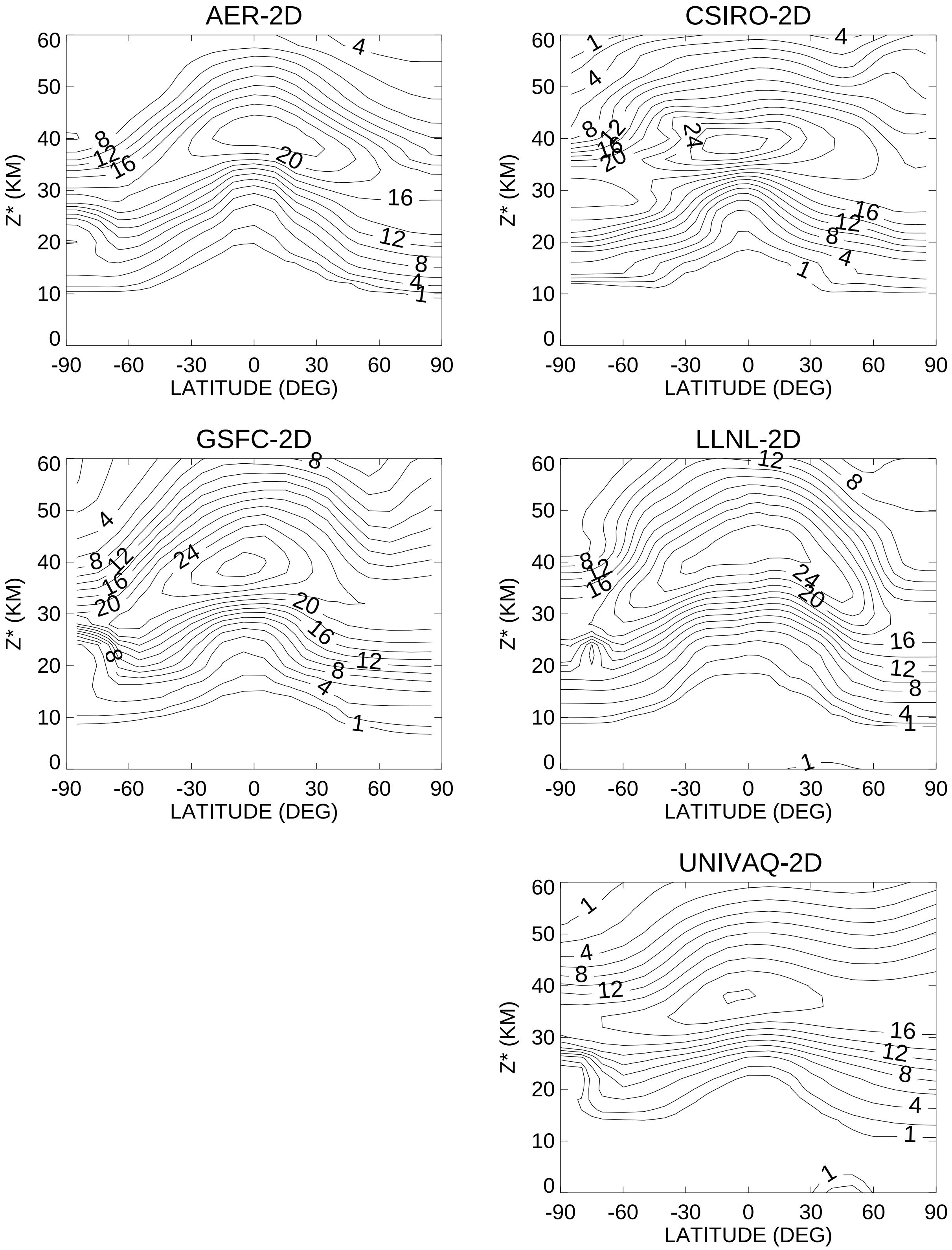

Figure 3.65: Calculated NO_y mixing ratios (ppbv) as a function of latitude and altitude in June for Scenario D9, the 2050 background atmosphere. Contours are 1 and 2 to 28 by 2 ppbv.

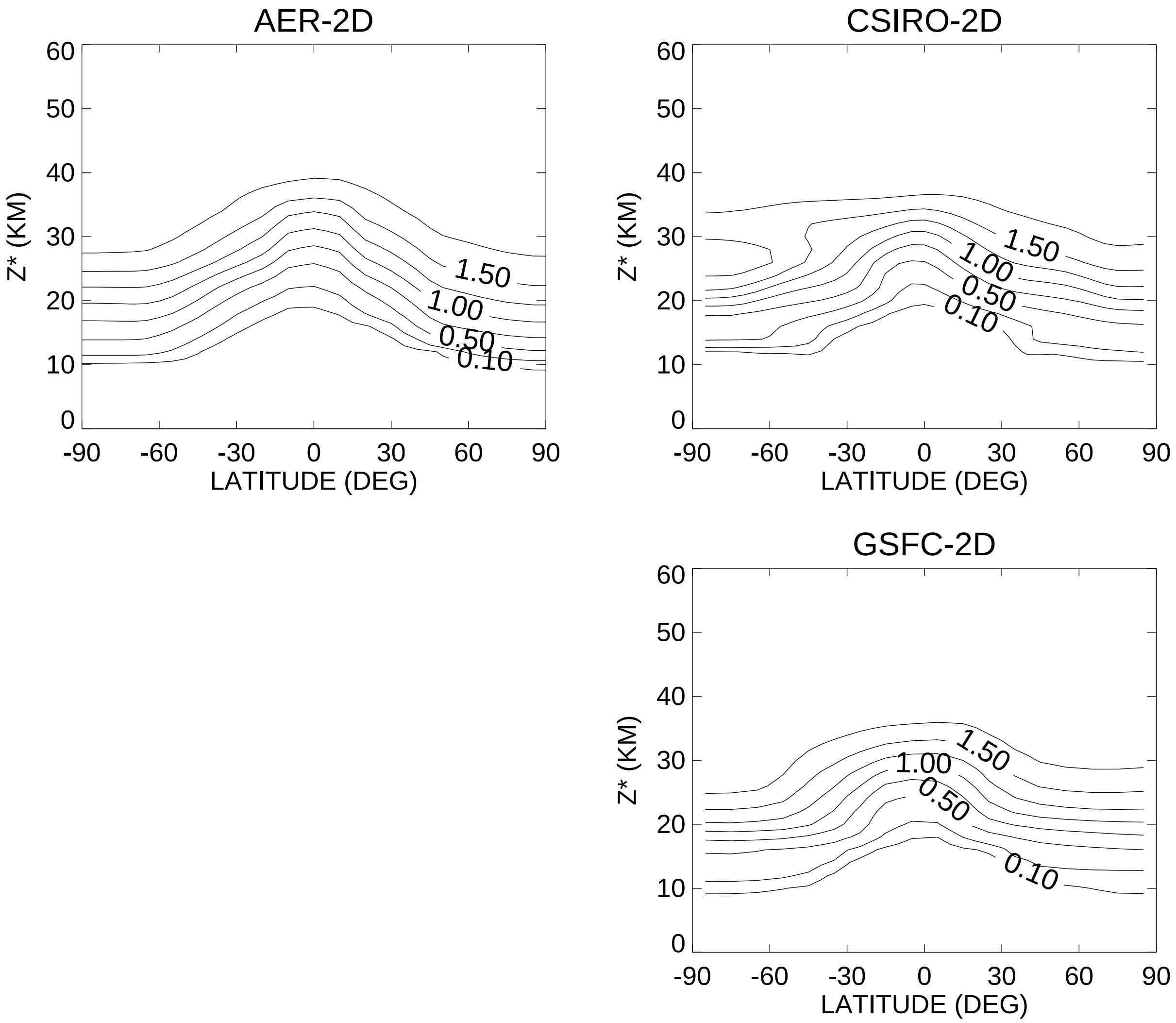

Figure 3.66: Calculated Cl_y mixing ratios (ppbv) as a function of latitude and altitude in June for Scenario D9, the 2050 background atmosphere. Inorganic chlorine loading is approximately 2 ppbv. Contours are 0.1 and 0.25 to 1.75 by 0.25 ppbv.

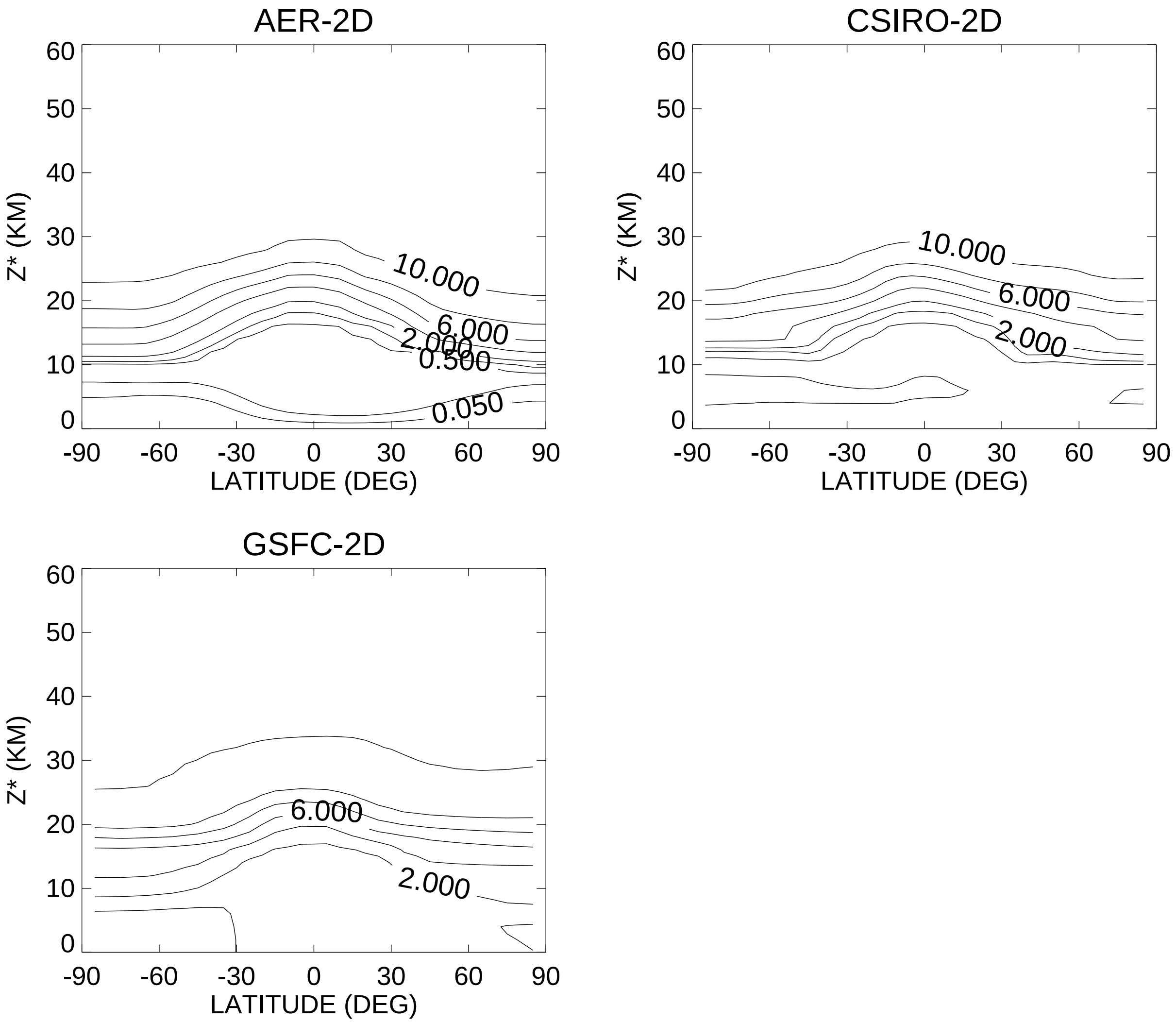

Figure 3.67: Calculated Br_y mixing ratios (ppbv) as a function of latitude and altitude in June for Scenario D9, the 2050 background atmosphere. Inorganic bromine loading is approximately 11 pptv. Contours are 0.05, 0.1, 0.5, 1.0, and 2 to 12 by 2 pptv.

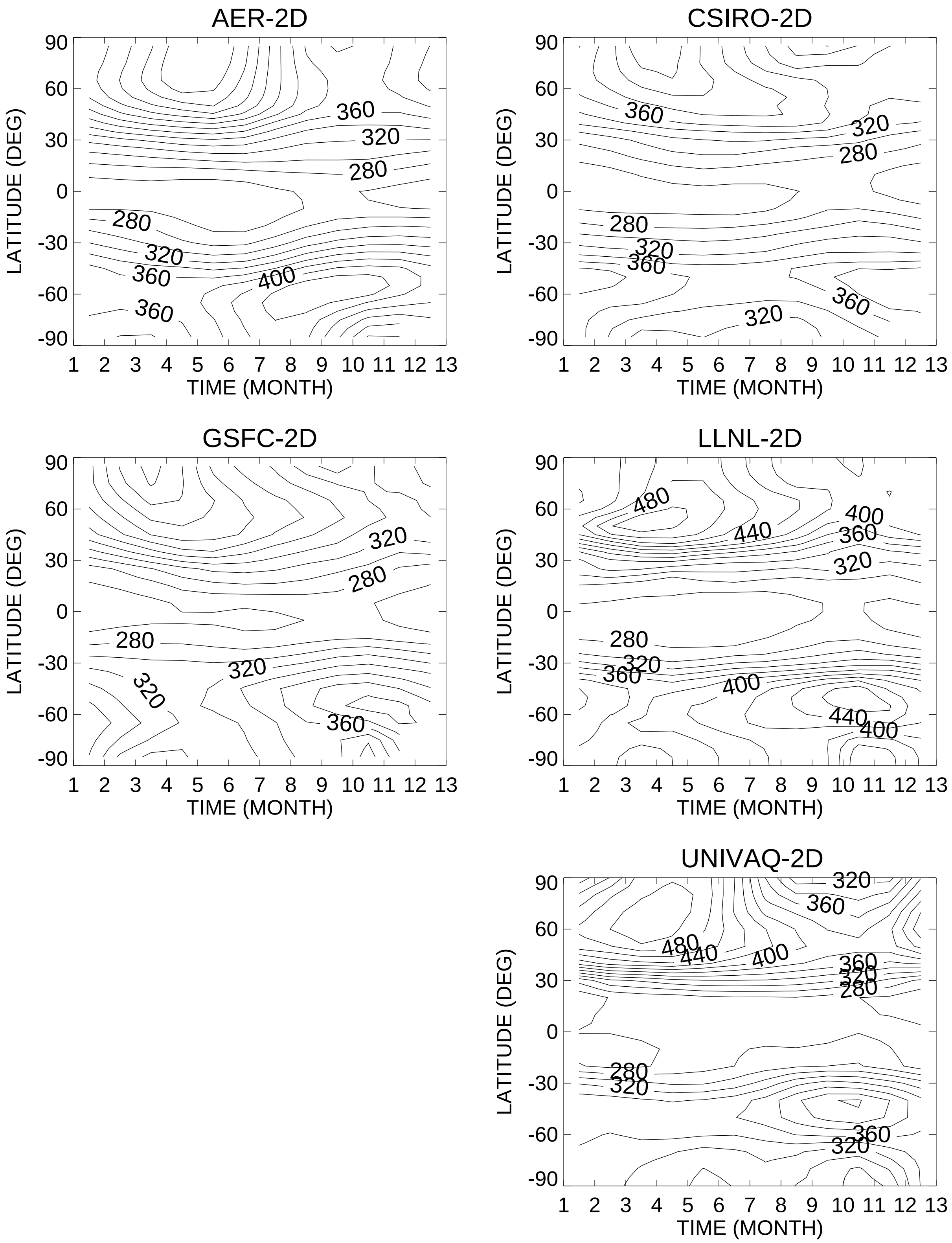

Figure 3.68: Total ozone column (Dobson Units) as a function of latitude and season as calculated by the models for Scenario D9, the 2050 background atmosphere including subsonic aircraft. Contour interval is 20 DU.

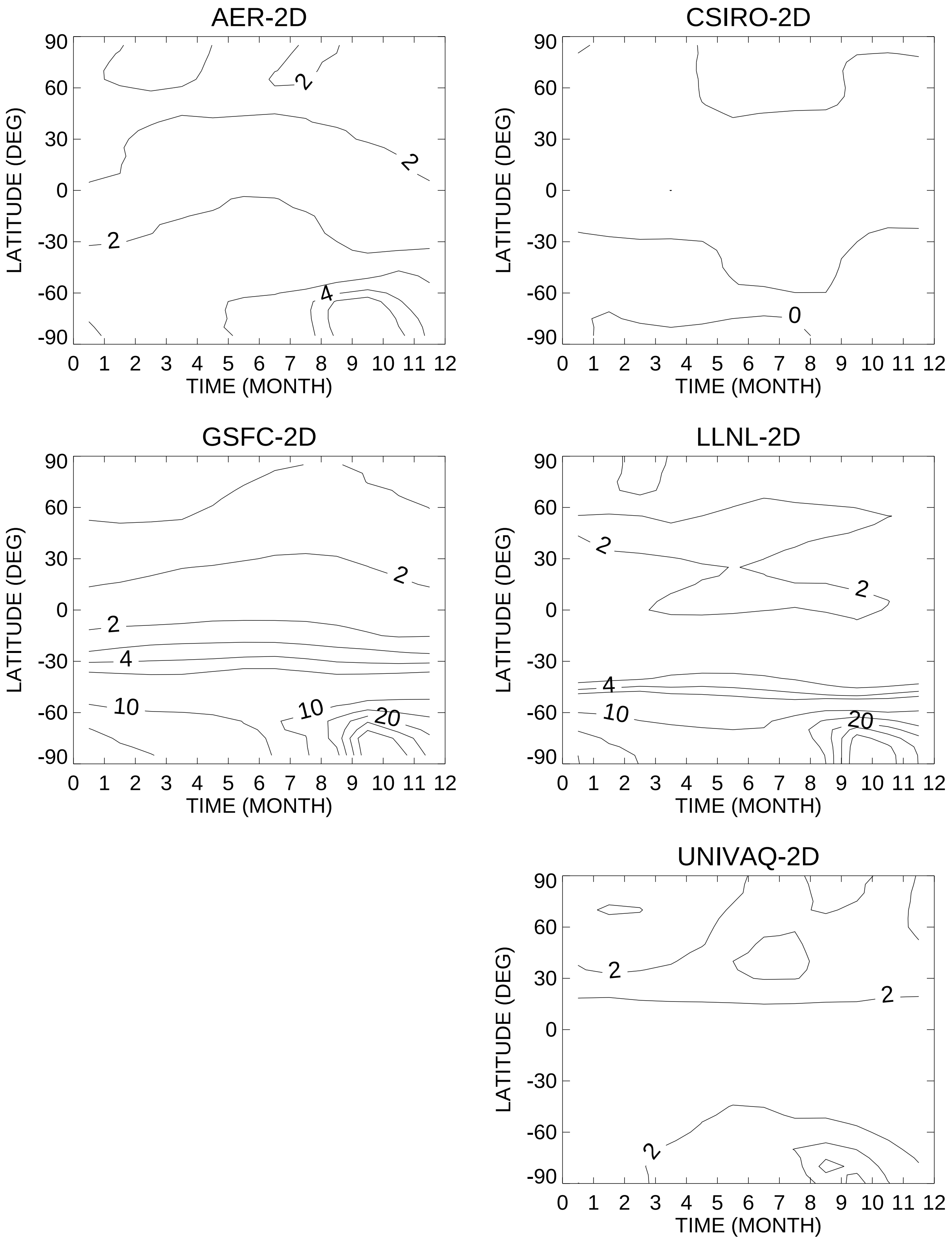

Figure 3.69: Percent change in total ozone column between Scenarios D9 and D. Scenario D9 represents 2050 and Scenario D 2015. The same subsonic aircraft fleet is included. Contours are 0 to 5 by 1 and 10 to 30 by 5.

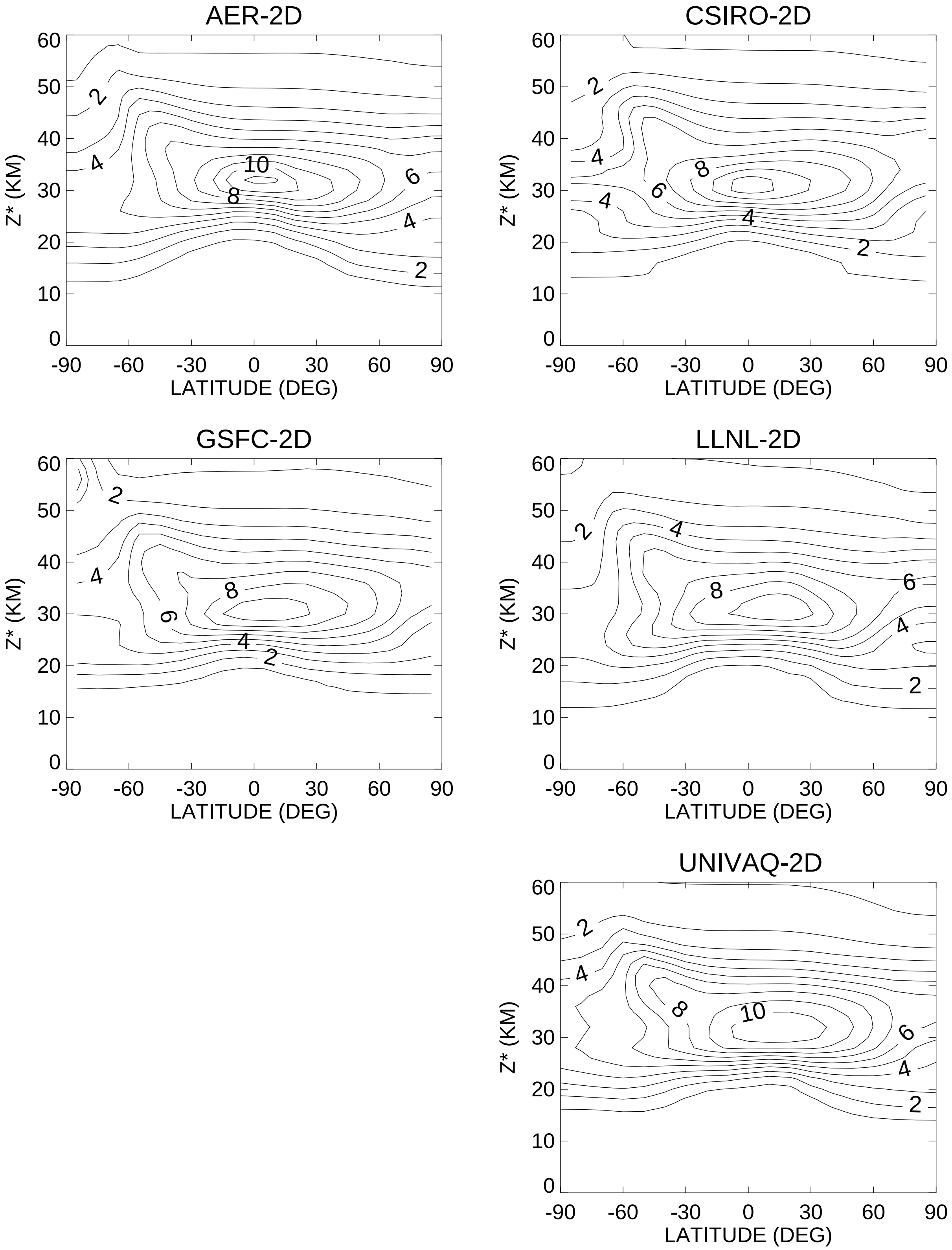

Figure 3.70: Calculated ozone mixing ratios (ppmv) as a function of latitude and altitude for Scenario D9 in June of 2050. Contour interval is 1 ppmv.

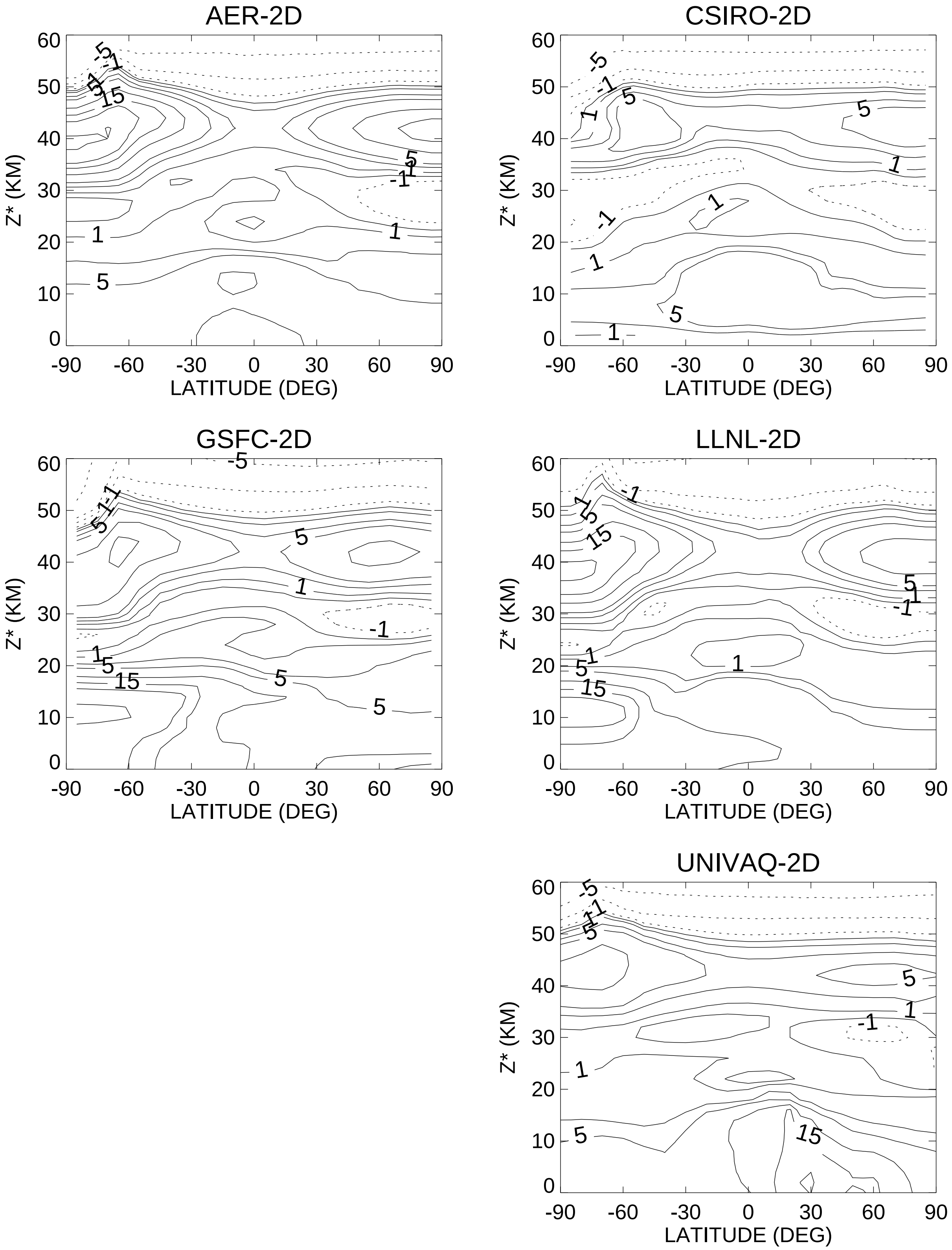

Figure 3.71: Percent change in ozone concentration between Scenarios D9 and D in June of 2015. Scenario D9 represents 2050 and Scenario D 2015. Contours are -1, 0, 1, 3, and 5 to 25 by 5.

3.9 Scenario F Results

This is an alternate 2050 background atmosphere with the subsonic fleet described by the IPCC IS92a scenario. The total fleet fuel burn is 471 Tg/yr for the 2050 IS92a scenario, compared with 309 Tg/yr for the 2015 subsonic scenario. Subsonic aircraft emissions perturb tropospheric NO_y concentrations. Figure 3.72 shows NO_y mixing ratios as a function of latitude and altitude for June for Scenario F. Figure 3.73 shows percent differences in NO_y concentration between Scenarios F and D9. NO_y concentrations in the troposphere are increased by only 0.5% due to increases in aircraft-emitted NO_y of 50%. Aircraft emissions of NO_y are small relative to other tropospheric sources, and tropospheric removal rates are large. The percent change in ozone mixing ratio for June for Scenario F relative to Scenario D9 is shown in Figure 3.74. The AER, CSIRO, and GSFC models show ozone increases of up to 5% in the troposphere, while changes in the UNIVAQ model are smaller.

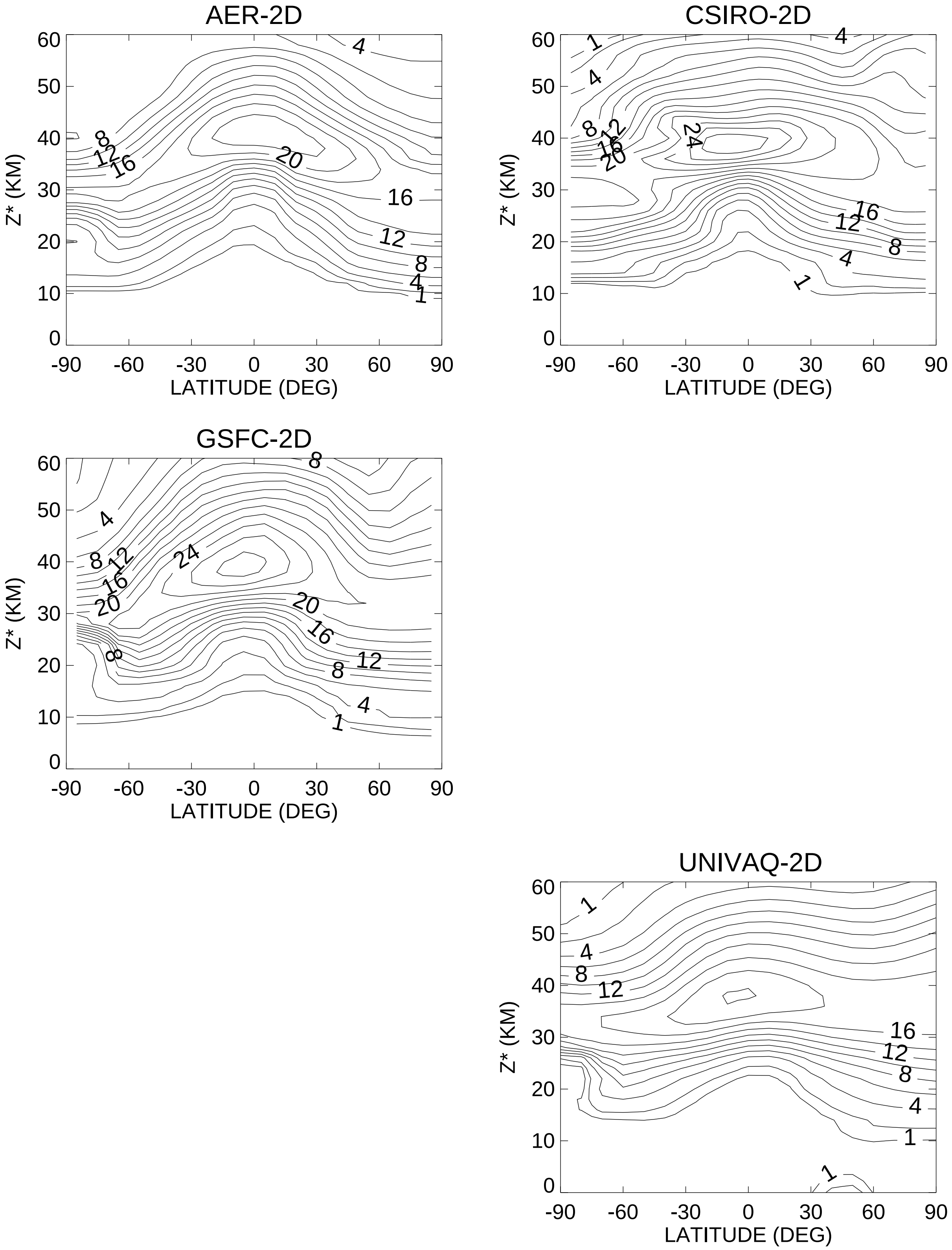

Figure 3.72: Calculated NO_y mixing ratios (ppbv) as a function of latitude and altitude in June for Scenario F, the 2050 background atmosphere with the subsonic fleet projected to 2050 using the IPCC IS92a scenario. Contours are 1 and 2 to 28 by 2 ppbv.

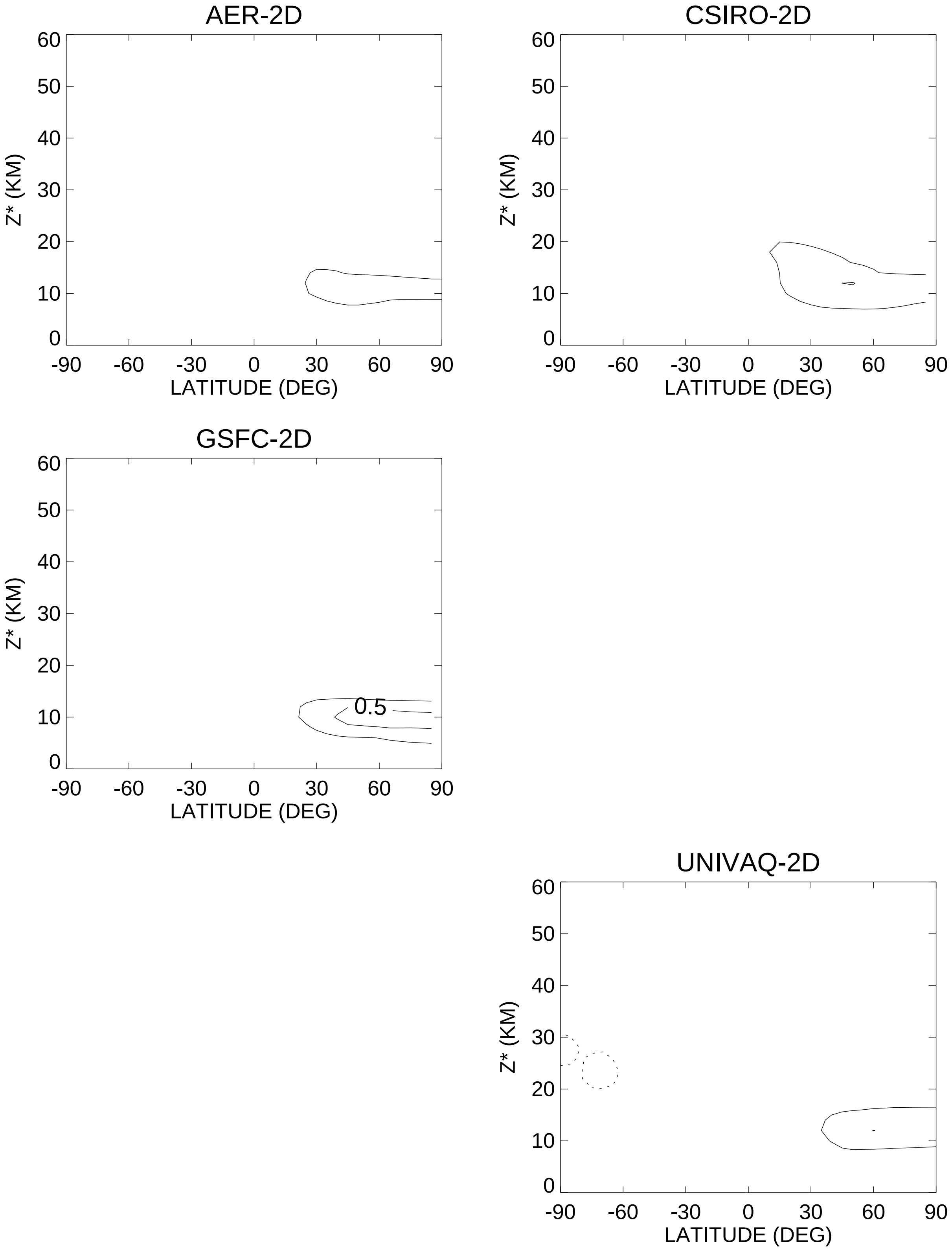

Figure 3.73: Percent change in calculated NO_y mixing ratio (ppbv) in June for Scenario F relative to Scenario D9. Scenario F uses a subsonic fleet projected to 2050 using the IPCC IS92a scenario, while Scenario D9 used the 2015 projected subsonic fleet. Contours are -0.5, 0, 0.5.

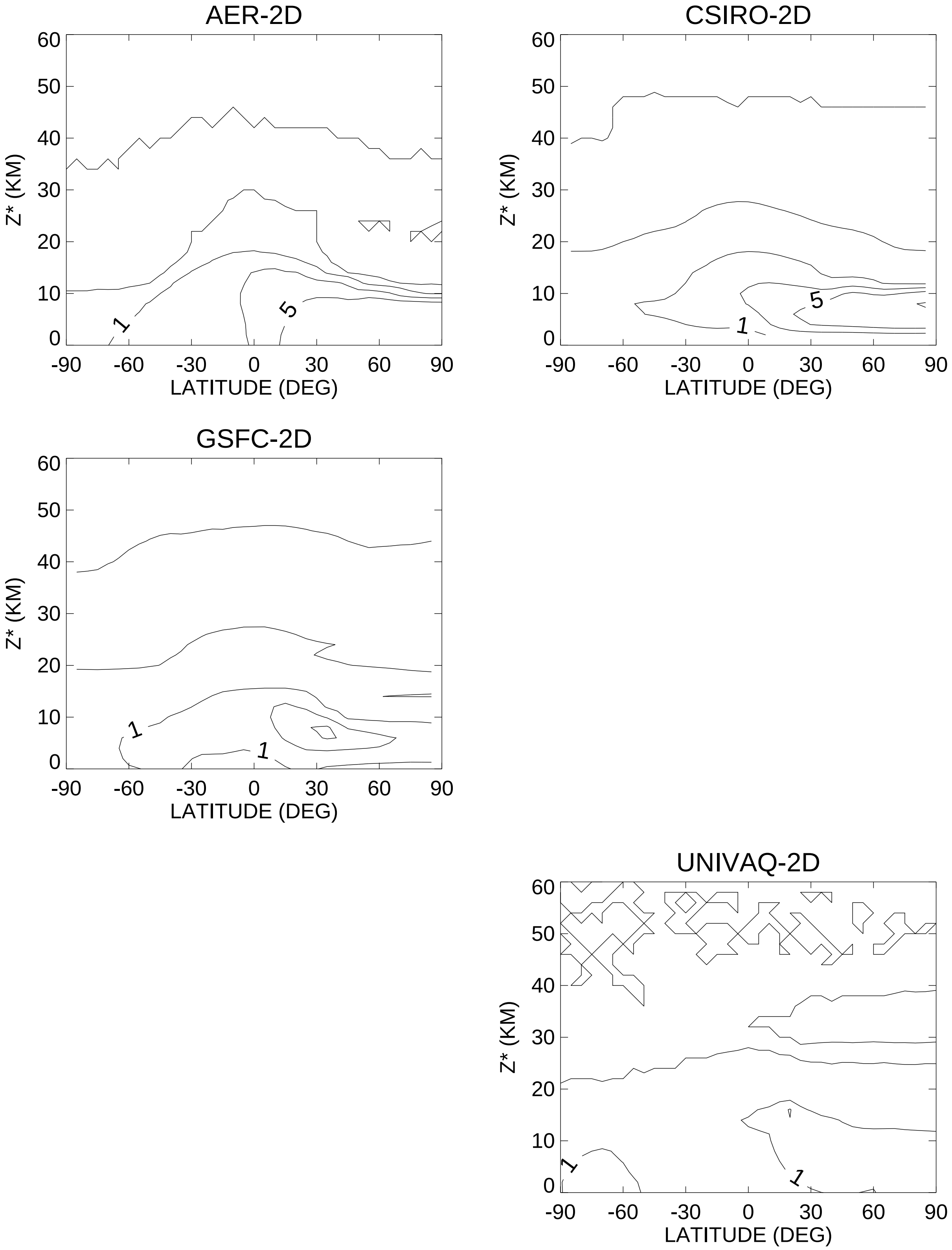

Figure 3.74: Percent change in ozone concentration between Scenarios F and D9 in June of 2015. Scenario F uses a subsonic fleet projected to 2050 using the IPCC IS92a scenario, while Scenario D9 used the 2015 projected subsonic fleet. Contours are 0, 1, 3, and 5.

3.10 Scenario G Results

This is an alternate 2050 background atmosphere with the subsonic fleet described by the IPCC IS92e high demand scenario. Total fuel burn from subsonic emission is 744 Tg/yr, an increase of 130% over the 2015 subsonic fleet. NO_y mixing ratios for June for this scenario are shown in Figure 3.75. Changes in NO_y mixing ratio relative to Scenario D9 are shown in Figure 3.76. Increases in NO_y of up to 1.5% are seen for the GSFC model and up to 1.0% for the CSIRO and UNIVAQ models. The AER model shows a smaller increase. The corresponding changes in ozone mixing ratio for June are shown in Figure 3.77. The CSIRO model shows tropospheric ozone changes as large as 20%.

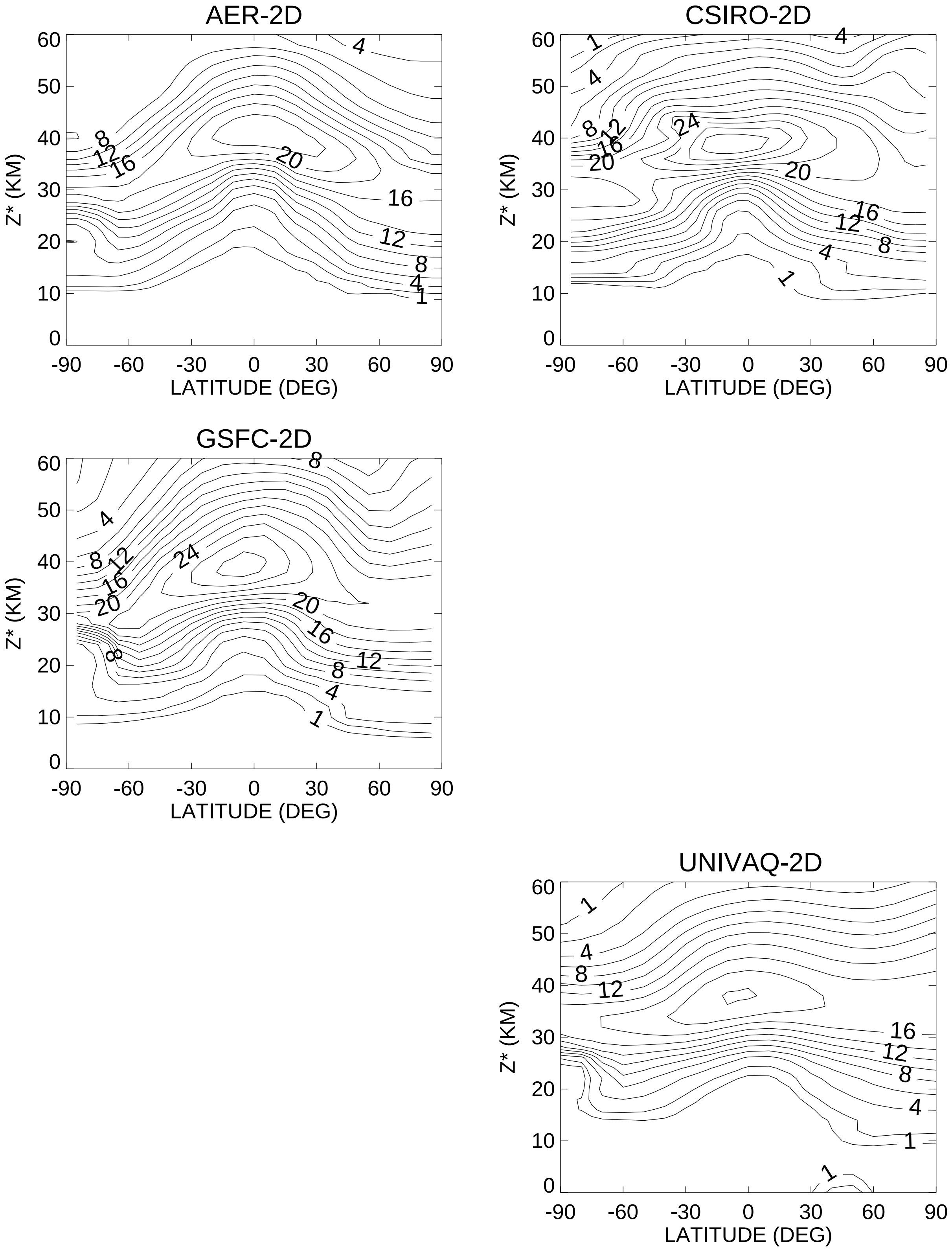

Figure 3.75: Calculated NO_y mixing ratios (ppbv) as a function of latitude and altitude in June for Scenario G, the 2050 background atmosphere with the subsonic fleet projected to 2050 using the IPCC IS92e high demand scenario. Contours are 1 and 2 to 28 by 2 ppbv.

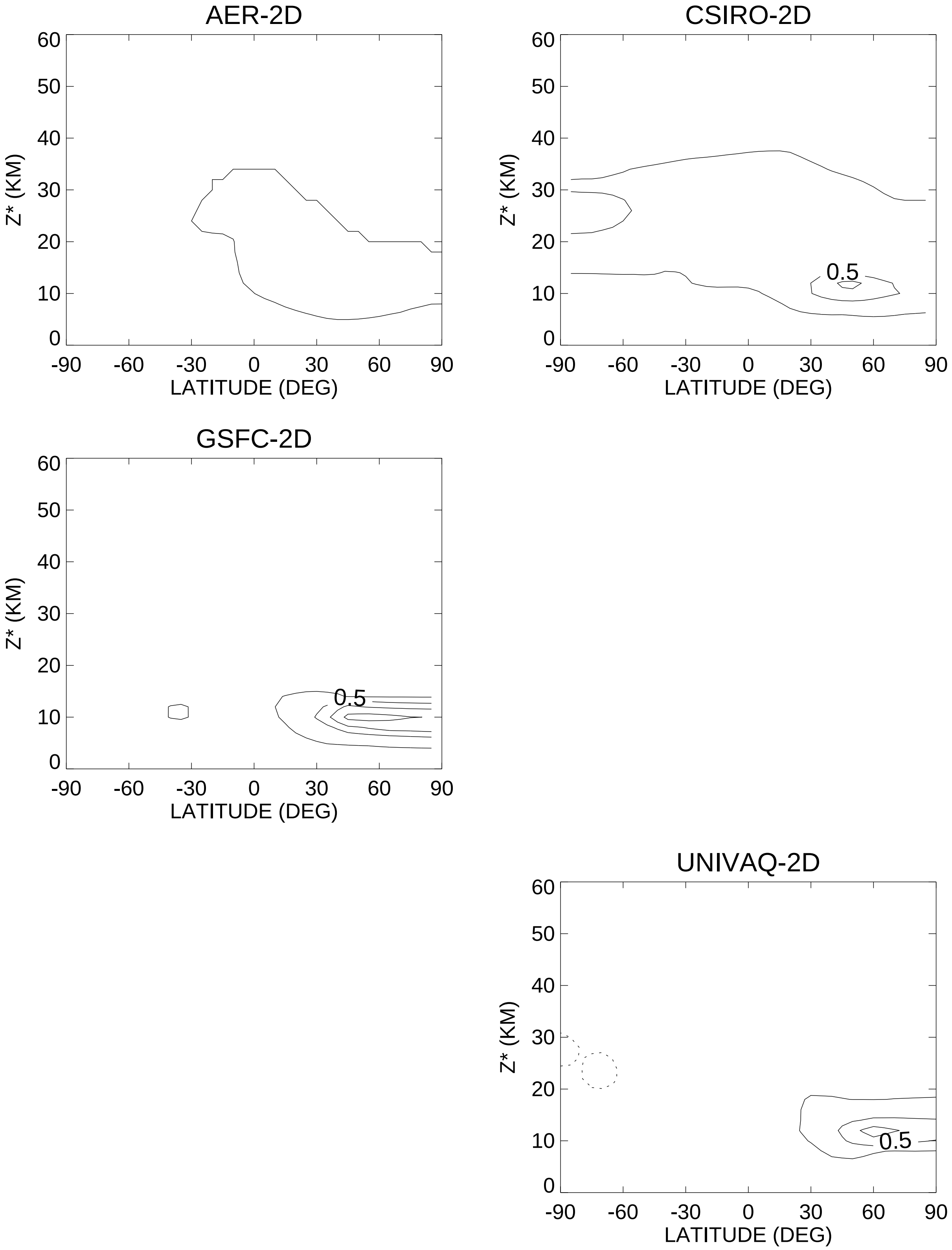

Figure 3.76: Percent change in calculated NO_y mixing ratio (ppbv) in June for Scenario G relative to Scenario D9. Scenario G uses a subsonic fleet projected to 2050 using the IPCC IS92e high demand scenario, while Scenario D9 used the 2015 projected subsonic fleet. Contours are -0.5, 0, 0.5, 1.0, and 1.5.

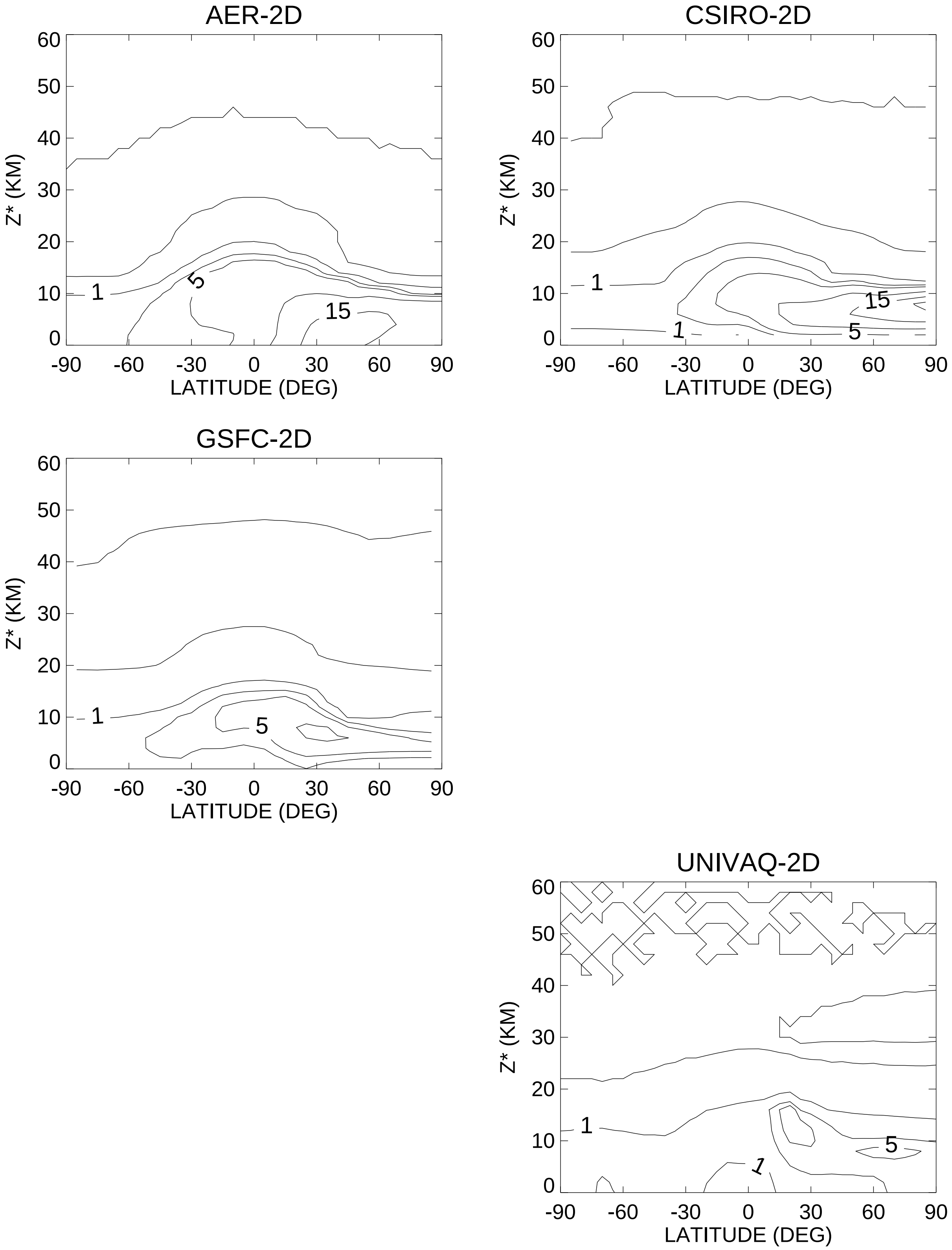

Figure 3.77: Percent change in ozone concentration between Scenarios G and D9 in June of 2015. Scenario G uses a subsonic fleet projected to 2050 using the IPCC IS92e high demand scenario, while Scenario D9 used the 2015 projected subsonic fleet. Contours are 0, 1, 3, 5, 10, 15, and 20.

Bibliography

[1] IPCC (International Panel on Climate Change), *Climate Change 1992: The Supplemental Report to the IPCC Scientific Assessment,* J. T. Houghton, B. A. Callander, and S. Varney (Eds.), Cambridge University Press, Cambridge, U.K., 1992.

[2] IPCC (International Panel on Climate Change), *Climate Change 1995: The Science of Climate Change,* J. T. Houghton, L. G. Meira Filho, B. A. Callander, N. Harris, A. Kattenberg, and K. Maskell (Eds.), Cambridge University Press, Cambridge, U.K., 1995.

[3] World Meteorological Organization (WMO), Scientific Assessment of Ozone Depletion: 1991, Global Ozone Res. and Monit. Proj., *Rep. 25,* Geneva, Switzerland, 1992.